FTIR and Raman spectroscopy in characterization of bioreactor cultured prostate cancer extracellular vesicles

Master's Thesis

University of Turku

MSc Degree Programme in Biomedical Sciences,
Drug Discovery and Development

December 2020

Laura Mäntylä, BSc

Jacopo Zini, MSc
Doctoral Student, Division of Pharmaceutical Biosciences
Faculty of Pharmacy, University of Helsinki

Marjo Yliperttula, PhD,
Professor, Division of Pharmaceutical Biosciences
Faculty of Pharmacy, University of Helsinki

Ullamari Pesonen, PhD
Professor, Institute of Biomedicine,
Faculty of Medicine, University of Turku

ABSTRACT
UNIVERSITY OF TURKU
Institute of Biomedicine, Faculty of Medicine

MÄNTYLÄ, LAURA: FTIR and Raman spectroscopy in characterization of bioreactor cultured prostate cancer extracellular vesicles
Master's Thesis, 79 pages, 2 appendices
MSc Degree Programme in Biomedical Sciences
Drug Discovery and Development
March 2021

Background Extracellular vesicles (EVs) are nano-sized cell membrane derived structures that function as intercellular messengers and hold potential for applications in diagnostics and drug delivery. There is a need to establish efficient methods of production and quality control for EV preparations. The International Society for Extracellular Vesicles has suggested the protein/lipid ratio of the vesicle components as a measure of purity for EV samples. Spectroscopic methods such as FTIR and Raman are promising options for characterization of these EV biomolecular properties. Hypoxia is a common feature of solid tumors such as prostate cancer and increases the secretion of EVs from cells.

Aims The aims for this study were to 1) establish a bioreactor cell culture protocol for 22Rv1 and RWPE-1 cell lines, 2) characterize the EVs obtained from these cell lines using Raman and FTIR spectroscopy and subsequently obtain the spectroscopic protein/lipid (P/L) ratio, and 3) to analyze the spectroscopic P/L ratio as a measure of EV composition and purity as a function of time in cell culture 4) to investigate EV secretion from these cell lines under hypoxic conditions.

Methods Prostate cancer (22Rv1 and PC3) and normal prostate cell lines (RWPE-1 and PNT2) were cultured in CELLine bioreactor conditions, and EVs were extracted from the cell culture media once per week. The collected culture media was subjected to a series of (ultra)centrifugations and size-exclusion chromatography to purify the vesicles. The purified vesicles were characterized by means of Western blotting, nanoparticle tracking analysis and Raman and ATR-FTIR spectroscopy, and the spectral protein/lipid ratios were analyzed. Culturing of 22Rv1 and RWPE-1 cell lines in hypoxic conditions was also attempted.

Results The obtained results suggest that this protocol was effective for producing purified EV preparations. However, notable variation in EV sample protein/lipid ratios between weekly samples from newly established bioreactor cultures was detected. These results highlight both the utility of spectroscopic methods in distinguishing the biomolecular compositions of different EV populations, and the volatility of EV preparations to changes in the cell culture, therefore indicating a need to carefully optimize stable EV culture conditions.

Keywords Extracellular vesicles, prostate cancer, FTIR, Raman spectroscopy

Contents

1. Introduction

1.1 Prostate cancer

1.1.1 Prostate cancer in Finland

Prostate cancer (PrCa) is the most commonly diagnosed cancer in adult men in Finland. With an average of about 5000 new cases diagnosed each year (2015-2017), PrCa accounts for 30% of all cancer diagnoses and it is the second most lethal cancer in males after lung cancer (Pitkäniemi et al., 2018). Age is a major risk factor for PrCa, and the current trend of increasingly ageing population means that the disease burden posed by PrCa on the Finnish society may be expected to further increase. It is estimated that the incidence of new PrCa cases will rise by more than 20% to 6600 new cases diagnosed per year by 2035 (Pitkäniemi et al., 2018).

The prognosis for PrCa has improved over the past decade, and the current 5-year survival rate for localised PrCa is good (94%) (Duodecim, 2014), Although most of the early-stage PrCas detected are curable, a notable segment of patients will experience disease progression with biochemical recurrence, defined usually as recurrence of increased prostate-specific antigen (PSA) levels (Hackman et al., 2019). In a Finnish trial evaluating the potential benefits of adjuvant radiotherapy after radical prostatectomy, 18% of the patients receiving adjuvant radiotherapy and 39% of those who did not, experienced biochemical recurrence of PrCa within 10 years of the surgery (Hackman et al., 2019).

For the 23% of patients initially diagnosed with locally advanced or metastatic PrCa, the 5-year survival rate is significantly poorer at 33% and the average life expectancy is only 2-3 years (Duodecim, 2014), indicating poor efficacy of currently available treatment options for advanced forms of PrCa. Treatment resistance acquired by the tumor cells is a problem especially with castration-based treatment approaches intended to inhibit androgen signalling to the tumor. Castration resistant prostate cancer (CRPC) is defined as progression of tumor growth even when the amount of testosterone in the serum is below castration level (Duodecim, 2014). While little current statistics exist regarding Finnish CRPC patients, the global estimates range from 20% of patients developing CRPC within 5 years of androgen deprivation therapy (ADT) to 28% developing

CRPC within 10 years (Kirby et al., 2011; Hirst et al., 2012). Most patients (86%) diagnosed with CRPC already have metastases at the time of diagnosis, and third of the patients initially diagnosed with non-metastatic CRPC may expect to develop tumors within two years of diagnosis (Kirby et al., 2011). The prognosis for CRPC patients is poor, with the median survival being14 months from CRPC diagnosis (Kirby et al., 2011; Hirst et al., 2012).

1.1.2 Current options for PrCa treatment

The choice of treatment for PrCa depends on the metastatic state of the tumor and the responsiveness to ADT. Non-metastasized, local tumors may be treated curatively by radical prostatectomy, and/or radiation therapy, and the prognosis for this type of cancer is good (Duodecim, 2014). However, within 10 years, 20–40% of patients will experience biochemical recurrence of the disease progression (Hackman et al., 2019).

For those patients who experience biochemical relapse after radical prostatectomy and/or radiation therapy, and patients initially diagnosed with metastatic PrCa, ADT is the first line of treatment recommended by both Finnish Current Care Guidelines and by the expert consensus of Advanced Prostate Cancer Consensus Conference 2017 (Duodecim, 2014; Gillessen et al., 2018). Androgens are known to promote growth of PrCa cells, and the aim of ADT is to slow down the growth and proliferation of the cancer cells by depriving the cancer of these hormones (Tammela, 2012). Suppression of the production of androgens can be achieved by blocking the function of the testes through castration. This may be achieved for example through surgical removal of the testes, however medical castration using drugs that lower the amount of testosterone made by the testicles is often preferred. Luteinizing hormone-releasing hormone (LHRH) agonists work by mimicking the hormones necessary for testosterone production and activating the body’s own negative feedback loop, drastically reducing the amount of testosterone produced in the body (Tammela, 2012). Alternatively, LHRH antagonists may be employed, with the advantage of avoiding the initial surge in testosterone production activated by LHRH agonists (Tammela, 2012). For patients diagnosed with an aggressively metastatic disease, addition of chemotherapy along with the hormonal therapy is

considered, and the preferred chemotherapeutic agent is docetaxel (Gillessen et al., 2018).

However, the response to ADT varies, and estimated 15% of men with metastatic disease primarily fail to respond to ADT, resulting in early treatment failure, defined as death within 12 months of ADT initiation (Varenhorst et al., 2016). Additionally, many PrCas become resistant to hormone treatment over long-term treatment (Kirby et al., 2011; Hirst et al., 2012).

For metastatic CRPC, the recommended first-line treatment approach is using antiandrogens, with the addition of docetaxel if the patient is symptomatic. Antiandrogen therapy utilizes androgen antagonists that block androgens from binding to their respective receptors by occupying androgen receptors (AR) themselves (e.g. enzalutamide, darolutamide), or androgen synthesis inhibitors to reduce the amount of androgens produced in the body (e.g. abiraterone). For those patients that have acquired resistance to antiandrogens, treatment with a taxane is the preferred first line approach, with docetaxel being the primary option, whereas if the patient has received docetaxel as part of the first-line treatment, abiraterone or enzalutamide are preferred as second-line treatment. Cabacitaxel or platinum compounds are only recommended as final treatment options for those patients who have already received docetaxel and/or abiraterone or enzalutamide during the first- and second-line treatment. (Gillessen et al., 2018)

Until recently, there has been no treatment options available specifically for the minority of CRPC patients with non-metastatic disease, and as such these patients would continue to receive ADT, either alone or possibly with added alternative hormonal therapies. However, treatment of non-metastatic CRPC has increasingly gained attention and research efforts in hopes of delaying disease progression to metastatic state. Today, three drugs exist that have been approved by The United States Food and Drug Administration (FDA) for non-metastatic CRPC specifically: apalutamide in 2018 (FDA, 2018a), enzalutamide, first approved for metastatic CRPC in 2012, with non-metastatic CRPC indication added in 2018 (FDA, 2012; FDA, 2018b), and the most recent addition, darolutamide in 2019 (FDA, 2019). All three have also received European Medicines Agency (EMA) authorization for use in the European Union for the

indication of non-metastatic CRPC (EMA, 2018; EMA,2019 ; EMA, 2020). These novel drugs are so called second-generation AR antagonists, and work similarly to traditional AR agonists, in that they inhibit androgen binding to AR receptors. The main improvements of second-generation AR antagonists include increased specificity to AR over steroidal receptors as well as a higher affinity to the AR receptors. As these novel drugs are almost exclusively antagonistic to AR, they do not induce androgen withdrawal syndrome in the case of treatment discontinuation (Rice et al., 2019). Benefits of darolutamide specifically include higher AR inhibition potency as compared to enzalutamide and apalutamide with less risk of central nervous system related side effects due to minimal blood-brain barrier penetration (Bastos and Antonarakis, 2019). Additionally, unlike enzalutamide and apalutamide, darolutamide does not activate mutant AR related to promiscuous AR activation (Bastos and Antonarakis, 2019).

1.1.3 Unmet medical need for targeted therapies

While progress has been made in the treatment of PrCa and specifically non-metastatic CRPC, the currently available treatment options for metastatic PrCA and CRPC remain insufficient. This is highlighted by the short life expectancy and poor overall survival of PrCa and CRPC patients with metastatic disease (Kirby et al., 2011; Hirst et al., 2012). Additionally, it is important to consider that as there is currently no cure for advanced PrCa, even the patients with a manageable form of the disease will require medical treatment for the rest of their lives. This subjects them to long-term treatment-related morbidities. Side-effects of PrCa therapies, especially chemotherapeutics, may be severe. With targeted delivery of anticancer therapeutics directly into the tumor cells, the therapeutic potential of the drugs could potentially be achieved without simultaneous induction of unwanted effects on healthy cells. This would allow for effective treatment options to be employed earlier on in treatment without as much concern for side-effects and likely increase the chances of achieving better treatment responses (Senapati et al., 2018).

1.1.4 Immortalized cell lines as *in vitro* models of PrCa

In vitro cell cultures of immortalized cell lines are a stable of biomedical research, due to their ability to be genetically modified to elucidate specific cellular mechanisms of diseases, as well as their cost-effectiveness. Numerous

immortalized cell lines have been established as *in vitro* models of PrCa, with each modeling different stages of the disease and exhibiting specific characteristics regarding AR expression and androgen responsiveness (Sampson et al., 2013). The first cell lines to be established for this disease, and still among the most commonly used PrCa cell lines are LNCaP (Horoszewicz et al., 1980)PC3 (Kaighn et al.,1979) and DU145 (Stone et al.,1978), whereas normal prostate epithelial cell lines PWR-1E (Webber et al., 1996), RWPE1 (Bello et al., 1997) and PNT2 (Berthon et al., 1995) are usually used as a normal prostate control for the disease model (Sampson et al., 2013).

For this thesis, 22Rv1 was chosen as the PrCa model. This cell line was established in 1999 by Sramkoski et al., through propagating a relapsed strain of an androgen-dependent parental xenograft in castrated mice. This parental xenograft was derived from a primary prostatic carcinoma from a patient with bone metastases. 22Rv1 therefore models primary, castration relapsed PrCa (Sramkoski et al., 1999). The cell line expresses AR receptors and is androgen responsive but not dependent on androgens for growth and compared to the androgen dependent LNCaPs the 22Rv1 cells express less AR (Sampson et al., 2013). Additionally, 22Rv1 has unique AR composition. Several alternatively spliced AR variants have been found to be expressed in 22Rv1 cells, for example a full-length AR with a mutation of lacking duplicated exon 3 and two truncated versions lacking the COOH terminal domain have been identified (Dehm et al., 2008; Marcias et al., 2010).These AR isoforms are functionally active, and the truncated isoforms specifically have been shown to be able to induce expression of many endogenous AR target genes, as well as the ligand independent growth of 22Rv1 cells in the absence of androgens. The existence of these truncated isotopes has been hypothesized to be the cause for the androgen-refractory phenotype of 22Rv1 (Dehm et al., 2008; Marcias et al., 2010) This unique AR composition allows for 22Rv1 to be utilized in studying AR function, as well as in screening of both existing and putative drugs for their anti-AR efficacy (Sampson et al., 2013). 22Rv1 cell line was chosen for this thesis due to its unique properties and relevance in PrCa research, as well as its relative underrepresentation in current PrCa research as compared to the more popular PC3 and LNCaP cell lines.

For the normal prostate control in this thesis, RWPE-1 was chosen. RWPE-1 is a commonly used model of benign prostate epithelial cells mainly employed as a control for carcinogenic cell lines when investigating drug efficacy or gene expression (Sampson et al., 2013). The RWPE-1 cell line was immortalized in 1997 by Bello et al. from human prostatic epithelial cells donated by a healthy male, using human papilloma virus 18. The cell line is androgen responsive, and expresses AR as well as PSA, however it is non-tumorigenic and does not form tumors when injected into immunocompromised mice (Bello et al., 1997). This allows for RWPE-1 to be used also in the screening of potential oncogenes or carcinogens, and as a model to investigate tumorigenesis and oncogenic transformation (Sampson et al., 2013).

1.2. Extracellular vesicles are messengers of cell signaling

Extracellular vesicles (EVs) are nano-sized cell membrane derived structures surrounded by a lipid bilayer. Such vesicles are secreted into the extracellular space and biofluids by all types of cells. What originally was thought as simply a mean of cellular waste excretion, has been since realized to be an important mechanism of intracellular communication (Van Niel et al., 2018). Today, EV mediated cell signaling has increasingly gained the attention of the scientific community for its continuously emerging roles in various physiological and pathological processes.

1.2.1 Classification and biogenesis

EVs are a highly heterogenous group of vesicles; within any population of EVs, diverse subpopulations of vesicles differing in size, morphology or composition may be found (Van Niel et al., 2018). This heterogeneity and lack of exact nomenclature and classification continue to propose challenges for characterizing specific properties and functions of EV subpopulations. Currently, the vesicles are commonly classified into two main categories based on the method of biogenesis; exosomes are typically smaller, 30-100 nm in diameter, and originate from the endosomal system. First, the EV precursors, titled intraluminal vesicles are formed by the inward budding of the outer membrane of multivesicular endosomes, and when the multivesicular endosomes fuse with the

plasma membrane releasing their contents, these vesicles are termed exosomes (Kowal et al., 2014). This biogenesis pathway has been found to be regulated mainly, although not solely, by the endosomal sorting complexes required for transport (ESCRT), as silencing genes of selected ESCRT components was found to affect EV production (Colombo et al., 2013). Microvesicles are typically larger structures of 50-1000 nm in diameter, and they are formed via outward budding of the cell's plasma membrane. When discussing microvesicles originating from cancer cells, the term oncosomes is often used (Van Niel et al., 2018).

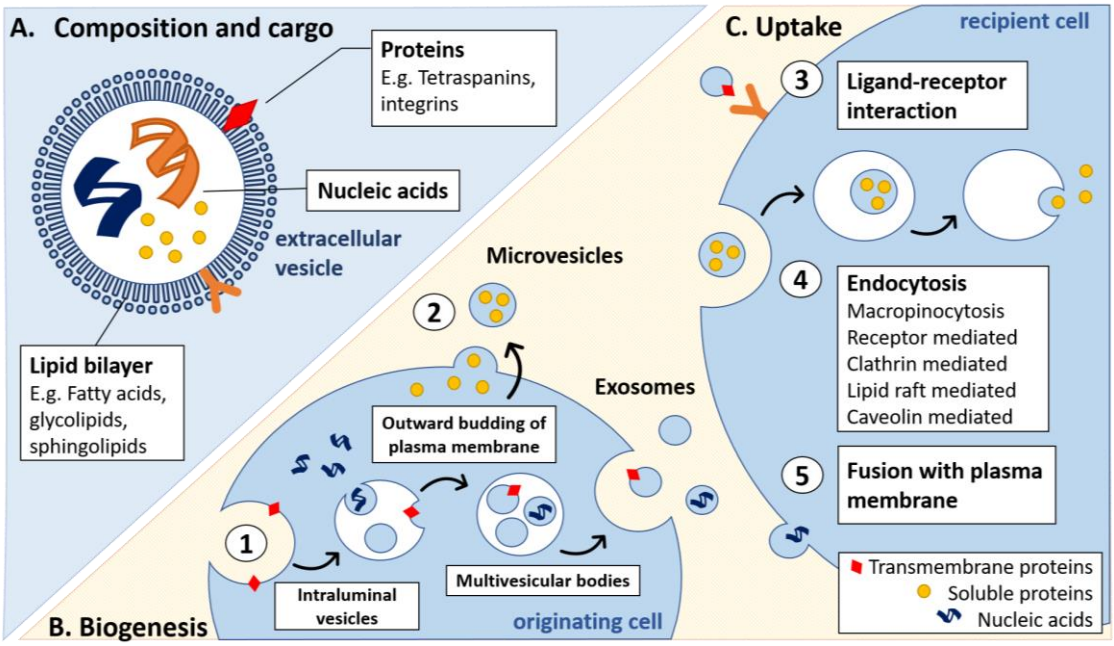

Figure 1 EV composition, biogenesis and uptake. A) EVs are nano-sized vesicles surrounded by a lipid bilayer, with transmembrane proteins embedded in the lipid bilayer. The lumen of EVs may contain many types of water-soluble cargo, including cytosolic proteins and nucleic acids. B) Exosomes originate via the endosomal pathway (1) intraluminal vesicles are formed by the inward budding of the outer membrane of multivesicular endosomes and are then released as exosomes as the multivesicular endosome fuses with the plasma membrane of the cell. Microvesicles originate from the outward budding of the cell plasma membrane (2). C) EV uptake by the recipient cells may happen via multiple mechanisms, including (3) receptor mediated interaction of the EV and recipient cell, (4) different forms of endocytosis, and (5) direct fusion with the plasma membrane.

While this exosome and microvesicle nomenclature remains popular in EV publications, it is however not recommended by International Society for Extracellular Vesicles (ISEV), as the method of biogenesis is difficult to determine from the extracted EV sample. Rather, classification by size into small, medium and large extracellular vesicle is encouraged (Théry et al., 2018). This classification is deemed more fitting also because the methods that are commonly employed with the purpose of separating EV subpopulations are

commonly ones based on the size or the density of the particles (eg. differential centrifugation, size exclusion chromatography (SEC), density gradients). According to ISEV, as sizes of exosomes and microvesicles overlap, this method of separation is insufficient for classifying the resultant EVs strictly as exosomes or microvesicles and thus methods to identify the biogenetic origin of the vesicles should be used if nomenclature specific to the vesicles secretion mechanisms is to be used. In this thesis, the umbrella term EVs will be used.

1.2.2 Cargo and molecular composition

The type and quantity of EV composition and cargo has been found to be specific to the secreting cell type, and it is influenced by the physiological or pathological condition of the cell; each cell type adapts EV biogenesis depending on its physiological state and releases EVs with distinct lipid, protein and nucleic acid compositions (Van Niel et al., 2018). EVs consist of a lipid bilayer originating from the plasma membrane, and the EV membrane is enriched in common plasma membrane lipids. Recently, this lipid composition of EVs was shown to be cell type dependent; Brzozowski et al., (2018a) evaluated the lipid composition of PrCa and normal prostate cell derived EVs and found that fatty acids, glycerolipids and prenol lipids were enriched in EVs from benign prostate cells, while EVs from PrCa cells were more abundant in sterol lipids, sphingolipids and glycerophospholipids. Hosseini-Beheshti et al., (2012) reported that EVs derived from PrCa cell lines contained significantly more cholesterol as compared to the benign RWPE-1 cell line. Differences between lipid compositions of EV subtypes separated by size have also been detected with small, exosome sized EVs being more enriched in glycolipids, free fatty acids and phosphatidylserine, whereas larger, microvesicle sized EVs were characterised by their abundance in ceramides and sphingomyelins (Haraszti et al., 2016).

The lipid membrane limits a small lumen containing proteins and metabolites from the secreting cell's cytosol. Additionally, transmembrane proteins are embedded in the lipid bilayer. The protein component of EVs consists of a specific subset of cellular proteins derived both from the plasma membrane and the cytosol. Additionally, vesicles formed via the exosome biogenesis pathway contain proteins from endosomes (Kowal et al., 2014). Evidence points to both the protein and lipid components being actively sorted into EVs during their biogenesis, rather than only spontaneously being tagged along from the secreting cells.

Hosseini-Beheshti et al., (2012) described enrichment of sphingolipids and glycosphingolipid in EVs, as EVs had higher content of these lipids compared to their PrCa and normal prostate parent cells. A comprehensive proteomic and lipidomic analysis of EVs revealed that the enrichment of specific proteins and lipids was cell type specific, however the EV proteome was more effective than the lipidome at distinguishing EVs secreted from different cell types (Haraszti et al., 2016)

Proteins commonly attributed as EV biomarkers include predominantly ones related to the lipid-bilayer structure of EVs, for example tetraspanins and integrins, proteins that bind to plasma membranes or to transmembrane proteins, such as flotillins, caveolins and heat shock proteins, and proteins associated with EV biogenesis, for example proteins related to the ESCRT pathway such as tumor susceptibility gene 101 (TSG101) and ALIX (Théry et al., 2018). A large proteomic study including EVs from 60 different cancer cell lines investigated the enrichment of the proteins traditionally thought of as universal EV biomarkers in cancer derived EVs. Out of 6000+ proteins analyzed, 213 were found to be expressed in all cancer EVs regardless of the tissue of origin, including cluster of differentiation (CD) 81, ALIX, and heat shock cognate 71 kDa protein. Most of these conserved EV proteins were found to be functionally linked to the EV biogenesis pathways. TSG101, syntenin-1, flotillin-1 and tetraspanins CD63 and CD9 were found to be present in two-thirds of the samples. However, the expression of some proteins previously thought of as universal EV markers, such as matrix metalloproteinase (MMP) -2 was found to be inconsistent and that expression of these proteins was dependent on their cellular origin rather than being constitutive in all vesicles. (Hurwitz et al., 2016)

In studies investigating proteins enriched in PrCa cell line derived EVs specifically, tetraspanins CD9 and CD81 were highly enriched in EVs from all the studied PrCa cell lines (Yoshioka et al., 2013). Other common EV proteins TSG101 and CD63 were also present in all PrCa EV samples, however the degree of enrichment of these proteins varied depending on their cancer cell line of origin. Another study found that all PrCa and benign prostate EV samples contained heat shock protein (HSP) 70, HSP90 and CD9, and that HSP90 which is a cellular stress marker often associated with cancer, was less abundant in benign RWPE-1 EVs than in cancer EVs (Hosseini-Beheshti et al., 2012). They

further identified 220 biomarker candidates specific to EVs of PrCa origin as opposed to normal prostate origin, including several which had been previously been suggested as biomarkers for PrCa diagnosis (e.g. annexin A2 and calsyntenin 1), and detected markers specific to AR negative (endoplasmin and annexin A2-like protein) and AR positive (e.g. trichoplein keratin filament-binding protein) PrCa cell lines only.

1.2.3 EV uptake

EVs are capable of transferring their cargo between cells and eliciting changes in the receiving cell's phenotype. As EVs are excreted into the extracellular space, they are able to enter the bloodstream, thus EV-mediated cargo transfer is possible both between long distances in the body as well as in an autocrine manner. EVs are targeted towards specific cell types based on the specific set of proteins enriched at their surface, which allow the vesicles to interact with the plasma membrane of the recipient cells. Known factors that mediate EVs cell-specific targeting include tetraspanins, integrins, leptins and heparan sulfate proteoglycans as well as certain lipids and components of the extracellular matrix (Van Niel et al., 2018).

Although the detailed mechanisms of EV uptake remain to be elucidated, it is known that there are a multitude of pathways through which an EV may be internalized by the receiving cells. The vesicles may be directly fused into the plasma membrane of the cell, or be taken up via different types of endocytosis, including phagocytosis, macropinocytosis, receptor mediated endocytosis and lipid rafts (Van Niel et al., 2018). In some cases, EVs need not to be internalized at all and instead will exert their effects by binding to receptors on the receiving cell's plasma membrane, activating downstream signaling cascades.

The preferred method of uptake is thought to be influenced by the specific compositions of the EV membrane and the receiving cell's plasma membrane as well as the size of the vesicles. For instance, clathrin-independent endocytosis and macropinocytosis have been reported as the predominant methods for EV uptake in human epidermoid and cervical carcinoma cell lines (Costa Verdera et al., 2017), whereas clathrin-dependent endocytosis was found to be more prominent in a study using PrCa cell lines (Tian et al.,2014). Saari et al. (2018) demonstrated that EV size affects their method of internalization. Studying the

utility of paclitaxel loaded PrCa derived EVs as drug carriers, they found that larger, microvesicles sized EVs entered the cells by both endocytosis and fusion with cell membrane, whereas the primary uptake pathway for smaller, exosome -sized vesicles was via endocytosis.

1.3 Role of EVs in PrCa development and progression

The hallmarks of cancer are a collection of properties deemed necessary for a cell to acquire to become malignant. Originally proposed by Hanahan and Weinberg in 2000, these hallmarks comprise of six key characteristics of a tumor cell: the ability to sustaining proliferative signaling, evade growth suppressors, resistance of cell death, replicative immortality, ability to induce angiogenesis, and activate invasion and metastasis. The authors updated this landmark article in 2011 by adding two emerging hallmarks, ability to avoid immune destruction and deregulation of cellular energetics, as well as two enabling characteristics, tumor-promoting inflammation and genome instability and mutation (Hanahan and Weinberg, 2011). EVs have been found to play crucial roles in the acquisition and development in these properties by cells, and therefore they seem to be pivotal in the development of cancer. Analysis of cancer cell derived EVs has shown the vesicles carry many cancer-enhancing signals; they are able to induce changes in the metabolism of tumor and tumor stomal cells, to suppress immune response, promote neoangiogenesis, and prep the tumor microenvironment to be hospitable to the cancer (Vlaeminck-Guillem et al., 2018).

1.3.1 EVs promote tumor cell growth and proliferation

Normal cells do not continue to proliferate in the absence of growth signaling, hence the hallmarks of cancer include self-sustaining of growth signaling as well as evasion of apoptotic signals (Hanahan and Weinberg 2011). Cancer cells acquire the capability to continue multiplying even in the absence of these signals, either by upregulating the amounts of certain receptors, alteration of extracellular growth signals or by initiation of autocrine proliferative signaling (Hanahan and Weinberg 2011). EVs are capable of transporting RNA and proteins that promote tumor cell growth and proliferation; Hosseini-Beheshti et al. (2016) investigated the effects of EVs derived from PrCa cell lines with different AR phenotypes were able to significantly reduce apoptosis, increase cancer cell

proliferation and promote cell migration in LNCaP and RWPE-1 cells, independently of the AR phenotype of the originating cells. Additionally, intravenous administration of DU145 EVs into xenografted mice showed that these EVs were able to increase both the tumor volume and the serum PSA levels *in vivo* (Hosseini-Beheshti et al., 2016*).* Soekmadji et al. (2016) elucidated some of the possible mechanisms behind this EV function by proposing that CD9 positive EVs are capable of modulating paracrine signalling, and therefore capable of promoting tumor growth and proliferation. They found that dihydrotestosterone treatment increased the secretion of CD9 positive EVs, and that treatment of cancer cells using EVs enriched in CD9 after dihydrotestosterone exposure was able to promote proliferation in androgen-deprived conditions. CD9 was suggested as a possible upstream regulator of AR, due to the finding that CD9 knockdown in LNCaP cells decreased expression of AR and PSA, as well as proliferation of the cells, but that knockdown of AR had no effect on CD9 expression (Soekmadji et al., 2016). Similar results were obtained using PC3 and LNCaP cells by Lázaro-Ibáñez et al. (2017); EVs from metastatic PC3 cells were capable of significantly increasing proliferation and migration of both cancer and benign PNT2 cells, whereas EVs derived from LNCaP cells increased proliferation of PNT2 but not PC3. EVs from PC3, LNCaP and primary PrCa cell line RC92a/hTERT were all able to induce increased migration of PC3 cells.

1.3.2 EVs promote tumor invasiveness and prepare the metastatic niche

Activation of invasion and metastasis is one of the original hallmarks of cancer (Hanahan and Weinberg, 2011).EVs originating from PrCa cell lines have been shown to promote cell migration on several occasions (Hosseini-Beheshti et al., 2016; Lázaro-Ibáñez et al., 2017). Brzozowski et al. (2018b) showed that the addition of EVs derived from modified RWPE1 cell lines with altered tetraspanin CD9 and CD51 expression to naïve RWPE1 cells induced a migratory and invasive phenotype in the originally non-malignant cell line. Some of the mechanisms behind the importance of EV mediated signaling in tumor cell migration were illustrated by Sung et al. (2015), as they showed autocrine EV secretion of fibrosarcoma tumor cells to be necessary for directionally persistent and effective cell migration due to the EV's role in promoting focal adhesion assembly and stabilizing of leading-edge protrusions.

EVs have also been hypothesized to be a key factor in a so-called seed-and-soil theory of metastasis; the idea first proposed by Stephen Paget in 1889 that circulating cancer cells seeding from the primary tumor prefer the microenvironment of certain organs over others (Paget, 1889) This theory arose from the observation that certain types of cancers tend to metastasize into distinct areas in the body, for example, PrCa is known to primarily metastasize in the bone. More recently, it has been suggested that tumor cells may also able to remotely prime these target sites to be more receptive to the tumor cells prior to metastasis (Langley and Fidler, 2011). Since EVs are able to circulate into any part of the body via bloodstream, it has been suggested that they would be involved in this phenomenon by carrying signals to prime the target sites for cancer cell invasion. This hypothesis is backed by studies showing that tumor derived EVs 1) are selectively biodistributed into tissues matching the organotropic distribution of the originating cancer cell line (Hoshino et al., 2015), 2) increase vascular permeability, potentially enabling the extravasation of cancer cells into new sites (Peinado et al., 2012) and 3) are able to condition the microenvironment of the premetastatic site to be more favorable for tumor cell growth via interactions with specific cell types (Hoshino et al., 2015; Peinado et al., 2012; Probert et al., 2018; Dai et al., 2019).

PrCa derived exosomes have been shown to be able to promote bone metastasis both *in vitro* and *in vivo*; Probert et al. (2018) reported that treatment with PC3 derived EVs significantly increased osteoblast viability and resulted in a supportive growth environment for subsequently cocultured PC3 cells. They further demonstrated the importance of tumor derived EV RNA cargo by showing that the transfer of RNA from PrCa cells to recipient osteoblasts via EVs was able to elicit the observed functional changes in osteoblast behavior. Dai et al. (2019) utilized EVs derived from metastatic PrCa cell lines PC3 and C4-2B to pretreat mice prior to inoculation of PrCa cells, and found that this pretreatment resulted in an increase in the number of metastatic sites and the total tumor burden compared with vehicle with both cell lines. The same pro-metastatic effect was obtained using EVs from serum of men with primary PrCa tumors but not with EVs obtained from healthy men. They further elucidated the pathway behind this effect and identified the EV mediated transfer of PrCa derived pyruvate kinase M2 (PKM2) protein in bone marrow cells and the subsequent upregulation of

stromal cell-derived factor 1 production in the target cells to be key mechanisms in supporting PrCa growth in the bone marrow, and demonstrated the clinical relevance of EV associated PKM2 by showing PKM2 expression in PrCa patient's serum EVs was associated with metastasis. These results implicate potential for EV PKM2 as a diagnostic marker of PrCa metastasis, but also as a potential drug target; consequently, it was demonstrated that inhibition of the stromal cell-derived factor 1 receptor decreased the ability of PKM2 EVs to induce bone metastasis (Dai et al., 2018).

1.3.1 EVs mediate signaling between the tumor and stromal cells

The tumor microenvironment (TME) is a complex and highly dynamic environment consisting not only of cancerous cells, but also other resident cells, including fibroblasts, endothelial cells, adipocytes and immune cells (Shiao et al., 2018). Cancer cells are capable of modulating this local environment and inducing a more tumor-favorable phenotype in the surrounding cells, and favorable tumor stroma is crucial in driving a more aggressive disease phenotype. EV mediated signaling has been proven to be an important mechanism in driving stromal differentiation to a tumor-promoting phenotype (Vlaeminck-Guillem, 2018).

One of the ways through which PrCa cells modify their microenvironment is by inducing transformation of stromal fibroblasts into cancer-associated fibroblasts. EVs present in the cancer cell secretome have been shown to be crucial factors driving this phenotype. Webber et al. (2015) found that EVs secreted from PrCa cell lines carry transforming growth factor beta 1 (TGFβ1), and these EVs were able to induce transformation of fibroblasts into myofibroblasts when fibroblasts were treated with PrCa cell conditioned, EV containing media. These myofibroblasts exhibited a pro-angiogenic and tumor growth -promoting phenotype distinct from that achieved by treatment with soluble TGFβ1. Furthermore, when EVs were eliminated from the conditioned media by centrifugation, this transformation was also abolished.

Additionally, EVs have been shown to have a similar effect on the differentiation of bone-marrow mesenchymal stem cells (BM-MSCs) (Chowdhury et al., 2015). Treatment of BM-MSCs with PrCa EVs induced the cells differentiation to lean towards alpha-smooth muscle actin positive myofibroblastic cells. The resulting

myofibroblasts were found to secrete high levels of vascular endothelial growth factor (VEGF), hepatocyte growth factor and matrix regulating factors like MMP-1, -3 and -13, they exhibited pro-angiogenic functions and were able to enhance tumor proliferation and invasiveness. As with the transformation of stromal fibroblast to cancer-associated fibroblasts, this observed BM-MSC differentiation to myofibroblasts was deemed dependent specifically on EV TGFβ1. Soluble TGFβ1 at matched dose did not generate a similarly tumor-promoting phenotype (Chowdhury et al., 2015). These findings indicate that EVs are key modulators of stroma in PrCa.

1.3.4 EVs promote angiogenesis

Tumor angiogenesis is pivotal for tumor survival and growth, and as such presents an important anticancer therapeutic target. Cancer cell derived EVS have been found to promote blood vessel formation within the tumor tissue by transporting pro-angiogenic cargo such as growth factors or MMPs, or by activating signaling cascades involved in angiogenesis (Aslan et al., 2019). VEGF is one of the best recognized mediators of angiogenesis. At least two distinct forms of tumor derived EV-associated VEGF have been found; a 189 amino acid isoform termed VEGF189 was determined to be bound to transmembrane heparin of small EVs derived from various cancer cell lines (Ko et al., 2019) and a ~90 kDa crosslinked form of VEGF termed VEGF90K was found to be associated to the surface of breast cancer cell line derived, microvesicle -sized EVs via HSP90 (Feng et al., 2017). Both of these EV-associated isoforms of VEGF were shown to 1) be insensitive to VEGF inhibitor bevacizumab and 2) able promote angiogenesis independently of soluble VEGF, therefore potentially enabling tumor treatment resistance by providing an additional mechanism for cancer cells to maintain angiogenic signaling even in the presence of antiangiogenic therapeutics targeting soluble VEGF. Subsequently, Feng et al. (2017) showed that by combining VEGF inhibitor Bevacizumab with an EV biogenesis inhibitor 17AAG the tumor growth inhibitory and antiangiogenic effect was significantly increased. These findings suggest that cancer derived EVs have a crucial role in promoting tumor angiogenesis and should therefore considered as additional targets of antiangiogenic therapies.

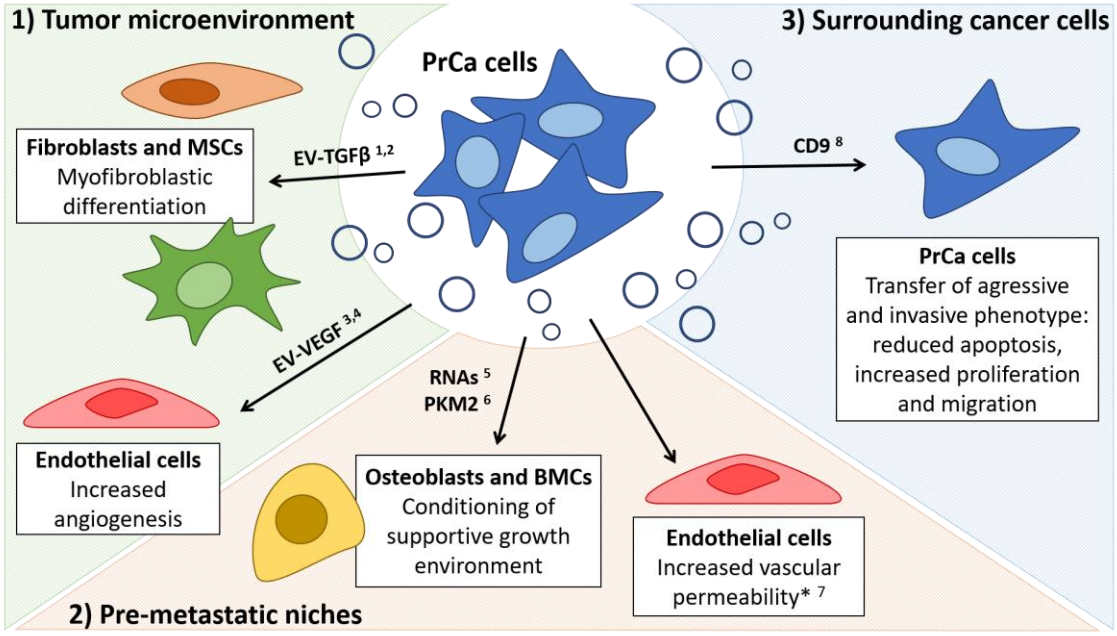

Figure 2. Functions of EVs in PrCa. EVs derived from PrCa cells have many functions in promoting prostate cancer survival, invasiveness, and metastasis. 1) EVs help promote a favourable TME. EV associated TGFβ1 induces myofibroblastic differentiation of fibroblasts and mesenchymal stem cells, inducing a pro-tumor phenotype ([1]Webber et al., 2015; [2]Chowdhury et al., 2015). EVs induce angiogenesis via EV associated VEGF signaling with vascular endothelial cells ([3]Feng et al., 2017; [4]Ko et al., 2019). 2) EVs prepare metastatic niches. EVs can travel to distant sites in the body via circulation and increase the permeability of blood vessels, allowing for extravasation of circulating tumor cells ([7]*Peinado et al., 2012). EVs condition osteoblasts and BMCs to create a favorable growth environment for metastasizing cancer cells ([5]Probert et al., 2018; [6]Dai et al., 2019). 3) EVs mediate signaling between cancer cells and transfer pro-survival traits from cells with a more aggressive and invasive phenotype to others, with EV associated CD9 identified as one potential mediator ([8]Soekmadji et al., 2016). *this function was reported on melanoma EVs but could be a function of other tumor derived EVs as well.

1.4 Hypoxia, a common feature of tumor microenvironment

Hypoxia is a common feature of the TME, specifically in the case of solid tumors and it is acknowledged to be a key element of the TME involved in tumor aggressiveness and metastasis (Petrova et al., 2018). Tumor hypoxia is a dynamic and heterogeneous with the oxygen levels within a tumor varying both temporally and regionally, thus it is common to find areas of varying oxygen levels within the same tumor, with hypoxic regions surrounded by normal oxygen level tissue (Saxena and Jolly, 2019).

Cellular hypoxia may be divided into three categories based on the origin and duration of oxygen deprivation, and these different types of hypoxia have distinct effects (Saxena and Jolly, 2019). Chronic hypoxia is characterized by extended periods of limited oxygen diffusion to the tumor tissue, caused by increasing

oxygen demand from rapidly proliferating cancer cells and lack of proper vasculature within the tumor mass. In acute hypoxia, also described as perfusion limited hypoxia, cells experience rapid episodes of hypoxia and reoxygenation caused by irregular flow of oxygen into the tumor tissue. This is due to the tumor induced angiogenesis often leading to structurally aberrant blood vessels with inefficient blood perfusion. Cyclic hypoxia is defined as the tumor cells experiencing intermittent hypoxic periods of varying duration, due to transient cessations in blood flow in the tumor vasculature. (Saxena and Jolly, 2019)

The best recognized mediators of the cellular effects of hypoxia are hypoxia inducible factors (HIF) 1 and 2, the induction of which depends on the duration of the low oxygen level conditions (Schöning et al., 2017). HIFs are heterodimeric transcription factors, consisting of a constitutively expressed β-subunit and an O2-regulated α-subunit. Under normoxic conditions, the α-subunits undergo rapid degradation via hydroxylation by prolyl hydroxylases or factor inhibiting HIF (FIH-1). In hypoxic conditions, beginning at approximately at below 5% oxygen conditions, prolyl hydroxylases and FIH-1 are inactivated, leading to the formation of HIF-α and HIF-β-complex and the subsequent induction of the transcription of HIF inducible genes, which include but are not limited to genes involved in the glycolysis pathway as well as stem cell regulating genes (Schöning et al., 2017).

Tumor hypoxia is a clinical predictor of poorer treatment outcomes. In an extensive clinical study by Milosevic et al. (2012), low partial pressure of oxygen within PrCa tumors was found to correlate with early biochemical relapse and with local recurrence after radiotherapy alone, or radiotherapy in combination with hormonal therapy. In a separate retrospective analysis of two randomized radiotherapy trials and one surgical cohort study, increased staining of HIF-1α as well as VEGF were both significant predictors of biochemical failure after radiotherapy or surgery (Vergis et al., 2008).

1.4.1 Hypoxia selects for more aggressive cancer subtypes and contributes to drug resistance

Hypoxia has been found to increase cancer cell motility as well as angiogenesis, and a high number of hypoxic cells in a tumor is associated with increased malignancy and metastasis potential (Zonneveld et al. 2019). This is due to the positive selection for cells exhibiting increased resistance to the apoptosis

pathways activated by hypoxia within the tumor. This acquired resistance to apoptosis within the tumor makes the cancer less susceptible to drug treatment and more aggressive. Butterworth et al. (2008) demonstrated the effect of hypoxia has on promoting tumorigenic properties by creating a hypoxia-induced subline of LNCaP PrCa cell line through exposure of the parental cell line to weekly cycles of severe 0.1% O2 hypoxia. The resulting subline, termed LNCaP-H1, showed significant hypoxia tolerance and resistance to mitochondria-mediated apoptosis. Though the parental cell line is androgen-dependent, LNCaP-H1 exhibited androgen independent growth both *in vitro* and *in vivo*. Additionally, these cells exhibited an altered genetic profile which made them more prone to metastasis in an *in vitro* invasion assay, as well as an *in vivo* metastasis study (Butterworth et al., 2008).

Besides exacerbating tumor growth and metastatic potential via selection for more aggressive cancer phenotype, hypoxia is also a major cause of treatment resistance. While the exact pathways behind hypoxia induced resistance remain unclear, several potential mechanisms contributing to it have been proposed, as summarized by Wilson and Hay (2011): hypoxia is usually associated with poor vasculature of the tumor, which translates to decreased distribution of circulating drugs into the tumor. Tumor cells adapt to hypoxia by reverting to glycolytic metabolism, which contributes to the acidification of the TME and may interfere with the function of certain anticancer therapeutics. Furthermore, hypoxia slows down the rate of cell proliferation and promotes a quiescent phenotype of cancer stem cells, an aggressive and poorly differentiated subtype of tumor cells, which renders the tumor less susceptible to therapies targeting rapidly proliferating cells (Schöning et al., 2017). It is worth noting that the effects of hypoxia in the drug response are dependent on the drug in question as well as the cell type, and in some cases, hypoxia may even increase chemosensitivity (Strese et al., 2013). While Strese et al. deemed docetaxel to work better under normoxic conditions in several other cancer cell lines, Forde et al (2012). found the docetaxel sensitivity of PrCa cells was not significantly decrease under hypoxia.

A study on ADT resistance reported that exposure to hypoxia induced adaptive androgen independence in originally androgen-dependent cell lines (Geng et al., 2018). LNCaP and LAPC4 cell lines acquired resistance to enzalutamide after repeated cycles of exposure to 1% hypoxia, while the same cell lines cultured in

normoxia remained sensitive to treatment. The molecular mechanism was identified to be mediated by activation of hypoxia-response genes, specifically glucose-6-phosphate isomerase. This gene is critical to cell survival under hypoxic stress, and it is normally attenuated by androgen signaling. Subsequently, the function of this gene and therefore cell adaptation and survival are restored by blocking androgen signaling during hypoxia. Furthermore, HIF-1α signaling has been found to promote proliferation PrCa cells independently of androgen signaling, providing a way for PrCa tumors to continue growing under hypoxia even when androgen signaling is blocked using ADT (Tran et al., 2020).

1.4.2 Exposure to hypoxia increases EV secretion from cells

The role of EV mediated signaling is amplified in cellular stress conditions, and hypoxia has been observed to have an effect of increasing EV production in several cell types (King et al., 2012; Zhang et al., 2017; Panigrahi et al., 2018). In a landmark article, King et al. found that EV secretion from several breast cancer cell lines increased significantly when cells were incubated under severe (0.1% O2) or moderate hypoxia (1% O2), as compared to normoxic conditions. Additionally, they found this increase likely to be HIF-1α mediated, as similar increase in EV production could be induced by treatment with dimethyloxallyl glycine, a pharmacological inducer of HIF (King et al. 2012). Accordingly, cells treated with HIF-1α targeting siRNA failed to show significant increase in EV release under hypoxia. Results supporting these findings were presented by Zhang et al. (2017), It was shown that that hypoxia increased exosome secretion from renal tubular cells in a time-dependent manner, and that this effect was lost in cells where HIF-1α induction was suppressed. In certain PrCa cell lines, EV secretion may increase up to 35.5 –fold under hypoxia as compared to normoxia (Panigrahi et al. 2018). Panigrahi et al. (2018) exposed several PrCa cell lines to moderate hypoxia (1% O2) and found that all PrCa cell lines tested exhibited a significant increase in EV production, with 22Rv1 specifically showing a dramatic change of 27.5 –fold between hypoxia and normoxia. In a recent study using pancreatic cancer cell lines, the hypoxia was found to increase release of small EVs specifically, shifting the size distribution of the secreted EV population towards smaller average size (Patton et al., 2019). Furthermore, small EVs specifically were determined to be important in promoting survival of hypoxic

cancer cells and both the altered EV release and EV mediated cell survival under hypoxia were linked to HIF-1α stabilization.

1.4.3 EVs promote cancer cell survival under hypoxia

Hypoxia-derived EVs (hEVs) have been shown to promote cell survival in low-oxygen conditions. hEVs were shown to have an inhibitory effect on apoptosis following ATP-depletion of hypoxia-naïve cells, an effect which could not be replicated in HIF-1α knockdown cells (Zhang et al. 2017). Additionally, hEVs secreted from hypoxic PrCa cells have been found to contain higher amounts of lactic acid than their normoxic counterparts, prompting the idea that hEVs may increase cell survival partly via eliminating metabolic waste accumulating under hypoxic conditions, which would otherwise induce cell death in severely hypoxic cells (Panigrahi et al. 2018).

The tumor-promoting effects of cancer derived EVs, including induction of angiogenesis and promotion of invasion and metastasis, are also prominent in hEVs. The hypoxia-induced aggressive phenotype may be transferred between cells via hEV signaling; Ramteke et al. (2015) found that co-culturing of hypoxia-naïve LNCaP and PC3 cells with hEVs increased their invasiveness and motility more efficiently than normoxic EVs. They further determined these hEVs contained increased amounts of specific signaling molecules and had a higher MMP activity than EVs secreted under hypoxia. Later it was also shown that treatment with hypoxic PrCa cell derived EVs was shown to promote MMP activity in possible metastatic sites, including lungs, liver and kidney in nude mice (Deep et al., 2020). This hEV mediated preparation of the metastatic sites is in accordance with the seed-and-soil theory discussed previously.

1.5 Potential applications of EVs in PrCa diagnostics and therapy

1.5.1 Biomarker potential of circulating tumor derived EVs

Liquid biopsy is a minimally invasive option for needle biopsies of tumor tissue as it is based on detecting circulating cancer biomarkers from biofluids such as blood, urine and seminal plasma (Pang et al., 2020). They avoid the complications associated with tissue biopsies and have the added benefit of providing a more comprehensive picture of the state of disease in the body. This

is because circulating biomarkers are homogeneously distributed in the biofluids, as opposed to tissue biomarkers which are heterogeneously localized within in the tumor tissue (Pang et al., 2020). As previously discussed, EVs are known to be excreted in all biofluids and to contain molecular cargo specific to the originating cells. This makes EVs and EV associated biomarkers of cancer promising targets for discovery of circulating biomarkers for liquid biopsy approaches.

Several methods have been approaches have been taken in the exploration of EVs for PrCa diagnostics; Pellegrini et al. (2017) analyzed RNA from urine EVs and determined them to be a viable source of RNA enriched with prostate-specific transcripts and that the levels of urinary PrCa biomarkers PCA3 and ERG, were significantly higher in the urine EVs of PrCa patients than those without PrCa, indicating that urinary EVs reflect the disease status and could be a source for future PrCa biomarker discovery. Puhka et al. (2017) utilized ultra-performance liquid chromatography-tandem mass spectrometry in a proof-of-concept study to profile over 100 small molecule metabolites in the urine and platelet EVs isolated from PrCa patients and healthy controls. Through normalization of the metabolomics data to EV quantity or ratio of metabolites, they identified glucuronate, D-ribose 5-phosphate and isobutyryl-L-carnitine as metabolites that were lower in pre-prostatectomy patient samples than post-prostatectomy and healthy control samples. It was suggested that this method of EV metabolomics analysis could be used for further EV biomarker detection for PrCa diagnostics Puhka et al. (2017). Analysis of EV molecular composition via vibrational spectroscopy methods has been employed for PrCa diagnosis as well (Krafft et al. 2017; Lee et al. 2018; Zlotogorski-Hurvitz et al. 2019; Romanò et al. 2020) and will be discussed in further detail in a following chapter (1.6.3 FTIR and Raman spectroscopy as promising tools for fast and easy characterization of EVs).

Some examples of the utility of EV associated protein markers in cancer diagnosis are assays developed Duijvesz et al. (2015) and Yoshioka et al. (2014). Duijvesz et al. (2015) developed a time-resolved fluorescence immunoassay for detection of CD9 or CD63 positive PrCa derived EVs directly in urine. They found that after correction for the relative amount of prostate fluid in the urine using

urinary PSA, the amount of both CD9 and CD63 positive EVs was significantly higher in men with PrCa, and that the CD63 based assay specifically had a higher diagnostic accuracy in detecting PrCa than traditional serum PSA assay. Yoshioka et al. (2014) developed the ExoScreen assay that detects CD147 and CD9 double-positive EVs in non-purified serum samples. CD147 had previously been identified as a potential colon cancer marker through proteomics analyses of EVs derived from colorectal cancer and normal colon fibroblast cell lines. This screening method was deemed sensitive enough to detect even early-stage colorectal cancers which would be difficult to diagnose using other existing methods, and it showed diagnostic advantage over other commonly used methods to detect colorectal cancer antigens (Yoshioka et al., 2014).

Besides diagnostic applications, analysis of the EV secretome from blood samples could be used for personalized medicine approaches in predicting the patient's treatment responses and therefore choosing the most suitable form of treatment for each patient. Several putative prognostic biomarkers of PrCa have been identified in EVs; Kharaziha et al. (2015) identified EV associated biomarkers predictive of docetaxel response through comparative proteomics analysis on EVs derived from docetaxel sensitive and resistance DU145 cells. They found major differences could be detected specifically in the amount of EVs secreted and the levels of EV associated CD82. Additionally, they identified a set of biomarkers, including multidrug resistance proteins 1 and 3, and polyadenylate-binding protein 4, which were enriched only in docetaxel resistant DU145 EVs. These results were further validated in a small cohort of docetaxel resistant and sensitive CRPC patients; in correlation with the *in vitro* data, proteins from the identified set of biomarkers were mainly detected in the EVs from docetaxel resistant CRPC patients.

Both have Del Re et al. (2017) and Joncas et al. (2019) reported that AR splice variant AR-V7 mRNA detected in plasma EV samples of CRPC patients is a potential biomarker of resistance to ADT. Del Re et al. (2017) reported that both median progression-free survival and overall survival were significantly longer in AR-V7 negative versus positive patients (20 vs 3 months and not reached vs 8 months, respectively). Joncas et al. (2019) found that AR-V7 positive status was associated with a shorter time to disease progression (16 vs 28 months) and correlated with low castrate androgen levels below the limit of quantification. Park

et al. (2016) collected plasma EVs from PrCa patients who had received surgical intervention and patients with benign prostatic hyperplasia and found that prostate-specific membrane antigen (PSMA)-positive EV concentration in the plasma could be used to differentiate between PrCa and benign prostate hyperplasia, as lower plasma PSMA-positive EV concentration was positively correlated with greater prostate volume, lower pathologic Gleason score and lower risk of biochemical failure in an 18-month follow-up period. Huang et al. (2015) screened plasma EV miRNAs from a cohort of 23 CRPC patients and found that higher levels of miR-1290 and -375 were significantly associated with poor overall survival; patients with high levels in both indicated miRNAs had a mortality rate of about 80% at 20-months of follow-up whereas the mortality rate of patients with low levels of both miRNAs was about 10% at the same timepoint. The results obtained by these studies exemplify the vast potential for using circulating EV associated molecules as diagnostic and prognostic biomarkers for PrCa.

1.5.2 EVs as vehicles for drug delivery

Optimizing drug delivery is crucial in improving safety and efficacy of cancer therapeutics. Many of the systemic side effects of current anticancer drugs could be avoided by the use of a targeted drug carrier. EVs possess many properties which make them interesting options to consider for vehicle for targeted delivery; 1) due to the mechanism of EV biogenesis, EVs naturally contain molecular signatures from their host cells, which are able to target these vesicles accurately to receiving cells, 2) EVs are not toxic or likely to elicit an immune response, 3) the structure of EVs allows for inclusion of both water and lipid soluble drug molecules, as the hydrophilic core is excellent for water transporting water soluble drugs, and lipid bilayer works to bind lipid soluble molecules (Li et al., 2019). EVs have also been reported to be able to pass through the blood brain barrier in danio rerio, although the exact mechanism is unclear (Yang et al. 2015). This property would allow for EV carriers to be used also in implications such as brain cancer and neurological diseases.

Anticancer drugs, most prominently paclitaxel and doxorubicin, have been successfully loaded into EVs in several experiments (Tian et a. 2013, Kim et al. 2015, Saari et al. 2015). In all these studies, encapsulation of the drug within EVs provided enhanced uptake and cytotoxicity compared to administration of free

drug. Kim et al. (2015) reported that EV-encapsulation provided a 50-fold increase in paclitaxel cytotoxicity in a multidrug resistant cell line *in vitro* as compared to administration of paclitaxel alone, suggesting that EVs may be an effective weapon in fighting multiple drug resistant cancers. The effectiveness of EVs against drug resistance was hypothesized to be due to the method of cell uptake; EVs may be taken up by endocytosis or via fusion with the plasma membrane, allowing the drug encapsulated in the EV to bypass the P-glycoprotein drug efflux system (Kim et al. 2015). Certain EVs seem to exhibit a natural preference for tumor tissue as further demonstrated by Kim et al. (2015); murine macrophage derived EVs administered *in vivo* via airway showed significant co-localization with pulmonary cancer metastases in a mouse model of Lewis lung carcinoma, and both EV-encapsulated paclitaxel and doxorubicin were found to mainly accumulate in cancer cells. Finally, it was shown that EV encapsulated paclitaxel produced a more effective antitumor effect than free paclitaxel in mice *in vivo*. EV target selectivity may be further enhanced by surface modifications, as did Tian et al. (2013) by engineering the EV producing mouse immature dendritic cells to express Lamp2b, a known exosomal membrane protein, fused with an iRDG peptide targeting alpha-v integrin. These modified EVs were shown to be highly specific in targeting alpha-v integrin overexpressing breast cancer cell lines *in vitro*, and when injected intravenously in xenografted mice these targeted EVs were able to deliver doxorubicin specifically to tumor tissue and induce inhibition of tumor growth.

EV mediated drug delivery may also enable the use of novel anticancer therapies. This was demonstrated by Usman et al. (2018), who described a red blood cell EV -based strategy for delivery of RNA drugs. They hypothesized that red blood cell derived EVs could overcome the drawbacks of currently available delivery vehicles such as viruses and lipid transfection reagents, which limit the usability of RNA based therapies due to problems such as low uptake efficiency and cytotoxicity. Consequently, it was shown that red blood cell derived EVs loaded with antisense oligonucleotides antagonizing miR-125b (an oncogenic microRNA upregulated in leukemia and breast cancer cells as well as in PrCa) were able to achieve an efficient, dose-dependent inhibition of miR-125b and the subtype miR-125a in myeloid leukemia cells *in vitro*, as well as suppressed breast cancer and acute myeloid leukemia xenograft growth *in vivo* following intratumoral

administrations, with no observed off-target cytotoxicity. The same delivery strategy was further validated for gRNA-mediated genome editing with CRISPR–Cas9 *in vitro* using myeloid leukemia cells (Usman et al., 2018).

While immunogenicity or toxicity have not presented as major problems with the use of EVs in *in vivo* and *in vitro* studies (Zhu et al., 2017; Saleh et al., 2019), concern may arise when taking into account the natural cancer-enhancing property that most cancer cell originated EVs possess and the possibility of horizontal gene transfer via EVs. While no reliable method of emptying EVs of their original contents has been reported, the option exists to utilize empty, red blood cell originated EVs or synthetic EV mimetics with surface modifications instead of autologous cancer EVs. However, when utilizing autologous EVs produced by PrCa cell lines to study EV mediated Paclitaxel drug delivery, Saari et al. (2015) found the EV mediated increase in paclitaxel cytotoxicity to be more prominent than the natural cancer-enhancing property of unmodified cancer EVs, providing an effective anticancer net effect.

A major hurdle in the way of efficient use of EVs in therapeutics is that EVs are difficult to produce in large quantities. Hypoxia has been found to increase EV production (King et al., 2010; Panigrahi et al.,) and this makes utilizing hypoxic conditions an interesting approach to enhancing EV production. However, as discussed previously, hypoxia also has the unwanted effect of providing the EVs loaded with aggressively cancer enhancing properties. Therefore, careful profiling of hypoxic EVs and thorough investigation into their efficacy and safety features are needed.

1.6 Challenges and future prospects in characterization and quality control of EV preparations

1.6.1 Methods for efficient EV production

A major challenge for EV research is their efficient production. EVs intended for therapeutic applications are typically extracted from cell culture conditioned media of cell lines, and large volumes of media is needed for extracting EVs in sufficient concentrations for most downstream analyses (Patel et al., 2018). This makes EV production in cell culture a laborious and time-consuming task. The use of bioreactor systems has gained traction as an option for traditional cell culture methods. These bioreactors are able to house 20 times more cells than a

T175 flask, and subsequently have been reported to be able to yield 100-fold more EVs (Palviainen et al., 2018). Although still not widely adopted for EV production, most commonly referenced commercially available bioreactors in EV publications are CELLine (Wheaton) and FiberCell (FiberCell Systems Inc.). The basic principle of both these bioreactor models is the same; both contain a matrix in which the cells grow, and a semi-permeable permitting nutrient and waste exchange with the surrounding media, but enclosing the cell product into a smaller volume, resulting in highly concentrated conditioned media. Both systems eliminate the need to passage cells after inoculation of the reactor. These factors greatly reduce the time spent on cell culture maintenance during EV production; a study on the efficacy of the CELLine bioreactor estimated that as many as ten traditional T175 flasks would have to be used each week to achieve the same EV yield. Other cell culture conditions also play a notable role in EV yield, and optimization of culture collection and purification protocols have been found to have amplifying effects on the EV yield already in classic T-flask cell cultures (Patel et al., 2017).

The FiberCell culture system is a more refined system and is claimed by the manufacturer to model the mammalian circulatory system and provide *in vivo*-like conditions (Fibercell System Inc, 2020). This is achieved through the use of a hollow fiber system mimicking capillaries, and via a pump that circulates medium through the system, mimicking heart and blood, as well as an oxygenator for re-oxygenating the circulating media. The cells grow in a porous matrix permeated by the hollow fiber “capillaries” coated with a semi-permeable membrane, allowing for metabolic waste and the nutrients and oxygen in the circulating media to pass through, but containing the cellular product, in this case EVs, within the restricted cell space to be harvested in highly concentrated fractions (Fibercell System Inc, 2020). In comparison, the CELLine system is relatively simple, consisting of a large cell culture flask with two compartments separated by a semi-permeable membrane. In the model for adherent cells, the cell compartment contains a polyethylene terephthalate matrix which allow cells to grow in high density, 3D like formation (Guerreiro et al., 2018). Both of these systems have been utilised in EV production with good results. Watson et al. utilized the FiberCell system for production of EVs from a HEK293 cell culture and reported a 40-fold increase in EV particles per volume of conditioned medium as opposed

to conventional cell culture (Watson et al., 2016). Studies evaluating the efficacy of the CELLine bioreactor in EV production have reported 10-12 fold increases in EVs yield per ml of conditioned medium (Guerreiro et al., 2018; Mitchell et al., 2008), with Palviainen et al. (2018) reporting a more than 100 fold increase in yield measured as the total particles/ml isolated in one isolation round from a single T175 vs from the CELLine bioreactor.

When comparing the metabolic signatures of EVs from 2D and 3D cultures, Palviainen et al. (2018) identified some cell culture system dependent differences between the resulting EVs; while the bioreactor cultured EVs exhibited all the same metabolic pathways as their 2D cultured counterparts, the total number of identified metabolites in the bioreactor derived EVs was lower. Other factors considered to influence this difference were medium composition and the frequency of culture maintenance. Their finding not only highlights the necessity of carefully optimising and reporting the culture conditions, but also suggests that EVs may be customised for the desired downstream applications by modifying the culture conditions, e.g. metabolite poor EVs could be desirable for drug delivery applications (Palviainen et al., 2018).

In conclusion, bioreactor cell culture approaches help overcome the challenge of sufficient sample material production, and they should be combined with suitable media modifications to achieve optimal efficacy. It is worth noting that even with these high yield approaches, EV production remains to be a bottleneck for larger scale *in vivo* studies for example, and to fully realise EV's therapeutic potential, methods to scale up this production towards industrial magnitude of EV manufacturing will need to be looked further into (Patel et al., 2018).

1.6.2 Current methods and guidelines for separation, purification and characterization of EV preparations

There is a lack of standardization regarding methods of EV isolation and characterization which hinders the translation of EV-based diagnostics into clinical use. ISEV is currently the major proponent for harmonizing EV research, and they have published position statements regarding best practices of EV research, most recently Minimal information for studies of extracellular vesicles 2018 (MISEV 2018), in which recommendations are made about EV isolation,

purification and characterization, as well as on the best practices on reporting EV studies, based on current expert consensus (Théry et al., 2018)

EV separation and purification

Currently there is no golden standard on the methods of EV collection, and several different methods are employed, with differential ultracentrifugation as the currently most commonly used technique for primary EV separation and concentration (Gardiner et al., 2016). Other techniques such as density gradients, ultrafiltration, SEC or ion exchange chromatography, and immunoisolation are also being employed to varying degrees. It is also increasingly common to use a combination of these methods when seeking to achieve optimal purity or separate EV subtypes.

Each of these methods have their advantages and disadvantages regarding EV yield and the possible impact of the isolation method on the EV integrity. For example, it has been suggested that the popular isolation technique, ultracentrifugation, does induce aggregation of the EV particles (Linares et al., 2015). Comparison of the different purification methods has been difficult as EVs from several different origins have been purified using different methods. However a comprehensive study of several purification methods, including differential centrifugation, ultra-filtration, density gradients, precipitation methods, SEC as well as combinations of these methods, and in which all the EVs studied were of the same cellular origin was recently conducted by Zini et al. (Data presented in ISEV annual meeting, Barcelona 2018). Based on that data by Zini et al., the combination of differential centrifugation with size-exclusion chromatography was found to be one of the most effective methods of EV separation and purification, prompting the approach to be employed also in this thesis.

Characterisation

MISEV2018 recommends utilizing multiple methods for comprehensive characterisation of EVs, and highlights three key features of EV preparations considered to be necessary to report for all studies (Théry et al., 2018). Firstly, the source from which the vesicles have originated, should be quantitatively defined, by using measures such as the number of cells in a culture, the volume

of a biofluid or mass of tissue. It is recognised that this is not feasible for all studies, due to restrictions arising from the cell culture methods, pointing for example to continuous bioreactor-based cultures, which was the culture method in this thesis as well. For these instances MISEV2018 recommends reporting instead the number of cells at initiation of culture, expected doubling time, and frequency of collection, which this thesis complies with. (Théry et al., 2018)

Secondly, the vesicles themselves should be characterised using methods that provide information on the quantity of EVs extracted (Théry et al., 2018). Methods which provide direct information of particle number in suspension include for example nanoparticle tracking analysis (NTA), flow cytometry and dynamic light scattering. Although these are the most effective methods currently used for particle counting, such methods based on light scattering have their disadvantages, mainly the fact that they are not EV specific but count any particles in the suspension, and the tendency of these methods to be biased towards detecting smaller vesicles (Théry et al., 2018). NTA estimates the concentration and size of particles based on the Brownian motion of a small aliquot of the particles over a definite period of time, thus the results may be analyzed statistically but may not be predicted precisely. Moreover, NTA is quite user-dependent and heterogeneous suspension of particles in size and composition can make the analysis difficult (Gardiner et al., 2013)

Methods which determine the total lipid or protein content of a sample may be used as substitute for particle number analyses, however this is not preferred as these measures may not be directly correlated with the particle number. For example, total protein quantification could result in overestimation of EV abundance due to co-isolated protein contaminants from the culture media or biofluid. While lacking as sole measures of particle number, MISEV2018 notes that total protein and lipid measures, and specifically the ratio of these components, could be utilized as an additional measure of purity of the EV preparation. (Théry et al., 2018)

The third necessary means of characterisation is the detection of EV associated, as well as EV negative biomarker proteins, using for example Western blot. If a publication seeks to ascribe findings to certain EV subtypes (e.g. exosomes vs microvesicles), biomarkers associated with the specific method of biogenesis

should be detected. The current recommendation for selection of biomarker proteins calls for biomarkers from at least three distinct categories to be detected; 1) at least one transmembrane or glycosylphosphatidylinositol anchored protein (e.g. tetraspanins, integrins) 2) at least one cytosolic protein with ability to bind to lipid membranes or transmembrane proteins (e.g. TSG101, ALIX) and optionally other proteins with more promiscuous incorporation in EVs (e.g. HSP70, tubulin) 3) negative purity control of possible source related contaminants (e.g. apolipoproteins, urine) (Théry et al., 2018). Additionally, two more categories of proteins have been listed in MISEV2018 for further characterisation of the EV subpopulation and functions; 4) EV subtype-specific proteins and 5) soluble extracellular proteins with functional activities and their mode of binding to EV associated receptors.

1.6.3 FTIR and Raman spectroscopy as promising tools for fast and easy characterization of EVs

In order for EV based preparations or diagnostic methods to be translated into clinical use, it is necessary to establish reproducible and efficient methods of characterization and quality control of EV preparations. ISEV has suggested using the protein/lipid ratio of the vesicle components as a possible measure of purity for the sample. Spectroscopic methods such as Fourier-transform infrared spectroscopy (FTIR) and Raman spectroscopy have recently been raised as promising options for characterization of the vesicles' biomolecular properties (Mihaly et al. 2017; Gualerzi et al.,2017). The main advantages of these spectroscopic techniques is that they provide reproducible results in a label-free manner, are relatively simple with minimal sample preparation and short acquisition times, and require only small amounts of material (micrograms to nanograms), a considerable advantage recalling that one of the major challenges in EV research is efficient production of sample material (Movasaghi et al., 2008).

Vibrational spectroscopic techniques like FTIR and Raman are based on exciting the sample material at specific light wavelengths and recording the absorption or Raman scattering, respectively, of the light by the molecules in the sample. Both FTIR and Raman spectra result from changes in vibration modes of the molecule. Changes in the dipole moment of a molecule are IR active, while vibrations that affect the dipole moment are Raman active. Raman and FTIR are complementary techniques due to the rule of mutual exclusion: in molecules that present a center

of symmetry, Raman active vibrations are IR inactive and vice versa (Campanella et al., 2021). FTIR and Raman spectra are graphed with the frequency (wavenumber) on the X axis and the intensity on the Y axis. The intensity is proportional to the vibration of the electric or magnetic dipole, IR and RS respectively. The spectral peak positions have further been attributed to molecular conformations, bonds and functional groups (Table 1, Table 2), thus a FTIR or Raman spectrum is able to provide detailed information of the biomolecular constitution of the sample (Movasaghi et al., 2008). While still a novel application, EV component characterization using these methods is increasingly gaining the attention of the scientific community. A new concept of spectroscopic protein/lipid ratio, calculated from IR or Raman spectra based on the areas of peaks with known protein or lipid attributions, as measure of EV sample quality was first proposed and validated for FTIR by Mihaly et al. (2017) and since then has been demonstrated also with Raman (Gualerzi et al., 2019).

Table 1. FTIR peak assignments. Literature assignments of common spectral features of EV (Drozdz et al., 2020; Movasaghi et al., 2008).

Position (cm^{-1})	Functional Group, Assignment
990	C-O of ribose
1050	C-O-C stretching of DNA and RNA, C-O stretching coupled with C-O bending of carbohydrate C-OH bonds, phosphate
1230	C-N stretching of proteins (amide III) and nucleic acid phosphate vibration
1400	CH_3 bending of lipids and proteins
1450	CH_2 scissoring of lipid acyl
1545	N-H bending of peptide groups (amide II)
1650	C=O stretching of peptide backbone (amide I)
2800-2900	CH_2 asymmetric and symmetric stretching of lipids
2900-3000	CH_3 asymmetric stretching of lipids
3300	N-H, O-H stretching, water

Table 2. Raman peak assignments. Literature assignments of common spectral features of EV Raman spectra (Smith et al., 2015 and Gualerzi et al., 2017).

Position (cm^{-1})	Functional Group, Assignment
700	Cholesterol ester
720-820	Nucleic acids backbone
880	Tryptophan side-chain in proteins
1003	Phenylalanine
1065-1095	C-C strectching in lipids and carbohydrates
1200-1300	C-N stretching, Amide III
1450	CH_2/CH_3 scissoring in lipids and proteins
1558	Tryptophan aromatic ring
1661	C=O stretching, Amide I

FTIR

Among the first to comprehensively characterize EVs using FTIR were Mihaly et al (2017). In this study, EVs were separated from Jurkat T-cell line as well as red blood cells using ultracentrifugation and analyzed using attenuated total reflection (ATR)-FTIR. It was found that the amide I (1650 cm^{-1}) and C-H stretching peak (2800-3000 cm^{-1}) intensity ratios, corresponding to protein and lipid components of the spectra respectively (Table 1) were specific to the EV subpopulation studied. They were also the ones to initially suggest the spectroscopic protein to lipid ratio as a tool to measure EV purity. Zini et al. utilized this spectroscopic ratio in a study comparing EV purification methods using both FTIR and Raman with results confirming the applicability of this method (2018).

Paolini et al. (2020) studied different subpopulations of EVs secreted from two murine prostate and melanoma (TRAMP and B16) cell lines and separated by size by utilizing differential centrifugation. It was found that through principal component analysis (PCA) (Ringnér, 2008) of the obtained IR spectra, it was possible to distinguish among the different subpopulations and discriminate between large, medium, and small EVs of same cell line. It is theorised here that through establishing spectral fingerprints, FTIR spectroscopy could be used to quickly fingerprint EV subpopulations and could potentially be considered as a

means of characterisation in lieu of attempting to establish specific protein biomarkers for the inherently heterogenous EV subpopulations.

The ability of FTIR based characterization to distinguish between EV subpopulations further holds potential to be used in cancer diagnosis; Zlotogorski-Hurvitz et al. (2019) studied EVs for early diagnosis of oral cancer using EVs isolated from saliva samples of healthy donors and oral cancer patients. They utilised ATR-FTIR spectroscopy for characterisation of the EVs and machine learning techniques to distinguish EVs from healthy and cancerous origins. The FTIR spectra were found to have significant differences between the EV populations and based on this a highly sensitive (100%) specific (89%) and accurate (95%) classification method for the samples could be developed. Romanò et al. (2020) utilised FTIR and set up an automated method for classification of cancer cell derived EVs. They studied the effects of starvation on EV composition by analysing vesicles released from human colorectal adenocarcinoma cancer cells cultured in two different media compositions and found statistically significant differences between the starvation and well-fed conditions in the shape of the Amide I and II peaks. Using PCA, they were able to establish a highly accurate automated classification of EVs derived from the different conditions.

Raman

Raman spectroscopy has recently gained interest as a promising method for two distinct EV related applications; quality control of EV preparations as well as in disease screening by identifying Raman fingerprints of EV subpopulations. Raman spectroscopy has already been applied to EV characterization with both quality control and diagnostic purposes, and promising results have been obtained from these studies, reviewed below.

The capability of Raman to differentiate between EVs based on their tissue and cellular origin has been demonstrated in several studies: Gualerzi et al. (2017) utilized this method in their study comparing the Raman spectra of spectra of the EVs of differentiated fibroblasts and MSCs derived from bone marrow and adipose tissue. By applying PCA of the Raman spectra, this method was found

to be able to distinguish not only EVs from two different cell types (fibroblasts and MSCs) but also between MSCs from different tissue origins, with the reported accuracy of 93.7%. In another study by them, it was demonstrated that besides being able to discriminate between EVs from different cell types Raman spectroscopy could also be used to differentiate EV preparations based on the isolation procedure and level of purity (Gualerzi et al. 2019). This was achieved by applying the spectroscopic P/L proposed by Mihaly et al. (2017) on Raman spectra. Similarly promising results were obtained by Zini et al. (2018) in a study comparing the efficacy of different EV purification methods, further verifying the applicability of Raman spectrometry and spectroscopic P/L ratio as an additional tool for EV preparation characterization and quality control.

Raman spectroscopy -based characterization of EVs could also provide a new method for cancer screening. Lee et al. (2018) employed single-EV characterization using Raman optical tweezers to detect differences in EV samples from four different cell types. The Raman spectra of red blood cell and platelet derived EVs, as well as EVs from PC3 and LNCaP PrCa cell lines were analyzed using PCA, and found that this method was able to discriminate the EVs in distinct groups based on the cellular origins (blood vs PrCa) (Lee et al., 2018). Krafft et al. (2017) utilized both IR and Raman spectroscopy in a comprehensive comparative analysis of cancer versus non-cancer EV and patient screening. EVs were separated from the blood and plasma of healthy donors and cancer patients by differential ultracentrifugation. They detected the reduction of alpha-helix-rich proteins and enhancement of beta-sheet-rich proteins to be a specific feature of EVs from the blood of cancer patients and determined this as a prospective cancer-specific EV signature.

A major challenge with Raman spectroscopy, especially when analyzing biological samples, has been the low Raman signal as compared to background. Sensitivity of Raman spectroscopy may be enhanced by utilizing surface enhanced Raman scattering (SERS). With the use of specific plasmonic surface substrates, such as noble metal nanoparticles or other nanostructures, enhancement of the Raman signal may be achieved at up to 10^{10} -10^{11} factor (Sharma et al., 2012). Park et al. (2017) utilized SERS in combination with PCA and found that this method allowed for exosomes derived from lung cancer cell

lines to be distinguished from normal alveolar cell derived exosomes with 95.3% sensitivity and 97.3% specificity, highlighting the potential of extracellular vesicles as diagnostic markers for cancer.

While state-of-art Raman spectrometers are still expensive and large pieces of equipment that require thorough training to use, portable Raman spectrometers are continually being developed to be better and more accurate (Sharma et al., 2012). More basic research and robust and reproducible protocols still need to be developed for EV characterization. However, in the future it could be enough that after optimization of the production and purification protocol of an EV preparation, the Raman fingerprint could be characterized and future batches could be compared to the control sample using a quick, easy to operate handheld Raman device. Additionally, once comprehensive libraries of specific EV fingerprints have been created, the same method could potentially be applied in the clinical setting for screening of diseases.

1.7 Aims of the study

The aims for this study were to 1) establish a bioreactor cell culture protocol for 22Rv1 and RWPE-1 cell lines, 2) characterize the EVs obtained from these cell lines using Raman and FTIR spectroscopy and subsequently obtain the spectroscopic protein/lipid ratio, and 3) to analyze this spectroscopic P/L ratio as a function on time as weeks since bioreactor inoculation to find possible changes in EV composition over time. This was done both in order to assess the spectroscopic P/L ratio as a way to measure of EV purity and to evaluate the stability of the EV production in the established cell culture conditions. An additional aim was to investigate the potential of utilizing hypoxic conditions to increase EV production by establishing hypoxic 22Rv1 and RWPE-1 cell cultures. The PrCa cell line 22Rv1 was used due to its unique AR properties and relevance as a CRPC model, and RWPE-1 was used as normal prostate cell line control.

Efficient production of sufficient amounts of sample material is currently a technical bottleneck in EV research, however the CELLine bioreactor system has been utilized by a few research groups with significantly improved EV yields as compared to traditional culture flasks (Palviainen et al., 2018; Guerreiro et al.,

2018; Mitchell et al., 2008) In this study, the first aim was to achieve efficient EV production via the use of a CELLine bioreactor combined with media optimization. The EVs obtained were separated using a two-step approach of DC and SEC for enhanced purity, and according to MISEV2018 the EVs were characterized quantitatively using NTA and screened for enrichment of EV specific biomarkers proteins using Western blot.

Raman and FTIR spectroscopy are increasingly studied for applications in the EV field, and promising results have been obtained, with these methods being able to distinguish between EVs based on both cellular origins and separation method used to obtain them. Recently, a spectroscopic protein/lipid ratio was proposed as a measure of EV purity (Mihaly et al., 2017). Using this method, studies have been able to identify cellular origin and purity -based differences in EV preparations with both FTIR and Raman spectroscopy. Here, 22Rv1 and RWPE-1 cell line derived EVs are characterized using these methods for the first time, and the spectroscopic P/L ratio is calculated from the obtained spectra. Finally, the spectroscopic P/L ratios obtained from different weeks are compared and the EV composition is analyzed as a function of time since bioreactor culture initiation.

2. Results

2.1 Bioreactor cell culture and hypoxic conditioning

Effective production of EVs is currently a bottleneck for EV research and application. As one of the main aims of this study, CELLine bioreactor cultures were established for 22Rv1 and RWPE-1 cell lines. These cell lines have not been previously cultured in bioreactors, therefore a suitable culture method needed to be established. After careful optimization of the media composition, the average EV yield from one weekly harvest ranged between 10^{11} and 10^{12} particles/ml (Figure 3). The bioreactors continued to produce a stable yield for 12 weeks, at which point a bacterial contamination of the nutrition compartment was detected in the RWPE-1 bioreactor and both bioreactors were subsequently run down.

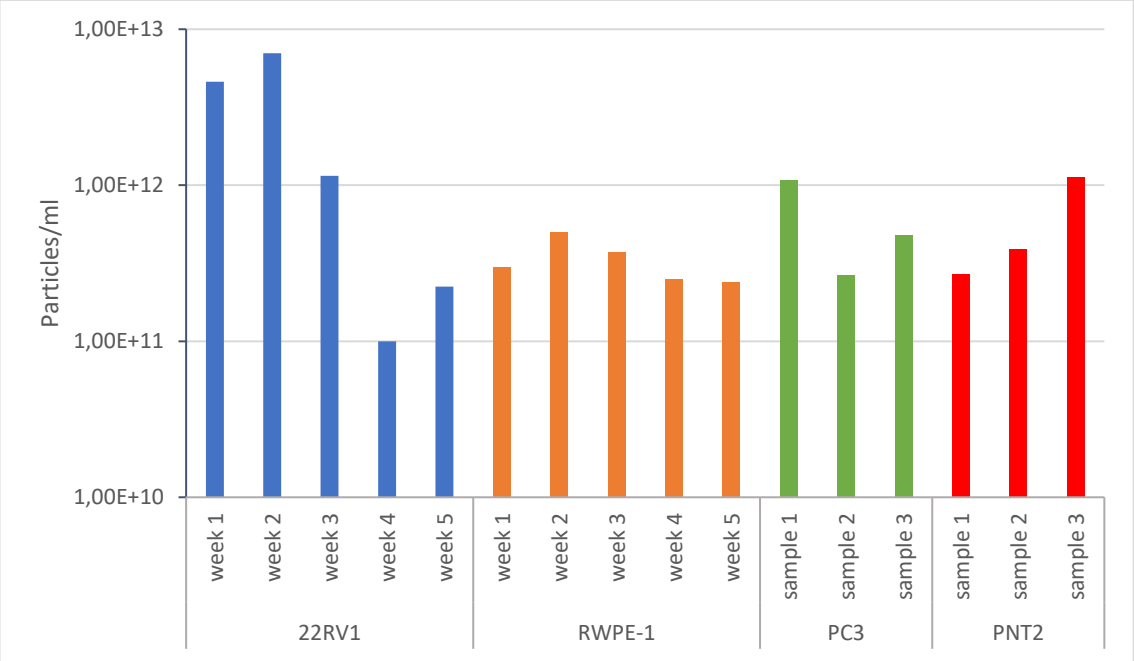

Figure 3. Particle concentrations measured with NTA (particles/ml in log10 scale, note that scale starts at 1E+10 instead of 0) of the EV samples derived from 22Rv1, RWPE-1 (new cultures, 1-5 weeks from inoculation), PC-3 and PNT2 cell cultures (stable cultures, 3+ months from inoculation).

An attempt was made to culture 22Rv1 and RWPE-1 cell lines long term in hypoxic conditions, in order to characterize differences in chronic hypoxia versus normoxia derived EVs. The cells were cultured in 0.1%, 1% and 4% O2 conditions. Unfortunately, the cells were unable to reach confluency in any of the abovementioned oxygen conditions within two weeks after the first passage, and therefore no hypoxic EV samples were obtained

2.2 Size-exclusion chromatography and NTA

EVs collected from the bioreactor cell cultures were purified using differential centrifugation at 20K and 110K g, and subsequent size-exclusion chromatography (SEC) using Superdex 200 column. The SEC fractions were collected 1ml/min, and the elution took place over 25 minutes. Most particles eluted at fractions 7 and 8, corresponding to the 7th and 8th ml of elute collected, as verified by NTA in Figure 3. The size of the particles collected from these main fractions of the SEC elute matches the typical small EV size with the particle diameter mean at 140 nm and mode at 145 nm (Figure 4A). SEC yield was analyzed by measuring the particle concentration of the sample both before and after SEC purification. The SEC method used had a yield of 21-25% (Figure 4B). The size distribution of the particles in the final sample of the concentrated SEC fractions was also analyzed with the NTA. For all samples analyzed the main peak of the size distribution is located at about 125-150 nm and remains mainly unchanged between different cell lines and different timepoints (Figure 4C). However, slightly more variation in the shape of the peak and the number of minor peaks at larger nm sizes can be seen between the EV samples of the 22Rv1 and RWPE-1 cell lines than with the PC3 an PNT2 cell lines derived EV samples, indicating greater heterogeneity of size distribution in the 22Rv1 and RWPE-1 EV populations, although for RWPE-1 this heterogeneity seems to be reducing over time (Figure 4C) .

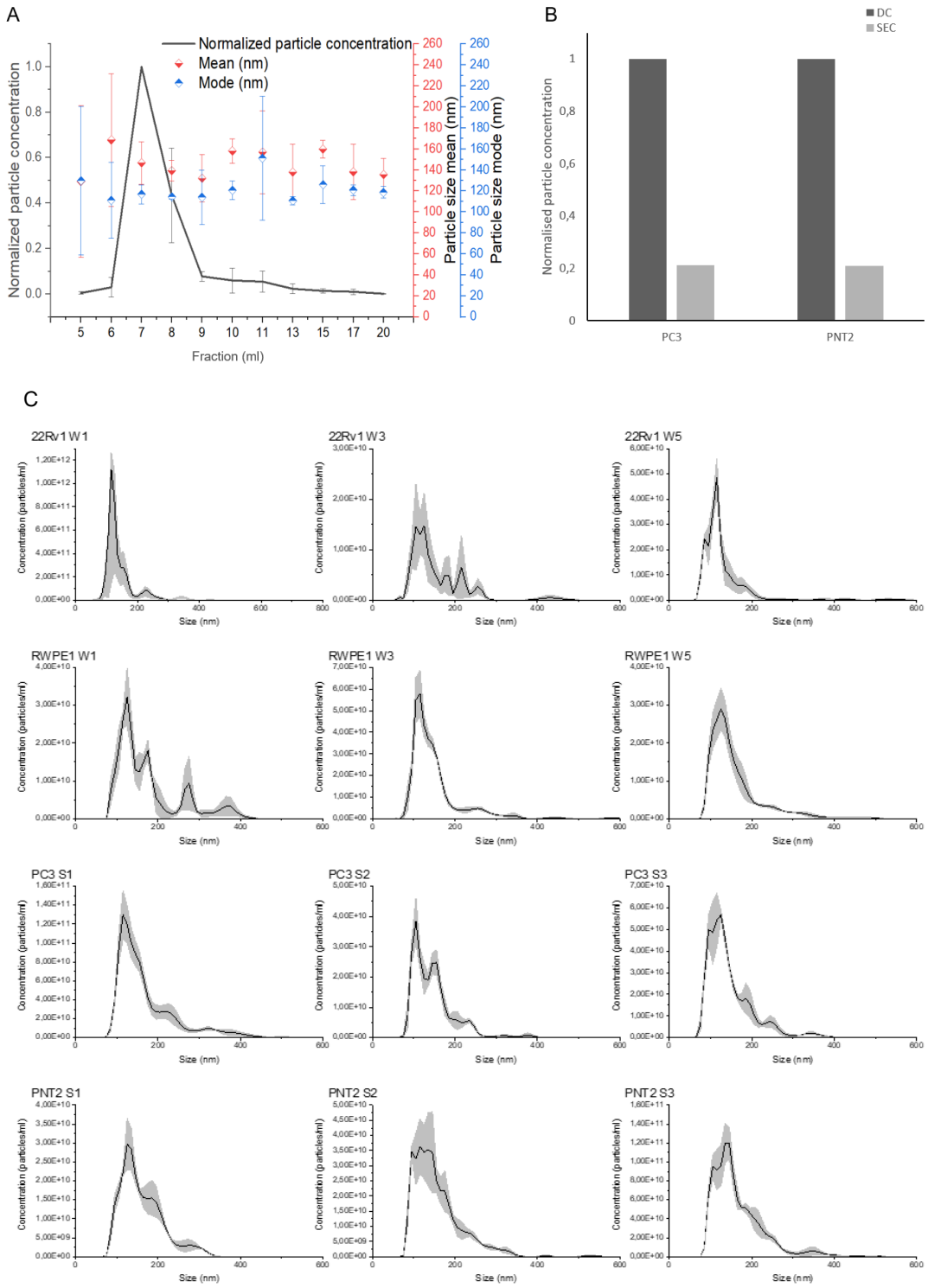

Figure 4. A) Normalised particle concentration (black line) and particle size mean (red diamonds) and mode (blue diamonds) of SEC fractions 5-20 measured using NTA show that most EVs eluted at fractions 7 and 8, and that the size of these particles was 145 nm on average. EVs were collected from bioreactor cultured 22Rv1 cell line, and purified using differential centrifugation and subsequent SEC. B) Particle concentration measured using NTA before and after SEC. The SEC purification method had yield of 21-25%. EVs were collected from bioreactor cultured PC3 and PNT2 cell line and purified using differential centrifugation and subsequent SEC. C) Representative size distributions obtained using NTA on EV samples of bioreactor cultures 22Rv1, RWPE-1, PC3 and PNT2 cell lines collected at different timepoints.

2.3 Western blot

For detection of EV biomarker proteins Hsp70, TSG101 and CD9, 10 µg of 22Rv1 and RWPE-1 derived EV samples and corresponding cell lysates were used for a Western blot analysis. Tubulin was used as loading control, and Golgi matrix protein GM130 was used as a negative control for EVs. Antibodies were chosen according to the guidelines presented in MISEV2018. The PC3 and PNT2 were obtained from Biopharmaceutics research group at Helsinki University and had already previously been characterized using the same antibodies (Zini et al., 2018), thus this analysis was not repeated for PC3 and PNT2 in this thesis. The tetraspanin CD9 could be detected in all of the EV samples, however it was absent in the cell lysates (Figure 5). Additionally, Hsp70 and TSG101 expression was detected in the 22Rv1 EV samples as well as both of the cell lysates, and TSG101 was faintly detected in one of the RWPE-1 EV samples, however Hsp70 was completely absent in the RWPE-1 EV samples. Tubulin, Tsg101 and GM130 bands could be detected in samples treated with reducing conditions, while CD9 and Hsp70 were visible only in non-denatured samples.

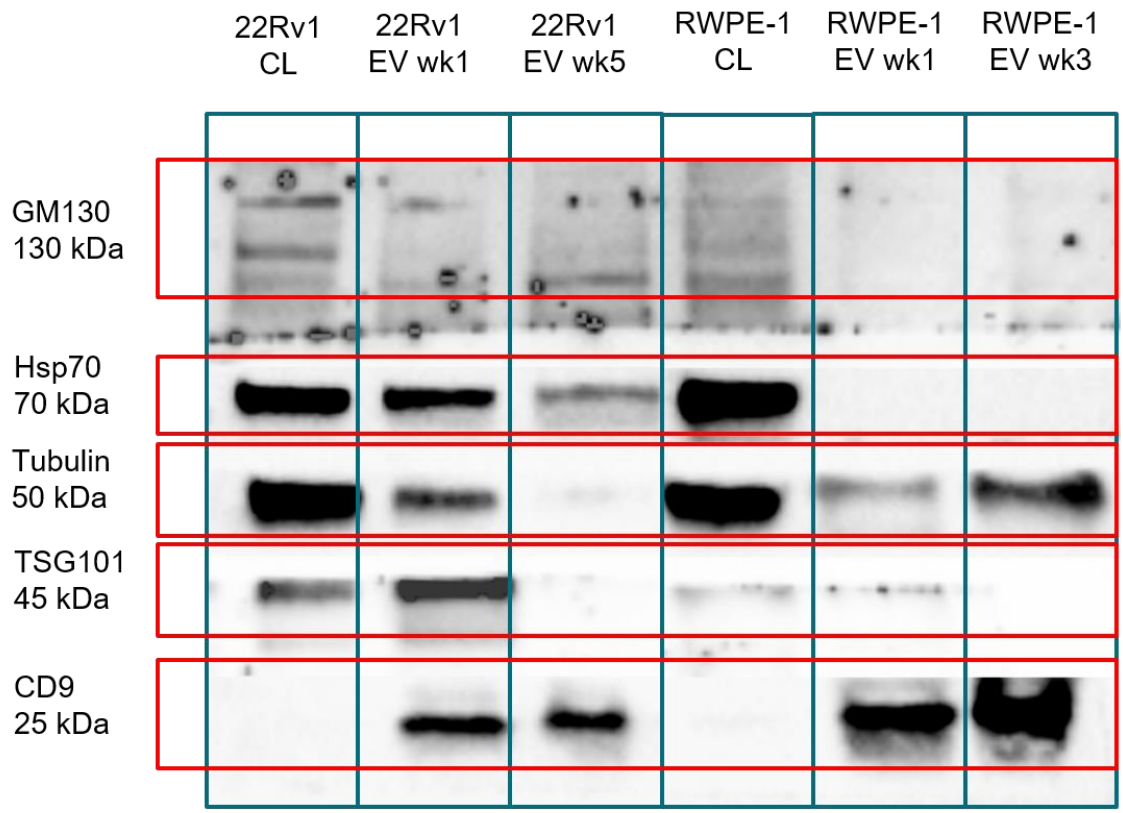

Figure 5. Western blot analysis of 22Rv1 and RWPE-1 EVs, verifying the presence of EV biomarker proteins CD9, TSG101 and HSP70 in the samples. Tubulin was used as loading control and GM130, a Golgi matrix protein, was used as negative EV control.

2.4 FTIR spectra

FTIR spectra were obtained using an IR- spectrophotometer, from a 5 µl droplet of EV suspension, air dried on top of an ATR crystal. Representative FTIR spectra were averaged from 4-5 EV samples of each cell line and three independent measurements of each sample (Appendix 1, Figures 1-4). Accumulation of 64 scans and nominal resolution of 4 cm^{-1} were used to acquire the spectra. All of the EV samples exhibit features common for most biological sample spectra (Figure 4.) From left to right, the strong peak at 1040 cm^{-1} is due to phosphate vibrations from PBS buffer (Mihaly et al., 2017; Movasaghi et al., 2008), the peaks at 1650 cm^{-1} and 1545 cm^{-1} are assigned as amide I and II respectively, with amide I arising from C=O stretching vibrations of the polypeptide backbone of proteins, and amide II from N-H bending vibrations of the peptide groups (Table 1). The small peak at around 1738 cm^{-1} originates from the C=O stretching of ester groups, arising e.g. from cholesterols and phospholipids. The peaks between 2800 and 3000 cm^{-1} are associated with the antisymmetric and symmetric stretching vibrations of lipid acyl CH_2 groups. The broad peak at 3300 is due to OH stretching vibrations of water molecules. For determination of the protein/lipid ratio the area of the amide I peak (centered at 1656 cm^{-1}) was determined by peak deconvolution using curve fitting with Lorentz-function. The area of the CH_2/CH_3 stretching vibration (2700 to 3000 cm^{-1}) representative of the lipid component was integrated (Figure 7.).

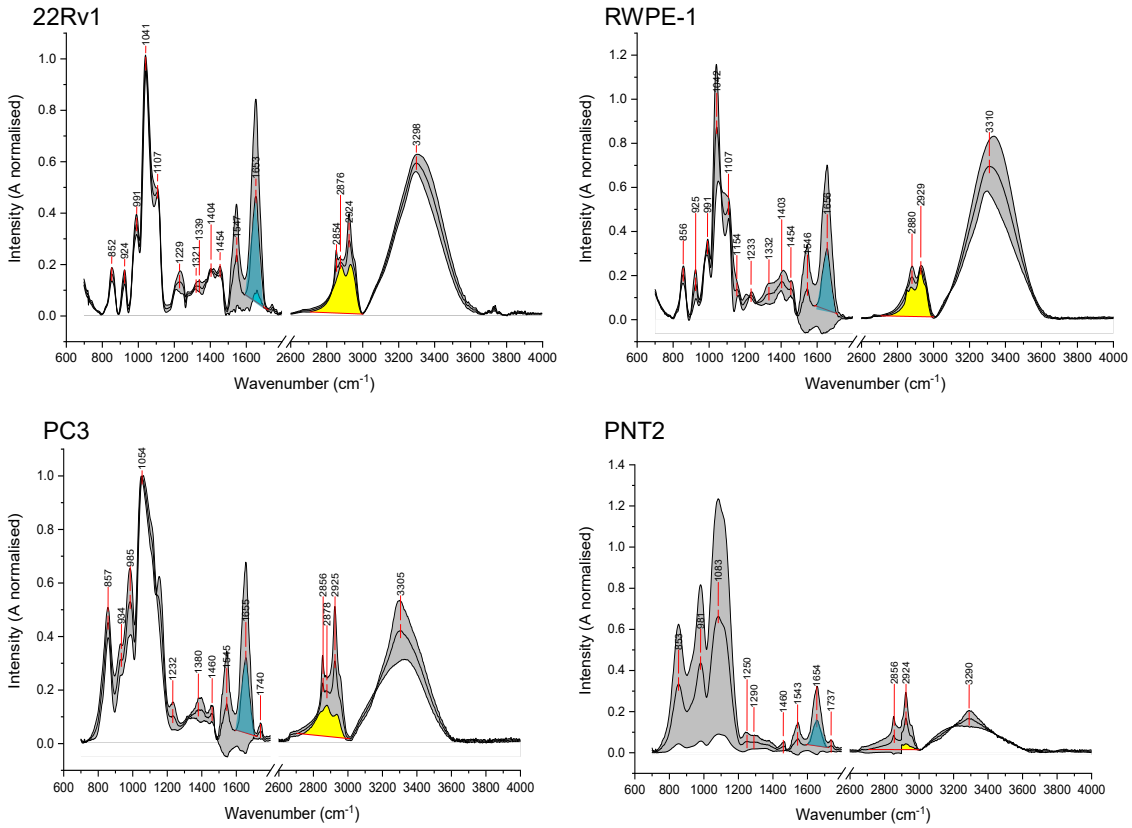

Figure 6. Representative FTIR spectra averaged from 4-5 EV samples from prostate cell lines 22Rv1 and PC3, and normal prostate cell lines RWPE-1 and PNT2 cultured in bioreactor cell culture and purified using differential ultracentrifugation and size-exclusion chromatography, presented as average (solid line)+-1 standard deviation(gray area) of 3 independent measurements.

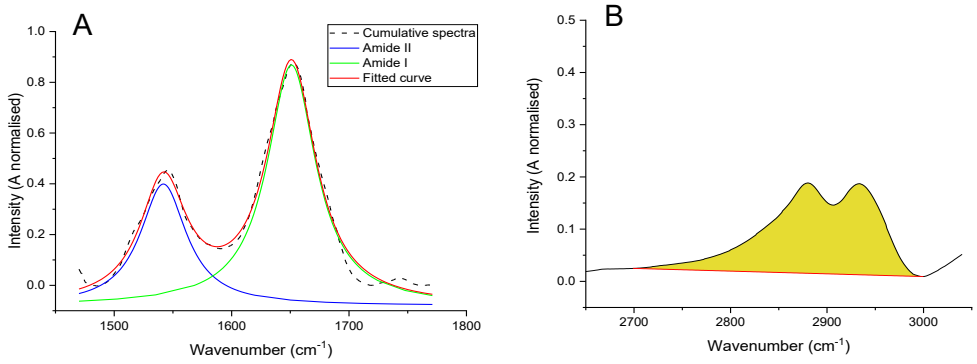

Figure 7. For determination of protein/lipid ratio from the ATR-FTIR spectra A) The area of the amide I peak centered at 1656 cm^{-1} (green line) was determined by peak deconvolution using curve fitting with Lorentz-function (red line) B) the area of the CH_2/CH_3 stretching vibration (2700 to 3000 cm^{-1}) representative of the lipid component was integrated.

2.5 Raman spectra

Raman spectroscopy is another spectroscopic method capable of quickly providing information of the molecular composition of a sample. In this study, Raman spectra of the EV samples were obtained from a 2 µl air dried droplet of EV suspension placed on top of a CaF_2 substrate slide and imaged with confocal Raman microscope (Figure 8.). Representative Raman spectra were averaged from 4-5 EV samples and three independent measurement (Appendix B, Figures 1-4). For determination of the protein/lipid ratio, the area of CH_2/CH_3 scissoring region (yellow 1416-1490 cm^{-1}, Figure 8) representing the lipid component and C=O peak (cyan, 1630-1710 cm^{-1}, Figure 8) chosen as representing the protein component were integrated. PC3 and PNT2 Raman spectra were obtained through collaboration with Jacopo Zini at University of Helsinki.

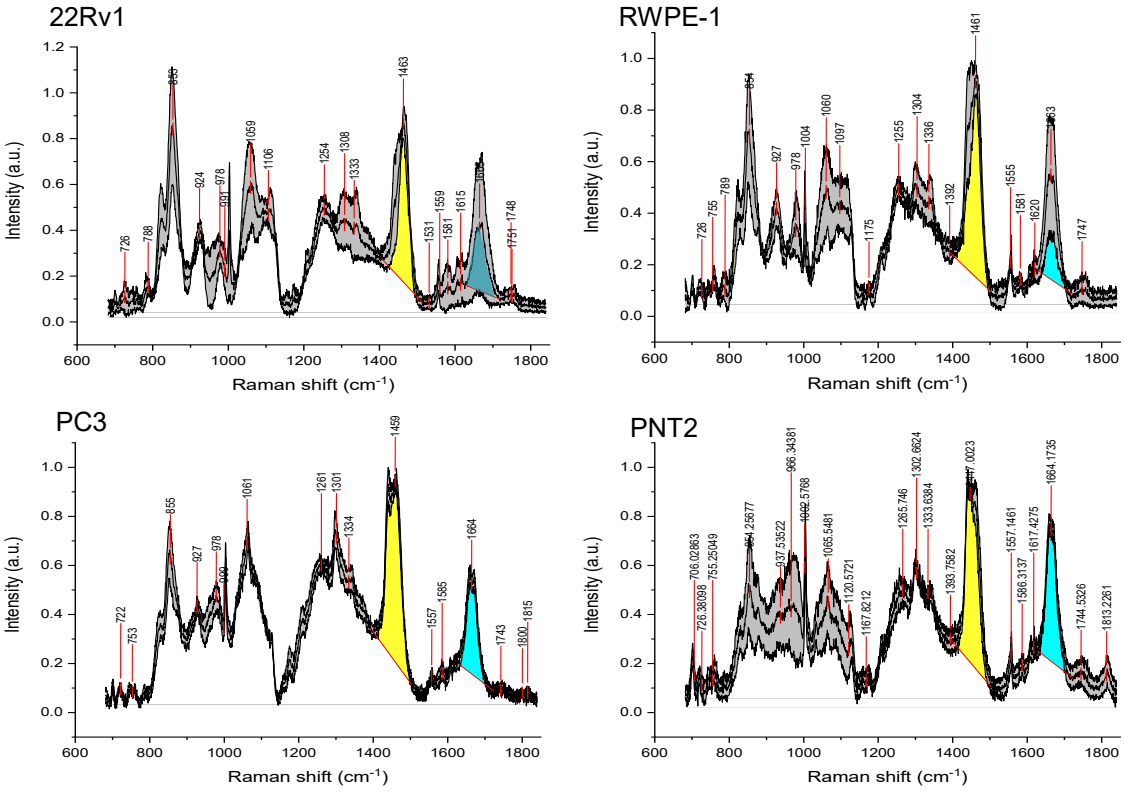

Figure 8. Representative Raman spectra, averaged from 4-5 EV samples from prostate cell lines 22Rv1 and PC3, and normal prostate cell lines RWPE-1 and PNT2 cultured in bioreactor cell culture and purified using differential ultracentrifugation and size-exclusion chromatography, presented as average (solid line) +/- 1 standard deviation (gray area) of 3 independent measurements. Integrated area of CH_2/CH_3 scissoring region (yellow 1416-1490 cm^{-1}) represents lipid component and C=O peak (cyan, 1630-1710 cm^{-1}) represents protein component.

2.6 Protein to lipid ratio as function of time

Recently proposed as a prospective additional measure of EV purity, the spectroscopic protein to lipid ratio was calculated from the EV FTIR and Raman spectra by dividing the area of the representative protein peak (P) with the area of the representative lipid peak (L). The P/L ratios calculated both from Raman and FTIR spectra of 22Rv1 and RWPE-1 derived EVs exhibit higher sample-to-sample variation than those of the EVs from PNT2 and PC3 cell lines. (Figure 9.) Data for independent spectra and determination of protein and lipid peak areas for each sample are included in the appendices.

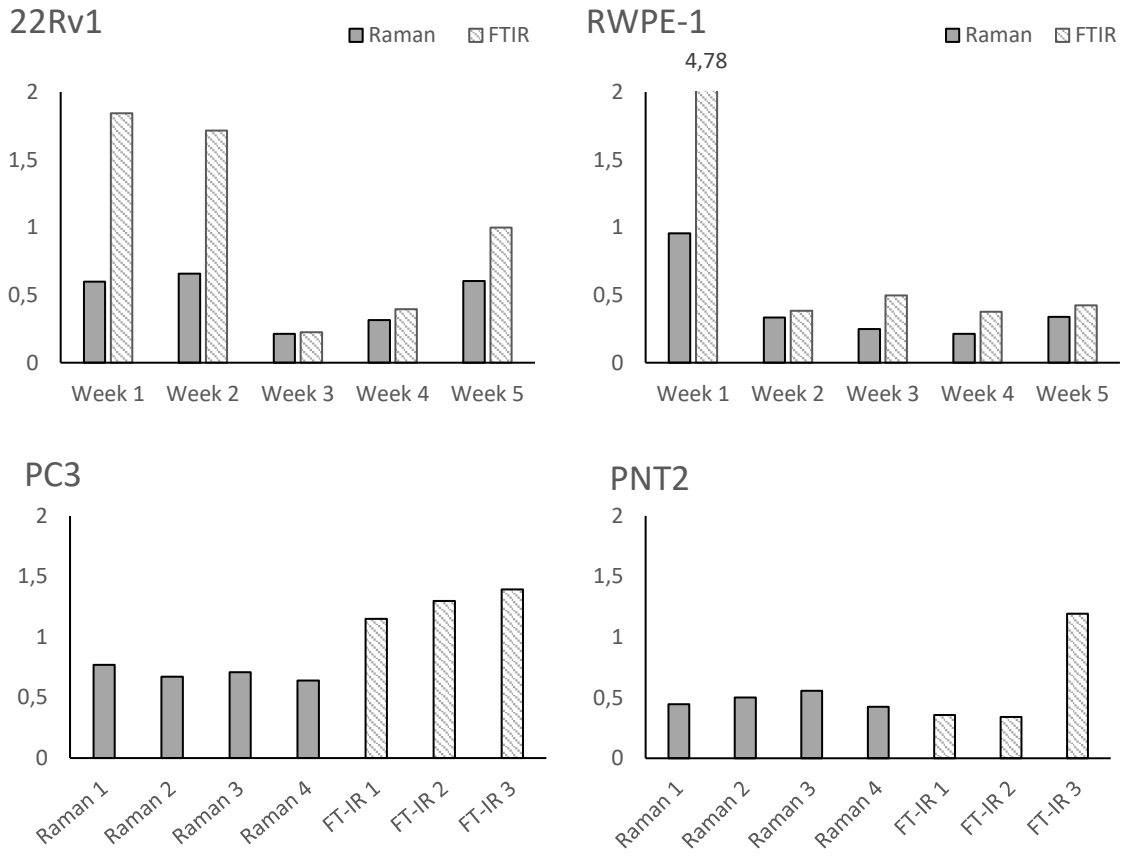

Figure 9. Protein-Lipid ratios for the FTIR were obtained by comparing the integrated peak areas of the amide II component centered at 1656 cm^{-1} for the protein component and the CH_2/CH_3 stretching vibration (2700 to 3000 cm^{-1}) representative of the lipid component from the FTIR spectra. Lipid-Protein Raman, the integrated areas of CH_2/CH_3 scissoring region (1416-1490 cm^{-1}) representing lipid component and C=O peak (1630-1710 cm^{-1}) representing protein component of the Raman spectra were compared.

3. Discussion

EVs play significant roles in both physiological and pathological states and the intrinsic properties of EVs make them potential for diverse array of uses in diagnostic and targeted drug delivery for diseases such as PrCa. In order to be able to utilize EVs in clinical settings, more research on EV subpopulations and their functions is needed. Important technical restraints for EV utilization lie in the need to establish robust methods for effective production and reliable characterization of the EV preparations. Currently, the EV research field is somewhat disorganized, and consensus and standardization are needed in methods for EV isolation and characterization. MISEV2018 outlines the current expert consensus and gives recommendations regarding the “best practices” of EV research.

The first aim of this study was to establish bioreactor cell cultures of 22Rv1 and RWPE-1 cell lines. The key advantages provided by the CELLine bioreactor as compared to conventional cell culture flasks are the increased yield and the reduced time needed for maintaining the culture. The CELLline bioreactor culture has been reported to increase EV yield up to 100-fold compared to a traditional T175 flask (Palviainen et al., 2018). Additionally, the cells in the CELLine do not need to be passaged after inoculation, which reduces the time it takes to handle the cells and to harvest the EVs compared to having to keep up several T175 flasks. After careful optimization of the growth medium, the EV yield achieved with the 22Rv1 and RWPE-1 cell lines was comparable to that achieved with other cell lines cultured in CELLine (Palviainen et al., 2018; Guerreiro et al., 2018) with weekly yield between 10^{11} to 10^{12} particles/ml EVs obtained once a week, after purification using DC and SEC.

The obtained vesicles were separated from the culture media by differential ultracentrifugation and purified further by using SEC as an additional separation method. A previously published protocol using Superdex 200 GL 10/300 SEC column was followed (Watson et al., 2018), and this method was analyzed with NTA to achieve a yield of 21-25%. Further sample analyses with NTA showed that compared to PC3 and PNT2 samples, the particle concentrations obtained

from 22Rv1 and RWPE-1 cell lines varied greatly on a week-to-week basis, and that while the size distribution main peak remained fairly consistently at 125-150 nm across different cell lines and different timepoints, slightly more variation in the shape of the peak and the amount of minor peaks at larger nm sizes can be seen between the EV samples of the 22Rv1 and RWPE-1 cell lines than with the PC3 an PNT2 derived samples. This sample-to-sample variation in the secreted vesicle properties could be linked to the duration that the cells have been cultured in the bioreactors, which will be discussed in further detail below.

EV biomarkers were detected using Western blotting. The biomarker proteins chosen included Tsg101, CD9 and Hsp70. The choice of these biomarkers reflects the older recommendations of MISEV2014 (Lötvall et al., 2014) and therefore the markers do not completely align with the newer, MISEV2018 recommendations (Théry et al., 2018). This is because the WB biomarker panel used had been optimized earlier by Zini et al., (2018) with markers chosen according to the previous recommendations. The MISEV2014 recommendations called for three classes of proteins to be detected; transmembrane proteins and cytosolic proteins with membrane-binding capacity, as well as proteins of endosomal origin not commonly enriched in EVs as a negative control (Lötvall et al., 2014). Tubulin was used as a loading control, and Golgi membrane protein GM130 was chosen as a negative control due to proteins from Golgi membrane and other cellular organelles not being prominent in EVs. Faint bands for TSG101 may be detected for RWPE-1 cell lysate and one EV lysate, however it is unclear as to why Hsp70 and TSG101 did not show up on RWPE-1 EVs. While studies have shown that biomarkers commonly attributed as universal EV markers are actually not constitutively enriched in EVs from all cell types (Hurwitz et al., 2016; Yoshioka et al., 2013), RWPE-1 EVs have been previously described to express Hsp70 (Hosseini-Beheshti et al., 2012). This difference could be due to the different cell culture and EV separation methods used in this thesis. However, on the basis of consistent CD9 expression (a biomarker strongly attributed to EVs and PrCa EVs specifically) in all EV samples analyzed, the particles obtained using the production and purification methods above may be identified as EVs

The second aim of this study was to characterize the obtained EVs using bio-photonic methods Raman and FTIR and to apply the method proposed by Mihály

et al. (2017) for determining the spectroscopic protein/lipid ratio as an additional measure of EV purity. These spectroscopic methods have recently gained interest as promising tools for efficient EV characterization, both of these methods have been applied to this purpose with promising results. According to MISEV2018, the protein to lipid ratio of an EV sample could serve as an additional measure of sample purity (Théry et al., 2018). The advantage of both FTIR and Raman spectroscopy is that they are able to quickly provide information on several biomolecular characteristics of the sample, including the protein and lipid component at once, which allows for the spectroscopic P/L ratio to be determined with just one measurement.

To our knowledge, the 22Rv1 and RWPE-1 cell line derived EVs have not been previously characterized using these methods. The spectra obtained from both methods were comparable to those obtained for prostate cell lines EVs in previous studies (Paolini et al.,2020; Lee et al.,2018; Krafft et al.,2017) and exhibited the characteristic peaks prominent in EV samples. The P/L ratios were calculated from both FTIR and Raman spectra by dividing the areas of the protein peak with the lipid peak of the spectra. The peaks chosen to represent protein and lipid components of the FTIR spectra are the amide I peak at 1656 cm^{-1} and the CH_2/CH_3 stretching vibration at 2700-3000 cm^{-1}, respectively. For Raman spectra, the C=O peak at 1630 -1710 cm^{-1} and the CH_2/CH_3 scissoring region at 1416-1490 cm^{-1} were chosen as representative of proteins and lipids, respectively. When analyzing the P/L ratios as function of time as weeks since initiation of the CELLine cell culture, it appears that new/fresh CELLine cultures exhibit greater week to week variation in the EV P/L as compared to 3+ months old bioreactors. This is hypothesized to be due to the cells needing more time than previously thought to fully adjust to the bioreactor conditions and for the EV production and composition to equilibrate. It is known that cells respond to stress via EV signaling, and that changes cell culture conditions effect EV production. Therefore, it would seem likely that when placed into a new environment the cells would respond by altering the EV production and composition before “settling in”, and once EV production has stabilized the sample-to-sample variation would be reduced over time. It was determined that this finding should be studied further to verify, as this phenomenon could have implications regarding the results of studies on EVs produced in bioreactor conditions. However, preliminary data of

EVs from newly established PNT2 and PC3 reactors obtained at University of Helsinki did not seem to exhibit as drastic weekly variation as the 22Rv1 and RWPE-1 EVs in this thesis, suggesting the phenomenon may also be cell line specific. Altogether this data highlights the importance of carefully reporting cell culture conditions including the age of the originating cell culture in EV publications. Although recommended also by ISEV (Thery et al., 2018) this practice seems to not yet have been widely adopted in publications.

It is worth noting, especially in the context of EV research, that the 22Rv1 cell line has been reported to produce high titers of a virus related to the human retrovirus xenotropic murine leukemia virus, and that these presumed viral particles were described to look similar to EVs at an approximated 100-nm size (Knouf et al., 2009). This virus was first described in 2006 from PrCa tissue samples by Urisman et al. but has been since been identified to most likely be a laboratory artifact and present in the 22Rv1 probably due to infection during the propagation of the cell line in mice (Sfanos et al., 2012). After learning of the virus, detection of extracellular biomarkers was deemed to be especially important when studying particles presumed to be EVs secreted by this cell line. However, the possibility of contamination of the EV samples derived from 22Rv1 cell lines by viral particles of the same size range cannot fully be ruled out with the characterization methods used, and therefore potential contribution of the viral proteins to the variation of the spectroscopic P/L ratio of the 22Rv1 derived EV samples is to be taken into account. A further avenue for EV studies using 22Rv1 cell lines could be to determine the extent of the contribution of viral particles versus EVs in the cell line's secretome.

Hypoxic EVs were an additional area of interest for this study. Cancer cells exposed to hypoxia have been shown to increase EV secretion, and that these EVs are involved in mediating many of the cells' hypoxia responses as described in section 1.4.3. This prompts the idea of hypoxic EVs being especially suitable as drug targets or diagnostic biomarkers. It is also worth noting that hypoxic cell culture conditions are more physiologically relevant, and the ambient 20% O2 conditions cell are usually grown in are actually hyperoxic in comparison; in normal tissues, oxygen levels range between approximately 5% and 10% O2, whereas in solid tumors, hypoxic conditions below 2% O2 are often present

(Saxena and Jolly, 2019). For this study, it was ultimately not feasible to set up a comparable bioreactor cell culture in hypoxic conditions to study the effects of chronic hypoxia on EVs. Most current studies on hypoxic EVs have been conducted by exposing cells to a short period of hypoxia (up to 72h) (King et al., 2012; Zhang et al., 2017; Panigrahi et al., 2019), or to repeated cycles of exposure to hypoxic conditions (Butterworth et al., 2008), however it is worth noting that using this method, reperfusion will also effect the results and therefore this is more of a model of acute or cyclic hypoxia. Few studies exist modeling truly long-term exposure of cells to hypoxia, and in these studies the cell lines have been meticulously conditioned by gradual lowering of oxygen levels, until a hypoxia resistant subpopulation remains (Kato et al., 2010). Such method was not, however, possible to attain within the timespan of this thesis. Another option utilized more often in hypoxic EV literature (King et al., 2012; Zhang et al., 2017; Panigrahi et al., 2019) would have been to expose the cells to a short periods of hypoxia, typically 24 to 72h, after which hypoxic EVs are collected and the cells are collected and lysed. However, this approach was not compatible with the CELLine bioreactor culture conditions utilized, where the cells are kept long term in a single culture vessel.

In conclusion, extracellular vesicles have great potential for future applications in targeted therapy and diagnostics. To achieve translation of this potential into clinic, robust and reproducible protocols for EV production, separation and characterization need to be established. This study presents a method for 22Rv1 and RWPE-1 bioreactor culture as an efficient method of producing EVs and is the first one to characterize EVs from these cell lines using both Raman and FTIR, spectroscopic methods that have gained popularity as potential tools for EV quality control. The spectroscopic protein/lipid ratio proposed by Mihaly et al. was explored as a measure of EV purity, and the results indicate a higher weekly variation of the protein and lipid components of EVs derived from newly established bioreactor cell cultures (Figure). This highlights the volatility of biological samples such as EVs to cell culture changes and the need to carefully report the culture conditions, preferably also culture age, a parameter that is rarely reported in EV publications despite recommendations in MISEV2018.

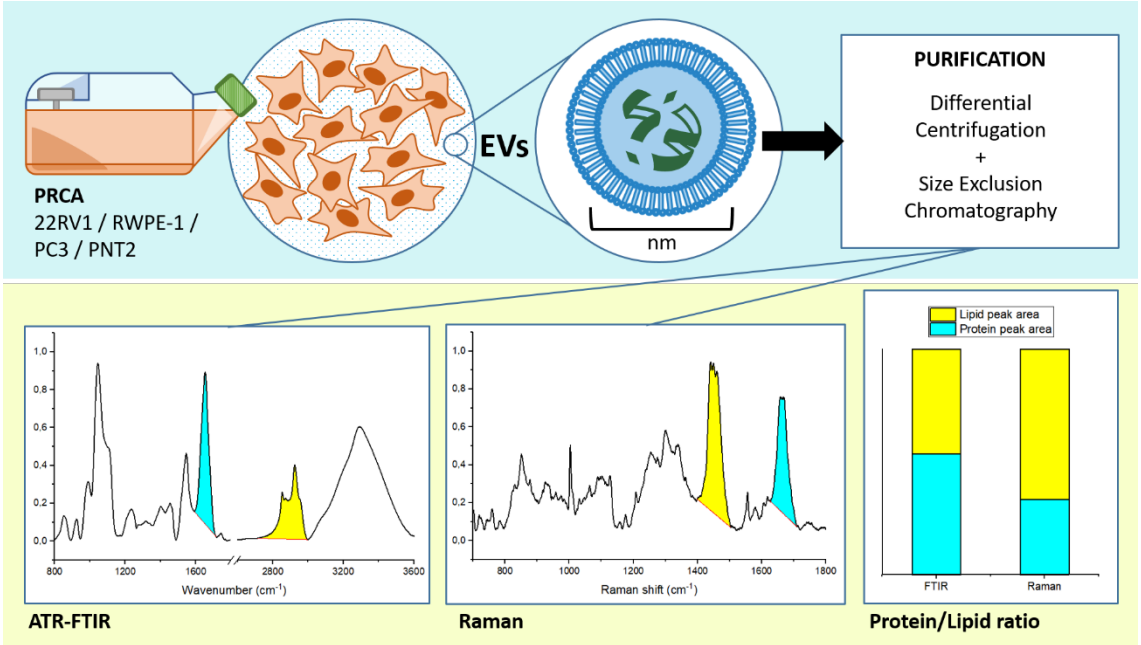

Figure 10. Overview of the study. In this study 1) a bioreactor cell culture protocol for 22Rv1 and RWPE-1 cell lines was established 2) the EVs obtained from these cell lines were purified using differential ultracentrifugation and SEC, characterised using Raman and FTIR spectroscopy, and subsequently the spectroscopic P/L ratio was calculated 3) the spectroscopic P/L ratio was analyzed as a measure of EV composition and purity over time in cell culture. The results indicate a higher weekly variation of the protein and lipid components of EVs derived from newly established bioreactor cell cultures as compared to long term, stabilised cultures, highlighting the volatility of biological samples such as EVs composition to cell culture changes.

4. Materials and methods

4.1 Cell culture

Cell lines, cell culture media and materials: RWPE-1, ATCC® CRL-11609™, American Type Culture Collection; 22Rv1, ATCC® CRL-2505™, American Type Culture Collection; RPMI 1640 Medium, GlutaMAX™ Supplement, Cat: 61870010, Gibco; Advanced RPMI 1640 Medium, Cat: 12633012, Gibco; Fetal Bovine Serum, exosome-depleted, One Shot™ format, Cat: A2720803; Keratinocyte-SFM Medium (Kit) with L-glutamine, EGF, and BPE, Cat: 17005075, Gibco; GlutaMAX™ Supplement, Cat: 35050038, Gibco D-(+)-Glucose solution, Cat: G8644, Sigma-Aldrich; DWK Life Sciences Wheaton™ CELLine™ Bioreactor Flask, Cat: 12811803, Thermo Fisher Scientific.

22Rv1 and RWPE-1 cell lines (American Type Culture Collection, ATCC) were cultured in bioreactor flasks at 37 °C and 5% of CO2. Conventional 2D cell culture flasks were maintained alongside the bioreactor cell culture in corresponding conditions and passaged twice a week. For conventional 2D cell cultures, the media compositions recommended for each cell line by ATCC were used. RPMI-1640 with 10% FBS was used for 22Rv1 and for RWPE-1, Keratinocyte Serum Free Medium supplemented with 0.05 mg/ml bovine pituitary extract and 5 ng/ml epidermal growth factor was used. For bioreactor cell culture, the media compositions were optimized for both high density cell culture and EV production purposes. The CELLine bioreactors consist of two compartments separated by a 10 kDa Nominal Molecular Weight Limit regenerated cellulose membrane. The cell compartment contains a polyethylene terephthalate matrix in which the cells grow in 3D like formation and allows for the cells to reach high numbers, whereas the nutrient compartment is able to house a large volume of nutrient rich medium.

For 22Rv1 cells, 750 ml of RPMI-1640 supplemented with 10ml glucose and 10% sterile-filtered FBS was used in the nutrition compartment, and 15 ml of advanced RPMI-1640 with 4 g/ml D-glucose, 4mM GlutaMAX and 1% commercial exosome-depleted FBS was used in the cell compartment. For RWPE-1 cells, 750 ml of Keratinocyte Serum Free Media supplemented with the included EGF+BPE and 10ml D-glucose was used in the medium compartment,

and 15 ml of KSFM+EGF+BPE, 4 g/ml D-glucose, 2 mM GlutaMAX was used in the cell compartment. No antibiotics were used in any of the culture media.

The nutrition compartment media was renewed once a week alongside EV collection. Conditioned media (CM) was collected from the cell compartment once weekly, and the compartment was subsequently washed twice with 15 ml of DPBS and added to collected CM to ensure optimal recovery of EV particles. The CM was then immediately centrifuged at 4°C, 2500 g for 25 min to remove cell debris. The supernatant was collected and stored at 4°C and proceeded to purification with differential centrifugation within the next 24 hours.

EV samples from PC3 and PNT2 cell lines were obtained from Biopharmaceutics research group at Helsinki University. These cells were cultured in corresponding bioreactor cell culture conditions (Zini et al., 2018) and the EV samples were collected and purified using the same methods described here.

Hypoxic cell culture

For hypoxic cell culture, T-75 flasks of 80% confluence were placed in hypoxia (SCI-tive Hypoxia Workstation, Baker Ruskinn) at 0.1%, 1% or 4% oxygen conditions with 5% CO2, 37°C. The cells were passaged 1:2-1:3 within the hypoxic workstation 24-48 hours after introduction to hypoxic conditions. All media and solutions were stored in 50 ml falcon tubes and placed in the hypoxic chamber to equilibrate for at least 20 minutes before passaging the cells. The media was renewed twice weekly after passaging.

4.2 EV separation and purification

Differential centrifugation

The CM supernatant was transferred into 38.5 ml polyallomer tubes (Beckman Coulter) and centrifuged using a swinging bucket rotor (SW 28 Ti, Beckman Coulter) at 4°C, 20 000 g for 1 h (Optima L-90K ultracentrifuge, Beckman Coulter). The resulting pellet was resuspended in 250 µl DPBS, and the supernatant was collected and centrifuged again at 4°C, 110 000 g for 2 h. The

110K pellet was resuspended in 250 µl DPBS, combined with the 20K pellet and stored at -80°C until SEC purification.

Size-exclusion Chromatography

SEC purification was conducted following a previously published protocol (Watson et al., 2018). The combined 500 µl sample was injected using a 1ml loop into a commercial, pre-packed Superdex 200 Increase 10/300 GL column connected to an Äkta Pure chromatography system (GE Healthcare) The volume of this column is 24 ml with 1.0 cm diameter and height of 24.0 cm, and the exclusion limit is 1.3×10^6 Da. For sample elution the mobile phase was PBS and a constant flow rate of 1ml/min was used. During the sample run, UV-absorbance at 215, 260 and 280 nm was monitored. Between each sample run, the column was washed with one column volume of 500 mM NaOH and one column volume of mQ water and equilibrated with two column volumes of PBS before application of the next sample. The 7^{th} and 8^{th} fractions, identified with NTA to contain the highest particle concentration, were pooled together and concentrated to a volume of 200-500 µl using Amicon Ultra 4 mL, 100 kDa MWL Centrifugal Filters (Millipore) at 4°C, 5000 g for 5x 5 min.

4.3 Nanoparticle tracking analysis

NTA was used to screen the SEC fractions to verify the fractions with the highest concentration of particles, as well as to determine the final concentration and size distribution of particles in the final, concentrated EV samples. NanoSight LM10 instrument and LM14C viewing unit equipped with a 405 nm blue laser were used with NTA 3.4 software (Malvern Panalytical). The samples were diluted in PBS to obtain a particle concentration suitable for detection. Three 60 s videos were recorded of each sample, using camera level of 15 and screen gain of 1. The videos were analyzedland particle concentration and size distribution data were obtained using NTA 3.4 software with detection threshold set at 5 and screen gain at 10.

4.4 Western blot analysis

To obtain the total protein content, duplicates of each EV sample and cell lysate (C.L.) were analyzed using Pierce BCA protein assay kit (Thermo scientific) according to manufacturer's instructions. The fluorescence signal was detected at 562 nm using Varioskan Flash multi-reader (v.2.4.3) (Thermo Scientific). For biomarker detection with Western blot, EV samples and C.L. were prepared by incubating them under reducing and non-reducing conditions at 95°C for at least 10 minutes. 10 µg of protein of each sample were loaded onto 4-20% Mini-PROTEAN TGX™ gels (Bio-Rad) for electrophoresis (80-120V). Following the SDS-page run the proteins were transferred onto polyvinylidene difluoride transfer membranes (Trans-Blot Turbo Mini 0.2 µg PVDF Transfer Pack, Bio-Rad), and the membranes were subsequently blocked with 3% (w/v) BSA in Tris-buffered saline Tween 20 (TBS-T) for 1 hr at RT.

All primary antibodies were diluted in 3% BSA in TBS-T and the primary antibody incubation took place at RT overnight. Primary antibodies used as EV positive markers were anti-Hsp70 (1:1000 Clone: 7/Hsp70, Isotype Mouse IgG1 Cat: 610607 BD Transduction Laboratories), anti-TSG101 (1:250 Clone: 51/TSG101, Isotype Mouse IgG1 Cat: 612697 BD Transduction Laboratories) and anti CD9 (1:1000, Clone: ALB 6 Isotype Mouse IgG1 Cat: HBM-CD9 Hansa Bio Med). For a negative EV marker, mouse monoclonal anti-GM130 (1:200, Clone: 35/GM130 Isotype Mouse IgG1 Cat: 610823 BD Transduction Laboratories) was used, and anti α-Tubulin (1:500, Clone: 6A204, Isotype Mouse IgG1, Cat: T9026 Sigma-Aldrich) was used as loading control. The membranes were washed five times in TBS-T and subsequently incubated for 1h at RT with secondary antibody, goat anti-mouse IgG-HRP (1:4000, Polyclonal Isotype: Goat IgG Cat Code: PA1-74421 ThermoFisher Scientific). The ECL+ system (Bio-Rad) was used to visualize the obtained protein bands.

4.5 ATR- FTIR

The ATR-FTIR spectra of each EV sample were obtained using an IR-spectrophotometer (Spectrum One spectrophotometer, Perkin Elmer Inc., Massachusetts, USA) equipped with a universal ATR sampling accessory

(Spectrum One spectrophotometer, Perkin Elmer Inc., Massachusetts, USA). A 5µl drop of the sample solution was placed over the ATR crystal and dried with a hairdryer to form a thin film on top of the crystal. The measurements were performed at RT, with accumulation of 64 scans and nominal resolution of 4cm^{-1}. Triplicate measurements of each sample were obtained. The results were analyzed using OriginPro 2020.

4.6 Raman spectroscopy

To measure the Raman spectra of 22Rv1 and RWPE-1 EVs, confocal Raman microscope (NT-MDT Ntegra, Russia) equipped with a 532 nm laser with an output power of ~ 20mW and a 100× objective (Leica) was used. Following a previously established protocol (Zini et al., 2018), the system was first calibrated using the Raman peak of silicon at 520.7 cm^{-1} by measuring the full width at half maximum of the peak. Spectral resolution of ~4.4 cm^{-1} was achieved with a grating of 1800/500. A 2 µl droplet of EV solution was placed on a CaF_2 substrate slide (LaserOptex) and let dry in ambient conditions. Raman spectra were measured on the edge of the dried sample droplet using exposure time of 6 s with the accumulation of 2 for the acquisition of one spectrum. Three measurement of each sample droplet were acquired. Due to time restrictions, Raman spectra could not be obtained for the PC3 and PNT2 samples. However, previously acquired Raman spectra for these same cell lines were kindly provided as a reference points by Jacopo Zini at Helsinki University.

5. Acknowledgements

I wish to sincerely thank my supervisors; Jacopo Zini, for all of his practical help and answers to my many questions, and for kindly providing me with some of his samples and data; Marjo Yliperttula, for her guidance and feedback throughout this thesis project and for insightful discussions; and my manager at Orion Corporation Orion Pharma, Jyrki Lehtimäki, for facilitating this project and providing his help and support throughout. Additionally, I would like to recognize my colleagues at Orion Corporation Orion Pharma, as well as at the Yliperttula research group at University of Helsinki, for providing me with their assistance, time and knowledge.

Furthermore, I am grateful for my teachers at the Institute of Biomedicine for their dedication, and my friends, especially my fellow students of the Drug Discovery and Development program, for providing me with encouragement and help whenever needed. I am lucky to have shared this journey with you. Finally, I want to thank my family for always encouraging me to pursue my academic goals and supporting me along the way.

I'd like to acknowledge Academy of Finland (314406) and Business Finland (1842/31/2019) for funding this project.

6. Abbreviations

ADT	androgen deprivation therapy
AR	androgen receptors
ATCC	American Type Culture Collection
ATR	attenuated total reflection
BM-MSCs	bone-marrow mesenchymal stem cells
CD	cluster of differentiation
CM	conditioned media
CRPC	castration resistant prostate cancer
EMA	European Medicines Agency
ESCRT	endosomal sorting complexes required for transport
EV	extracellular vesicles
FBS	fetal bovine serum
FDA	The United States Food and Drug Administration
FIH-1	factor inhibiting HIF
FTIR	Fourier-transform infrared spectroscopy
HIF	hypoxia inducible factor
HSP	heat shock protein
ISEV	International Society for Extracellular Vesicles
LHRH	luteinizing hormone-releasing hormone
MISEV 2018	Minimal information for studies of extracellular vesicles 2018
MMP	matrix metalloproteinase
NTA	nanoparticle tracking analysis
PKM2	pyruvate kinase M2
PrCa	prostate cancer
PSA	prostate-specific antigen
PSMA	prostate-specific membrane antigen
SEC	size exclusion chromatography
TBS-T	tris-buffered saline tween 20
TGFβ1	transforming growth factor beta 1
TME	tumor microenvironment
TSG101	tumor susceptibility gene 101
VEGF	vascular endothelial growth factor

7. References

Aslan, C., S. Maralbashi, F. Salari, H. Kahroba, F. Sigaroodi, T. Kazemi, and P. Kharaziha. 2019. Tumor-derived exosomes: Implication in angiogenesis and antiangiogenesis cancer therapy. J.Cell.Physiol. 234:16885-16903. doi: 10.1002/jcp.28374.

Bastos, D.A., and E.S. Antonarakis. 2019. Darolutamide For Castration-Resistant Prostate Cancer. Onco Targets Ther. 12:8769-8777. doi: 10.2147/OTT.S197244.

Bello, D., M.M. Webber, H.K. Kleinman, D.D. Wartinger, and J.S. Rhim. 1997. Androgen responsive adult human prostatic epithelial cell lines immortalized by human papillomavirus 18. Carcinogenesis. 18:1215-1223. doi: 10.1093/carcin/18.6.1215.

Berthon, P., O. Cussenot, L. Hopwood, A. Leduc, and N. Maitland. 1995. Functional expression of sv40 in normal human prostatic epithelial and fibroblastic cells - differentiation pattern of nontumorigenic cell-lines. Int.J.Oncol. 6:333-343. doi: 10.3892/ijo.6.2.333.

Brzozowski, J.S., D.R. Bond, H. Jankowski, B.J. Goldie, R. Burchell, C. Naudin, N.D. Smith, C.J. Scarlett, M.R. Larsen, M.D. Dun, K.A. Skelding, and J. Weidenhofer. 2018(b). Extracellular vesicles with altered tetraspanin CD9 and CD151 levels confer increased prostate cell motility and invasion. Sci.Rep. 8:8822-z. doi: 10.1038/s41598-018-27180-z.

Brzozowski, J.S., H. Jankowski, D.R. Bond, S.B. McCague, B.R. Munro, M.J. Predebon, C.J. Scarlett, K.A. Skelding, and J. Weidenhofer. 2018(a). Lipidomic profiling of extracellular vesicles derived from prostate and prostate cancer cell lines. Lipids Health.Dis. 17:211-x. doi: 10.1186/s12944-018-0854-x.

Butterworth, K.T., McCarthy, H.O., Devlin, A., Ming, L., Robson, T., McKeown, S.R. and Worthington, J. (2008), Hypoxia selects for androgen independent LNCaP cells with a more malignant geno- and phenotype. Int. J. Cancer, 123: 760-768. doi: 10.1002/ijc.23418.

Campanella, B., Palleschi, V. and Legnaioli, S. 2021. Introduction to vibrational spectroscopies. ChemTexts 7:5. doi: 10.1007/s40828-020-00129-4

Chowdhury, R., J.P. Webber, M. Gurney, M.D. Mason, Z. Tabi, and A. Clayton. 2015. Cancer exosomes trigger mesenchymal stem cell differentiation into pro-angiogenic and pro-invasive myofibroblasts. Oncotarget. 6:715-731. doi: 10.18632/oncotarget.2711.

Colombo, M., C. Moita, G. van Niel, J. Kowal, J. Vigneron, P. Benaroch, N. Manel, L.F. Moita, C. Thery, and G. Raposo. 2013. Analysis of ESCRT functions in exosome biogenesis, composition and secretion highlights the heterogeneity of extracellular vesicles. J.Cell.Sci. 126:5553-5565. doi: 10.1242/jcs.128868.

Costa Verdera, H., J.J. Gitz-Francois, R.M. Schiffelers, and P. Vader. 2017. Cellular uptake of extracellular vesicles is mediated by clathrin-independent

endocytosis and macropinocytosis. J.Control.Release. 266:100-108. doi: S0168-3659(17)30852-0.

Dai, J., J. Escara-Wilke, J.M. Keller, Y. Jung, R.S. Taichman, K.J. Pienta, and E.T. Keller. 2019. Primary prostate cancer educates bone stroma through exosomal pyruvate kinase M2 to promote bone metastasis. J.Exp.Med. 216:2883-2899. doi: 10.1084/jem.20190158.

Deep, G., A. Jain, A. Kumar, C. Agarwal, S. Kim, W.M. Leevy, and R. Agarwal. 2020. Exosomes secreted by prostate cancer cells under hypoxia promote matrix metalloproteinases activity at pre-metastatic niches. Mol.Carcinog. 59:323-332. doi: 10.1002/mc.23157.

Dehm, S.M., L.J. Schmidt, H.V. Heemers, R.L. Vessella, and D.J. Tindall. 2008. Splicing of a novel androgen receptor exon generates a constitutively active androgen receptor that mediates prostate cancer therapy resistance. Cancer Res. 68:5469-5477. doi: 10.1158/0008-5472.CAN-08-0594.

Del Re, M., E. Biasco, S. Crucitta, L. Derosa, E. Rofi, C. Orlandini, M. Miccoli, L. Galli, A. Falcone, G.W. Jenster, R.H. van Schaik, and R. Danesi. 2017. The Detection of Androgen Receptor Splice Variant 7 in Plasma-derived Exosomal RNA Strongly Predicts Resistance to Hormonal Therapy in Metastatic Prostate Cancer Patients. Eur.Urol. 71:680-687. doi: S0302-2838(16)30479-1.

Drożdż, A., A. Kamińska, M. Surman, A. Gonet-Surówka, R. Jach, H. Huras, M. Przybyło and E. Stępień. 2020. Low-Vacuum Filtration as an Alternative Extracellular Vesicle Concentration Method: A Comparison with Ultracentrifugation and Differential Centrifugation. Pharmaceutics, 12:872. doi: 10.3390/pharmaceutics12090872

Duijvesz, D., C.Y. Versluis, van der Fels, C A, Vredenbregt-van den Berg, M S, J. Leivo, M.T. Peltola, C.H. Bangma, K.S. Pettersson, and G. Jenster. 2015. Immuno-based detection of extracellular vesicles in urine as diagnostic marker for prostate cancer. Int.J.Cancer. 137:2869-2878. doi: 10.1002/ijc.29664.

Duodecim (Suomalaisen Lääkäriseuran Duodecimin ja Suomen Urologiyhdistys ry:n asettama työryhmä). 2014. Eturauhassyöpä. Suomalainen Lääkäriseura Duodecim, Helsinki. https://www.kaypahoito.fi/hoi11060 (accessed May 5, 2020)

EMA (European Medicines Agency). 2018. EMA/CHMP/784876/2018: CHMP summary of positive opinion for Erleada. https://www.ema.europa.eu/documents/smop-initial/chmp-summary-positive-opinion-erleada_en.pdf (accessed September 10, 2020).

EMA (European Medicines Agency). 2019. Xtandi. European Medicines Agency. Xtandi-H-C-2639-II-0039-G: EPAR assessment report - variation. https://www.ema.europa.eu/documents/variation-report/xtandi-h-c-2639-ii-0039-g-epar-assessment-report-variation_en.pdf (accessed September 10, 2020).

EMA (European Medicines Agency). 2020. EMA/32437/2020: CHMP summary of positive opinion for Nubeqa. https://www.ema.europa.eu/documents/smop-initial/chmp-summary-positive-opinion-nubeqa_en.pdf (accessed September 10, 2020).

FDA (The United States Food and Drug Administration). 2012. 2012 Notifications. https://www.fda.gov/drugs/resources-information-approved-drugs/2012-notifications (accessed September 9, 2020).

FDA (The United States Food and Drug Administration). 2018a. FDA approves apalutamide for non-metastatic castration-resistant prostate cancer. https://www.fda.gov/drugs/resources-information-approved-drugs/fda-approves-apalutamide-non-metastatic-castration-resistant-prostate-cancer (accessed September 9, 2020).

FDA (The United States Food and Drug Administration). 2018b. FDA approves enzalutamide for castration-resistant prostate cancer. https://www.fda.gov/drugs/resources-information-approved-drugs/fda-approves-enzalutamide-castration-resistant-prostate-cancer (accessed September 9, 2020).

FDA (The United States Food and Drug Administration). 2019. FDA approves darolutamide for non-metastatic castration-resistant prostate cancer. https://www.fda.gov/drugs/resources-information-approved-drugs/fda-approves-darolutamide-non-metastatic-castration-resistant-prostate-cancer (accessed September 9, 2020).

Feng, Q., C. Zhang, D. Lum, J.E. Druso, B. Blank, K.F. Wilson, A. Welm, M.A. Antonyak, and R.A. Cerione. 2017. A class of extracellular vesicles from breast cancer cells activates VEGF receptors and tumour angiogenesis. Nat.Commun. 8:14450. doi: 10.1038/ncomms14450.

Fibercell System Inc, 2020. Apparatus For Growing Cells. US6933144B2.

Forde, J.C., A.S. Perry, K. Brennan, L.M. Martin, M.P. Lawler, T.H. Lynch, D. Hollywood, and L. Marignol. 2012. Docetaxel maintains its cytotoxic activity under hypoxic conditions in prostate cancer cells. Urol.Oncol. 30:912-919. doi: 10.1016/j.urolonc.2010.08.015.

Gardiner, C., D. Vizio, S. Sahoo, C. Théry, K., Witwer, M. Wauben and A. Hill. 2016. Techniques used for the isolation and characterization of extracellular vesicles: results of a worldwide survey. J.Extracell.Vesicles, 5:32945. doi: 10.3402/jev.v5.32945

Gardiner, C., Y.J. Ferreira, R.A. Dragovic, C.W. Redman, and I.L. Sargent. 2013. Extracellular vesicle sizing and enumeration by nanoparticle tracking analysis. J.Extracell.Vesicles. 2:10.3402/jev.v2i0.19671. eCollection 2013. doi: 10.3402/jev.v2i0.19671.

Geng, H., C. Xue, J. Mendonca, X. Sun, Q. Liu, P.N. Reardon, Y. Chen, K. Qian, V. Hua, A. Chen, F. Pan, J. Yuan, S. Dang, T.M. Beer, M. Dai, S.K. Kachhap, and D.Z. Qian. 2018. Interplay between hypoxia and androgen controls a metabolic switch conferring resistance to androgen/AR-targeted therapy. Nat.Commun. 9:4972-16. doi: 10.1038/s41467-018-07411-7.

Gillessen, S., G. Attard, T.M. Beer, H. Beltran, A. Bossi, R. Bristow, B. Carver, D. Castellano, B.H. Chung, N. Clarke, G. Daugaard, I.D. Davis, J. de Bono, R. Borges Dos Reis, C.G. Drake, R. Eeles, E. Efstathiou, C.P. Evans, S. Fanti, F.

Feng, K. Fizazi, M. Frydenberg, M. Gleave, S. Halabi, A. Heidenreich, C.S. Higano, N. James, P. Kantoff, P.L. Kellokumpu-Lehtinen, R.B. Khauli, G. Kramer, C. Logothetis, F. Maluf, A.K. Morgans, M.J. Morris, N. Mottet, V. Murthy, W. Oh, P. Ost, A.R. Padhani, C. Parker, C.C. Pritchard, M. Roach, M.A. Rubin, C. Ryan, F. Saad, O. Sartor, H. Scher, A. Sella, N. Shore, M. Smith, H. Soule, C.N. Sternberg, H. Suzuki, C. Sweeney, M.R. Sydes, I. Tannock, B. Tombal, R. Valdagni, T. Wiegel, and A. Omlin. 2018. Management of Patients with Advanced Prostate Cancer: The Report of the Advanced Prostate Cancer Consensus Conference APCCC 2017. Eur.Urol. 73:178-211. doi: S0302-2838(17)30497-9.

Gualerzi, A., S.A.A. Kooijmans, S. Niada, S. Picciolini, A.T. Brini, G. Camussi, and M. Bedoni. 2019. Raman spectroscopy as a quick tool to assess purity of extracellular vesicle preparations and predict their functionality. J.Extracell Vesicles. 8:1568780. doi: 10.1080/20013078.2019.1568780.

Guerreiro, E.M., B. Vestad, L.A. Steffensen, H.C.D. Aass, M. Saeed, R. Ovstebo, D.E. Costea, H.K. Galtung, and T.M. Soland. 2018. Efficient extracellular vesicle isolation by combining cell media modifications, ultrafiltration, and size-exclusion chromatography. PLoS One. 13:e0204276. doi: 10.1371/journal.pone.0204276.

Gualerzi, A., S. Niada, C. Giannasi, S. Picciolini, C. Morasso, R. Vanna, V. Rossella, M. Masserini, M. Bedoni, F. Ciceri, M.E. Bernardo, A.T. Brini, F. Gramatica. 2017. Raman spectroscopy uncovers biochemical tissue-related features of extracellular vesicles from mesenchymal stromal cells. Sci Rep. 7(1):9820. doi: 10.1038/s41598-017-10448-1

Hackman, G., K. Taari, T.L. Tammela, M. Matikainen, M. Kouri, T. Joensuu, T. Luukkaala, A. Salonen, T. Isotalo, A. Petas, N. Hendolin, P.J. Bostrom, S. Aaltomaa, K. Lehtoranta, P. Hellstrom, J. Riikonen, M. Korpela, H. Minn, P.L. Kellokumpu-Lehtinen, E. Pukkala, A. Hemminki, and FinnProstate Group. 2019. Randomised Trial of Adjuvant Radiotherapy Following Radical Prostatectomy Versus Radical Prostatectomy Alone in Prostate Cancer Patients with Positive Margins or Extracapsular Extension. Eur.Urol. 76:586-595. doi: S0302-2838(19)30525-1.

Hanahan, D., and R. Weinberg. 2011. Hallmarks of Cancer: The Next Generation. Cell. 144:646-674. doi: 10.1016/j.cell.2011.02.013.

Haraszti, R.A., M.C. Didiot, E. Sapp, J. Leszyk, S.A. Shaffer, H.E. Rockwell, F. Gao, N.R. Narain, M. DiFiglia, M.A. Kiebish, N. Aronin, and A. Khvorova. 2016. High-resolution proteomic and lipidomic analysis of exosomes and microvesicles from different cell sources. J.Extracell Vesicles. 5:32570. doi: 10.3402/jev.v5.32570.

Hirst, C.J., C. Cabrera, and M. Kirby. 2012. Epidemiology of castration resistant prostate cancer: a longitudinal analysis using a UK primary care database. Cancer.Epidemiol. 36:349. doi: 10.1016/j.canep.2012.07.012.

Horoszewicz, J.S., S.S. Leong, T.M. Chu, Z.L. Wajsman, M. Friedman, L. Papsidero, U. Kim, L.S. Chai, S. Kakati, S.K. Arya, and A.A. Sandberg. 1980. The LNCaP cell line--a new model for studies on human prostatic carcinoma. Prog.Clin.Biol.Res. 37:115-132.

Hoshino, A., B. Costa-Silva, T.L. Shen, G. Rodrigues, A. Hashimoto, M. Tesic Mark, H. Molina, S. Kohsaka, A. Di Giannatale, S. Ceder, S. Singh, C. Williams, N. Soplop, K. Uryu, L. Pharmer, T. King, L. Bojmar, A.E. Davies, Y. Ararso, T. Zhang, H. Zhang, J. Hernandez, J.M. Weiss, V.D. Dumont-Cole, K. Kramer, L.H. Wexler, A. Narendran, G.K. Schwartz, J.H. Healey, P. Sandstrom, K.J. Labori, E.H. Kure, P.M. Grandgenett, M.A. Hollingsworth, M. de Sousa, S. Kaur, M. Jain, K. Mallya, S.K. Batra, W.R. Jarnagin, M.S. Brady, O. Fodstad, V. Muller, K. Pantel, A.J. Minn, M.J. Bissell, B.A. Garcia, Y. Kang, V.K. Rajasekhar, C.M. Ghajar, I. Matei, H. Peinado, J. Bromberg, and D. Lyden. 2015. Tumour exosome integrins determine organotropic metastasis. Nature. 527:329-335. doi: 10.1038/nature15756.

Hosseini-Beheshti, E., S. Pham, H. Adomat, N. Li, and E.S. Tomlinson Guns. 2012. Exosomes as Biomarker Enriched Microvesicles: Characterization of Exosomal Proteins Derived from a Panel of Prostate Cell Lines with Distinct AR Phenotypes. Mol. Cell. Proteom. 11:863-885. doi: 10.1074/mcp.M111.014845.

Hosseini-Beheshti, E., W. Choi, L.B. Weiswald, G. Kharmate, M. Ghaffari, M. Roshan-Moniri, M.D. Hassona, L. Chan, M.Y. Chin, I.T. Tai, P.S. Rennie, L. Fazli, and E.S. Tomlinson Guns. 2016. Exosomes confer pro-survival signals to alter the phenotype of prostate cells in their surrounding environment. Oncotarget. 7:14639-14658. doi: 10.18632/oncotarget.7052.

Huang, J., M. Shen, M. Yan, Y. Cui, Z. Gao, and X. Meng. 2019. Exosome-mediated transfer of miR-1290 promotes cell proliferation and invasion in gastric cancer via NKD1. Acta Biochim.Biophys.Sin.(Shanghai). 51:900-907. doi: 10.1093/abbs/gmz077.

Hurwitz, S.N., M.A. Rider, J.L. Bundy, X. Liu, R.K. Singh, and D.G. Meckes. 2016. Proteomic profiling of NCI-60 extracellular vesicles uncovers common protein cargo and cancer type-specific biomarkers. Oncotarget. 7:86999-87015. doi: 10.18632/oncotarget.13569.

Joncas, F.H., F. Lucien, M. Rouleau, F. Morin, H.S. Leong, F. Pouliot, Y. Fradet, C. Gilbert, and P. Toren. 2019. Plasma extracellular vesicles as phenotypic biomarkers in prostate cancer patients. Prostate. 79:1767-1776. doi: 10.1002/pros.23901.

Kaighn, M.E., K.S. Narayan, Y. Ohnuki, J.F. Lechner, and L.W. Jones. 1979. Establishment and characterization of a human prostatic carcinoma cell line (PC-3). Invest.Urol. 17:16-23.

Kato, Y., M. Yashiro, S. Noda, M. Tendo, S. Kashiwagi, Y. Doi, T. Nishii, J. Matsuoka, Y. Fuyuhiro, O. Shinto, T. Sawada, M. Ohira, and K. Hirakawa. 2010. Establishment and characterization of a new hypoxia-resistant cancer cell line, OCUM-12/Hypo, derived from a scirrhous gastric carcinoma. Br.J.Cancer. 102:898-907. doi: 10.1038/sj.bjc.6605543.

Kharaziha, P., D. Chioureas, D. Rutishauser, G. Baltatzis, L. Lennartsson, P. Fonseca, A. Azimi, K. Hultenby, R. Zubarev, A. Ullen, J. Yachnin, S. Nilsson, and T. Panaretakis. 2015. Molecular profiling of prostate cancer derived exosomes may reveal a predictive signature for response to docetaxel. Oncotarget. 6:21740-21754. doi: 10.18632/oncotarget.3226.

Kim, M.S., M.J. Haney, Y. Zhao, V. Mahajan, I. Deygen, N.L. Klyachko, E. Inskoe, A. Piroyan, M. Sokolsky, O. Okolie, S.D. Hingtgen, A.V. Kabanov, and E.V. Batrakova. 2016. Development of exosome-encapsulated paclitaxel to overcome MDR in cancer cells. Nanomedicine. 12:655-664. doi: S1549-9634(15)00202-6.

King, H.W., M.Z. Michael, and J.M. Gleadle. 2012. Hypoxic enhancement of exosome release by breast cancer cells. BMC Cancer. 12:421. doi: 10.1186/1471-2407-12-421.

Kirby, M., C. Hirst, and E.D. Crawford. 2011. Characterising the castration-resistant prostate cancer population: a systematic review. Int.J.Clin.Pract. 65:1180-1192. doi: 10.1111/j.1742-1241.2011.02799.x.

Knouf, E.C., M.J. Metzger, P.S. Mitchell, J.D. Arroyo, J.R. Chevillet, M. Tewari, and A.D. Miller. 2009. Multiple integrated copies and high-level production of the human retrovirus XMRV (xenotropic murine leukemia virus-related virus) from 22Rv1 prostate carcinoma cells. J.Virol. 83:7353-7356. doi: 10.1128/JVI.00546-09.

Ko, S.Y., W. Lee, H.A. Kenny, L.H. Dang, L.M. Ellis, E. Jonasch, E. Lengyel, and H. Naora. 2019. Cancer-derived small extracellular vesicles promote angiogenesis by heparin-bound, bevacizumab-insensitive VEGF, independent of vesicle uptake. Commun.Biol. 2:386-x. eCollection 2019. doi: 10.1038/s42003-019-0609-x.

Kowal, J., M. Tkach, and C. Thery. 2014. Biogenesis and secretion of exosomes. Curr.Opin.Cell Biol. 29:116-125. doi: 10.1016/j.ceb.2014.05.004.

Krafft, C., K. Wilhelm, A. Eremin, S. Nestel, N. von Bubnoff, W. Schultze-Seemann, J. Popp, and I. Nazarenko. 2017. A specific spectral signature of serum and plasma-derived extracellular vesicles for cancer screening. Nanomedicine (Lond). 13:835-841. doi: S1549-9634(16)30212-X [pii].

Langley, R.R., and I.J. Fidler. 2011. The seed and soil hypothesis revisited--the role of tumor-stroma interactions in metastasis to different organs. Int.J.Cancer. 128:2527-2535. doi: 10.1002/ijc.26031.

Lazaro-Ibanez, E., M. Neuvonen, M. Takatalo, U. Thanigai Arasu, C. Capasso, V. Cerullo, J.S. Rhim, K. Rilla, M. Yliperttula, and P.R. Siljander. 2017. Metastatic state of parent cells influences the uptake and functionality of prostate cancer cell-derived extracellular vesicles. J.Extracell Vesicles. 6:1354645. doi: 10.1080/20013078.2017.1354645.

Lee, W., A. Nanou, L. Rikkert, F.A.W. Coumans, C. Otto, Terstappen, Leon W. M. M, and H.L. Offerhaus. 2018. Label-Free Prostate Cancer Detection by Characterization of Extracellular Vesicles Using Raman Spectroscopy. Anal. Chem. 90:11290-11296. doi: 10.1021/acs.analchem.8b01831.

Li, Y.J., J.Y. Wu, X.B. Hu, J.M. Wang, and D.X. Xiang. 2019. Autologous cancer cell-derived extracellular vesicles as drug-delivery systems: a systematic review of preclinical and clinical findings and translational implications. Nanomedicine (Lond). 14:493-509. doi: 10.2217/nnm-2018-0286.

Linares, R., S. Tan, C. Gounou, N. Arraud, and A.R. Brisson. 2015. High-speed centrifugation induces aggregation of extracellular vesicles. J.Extracell Vesicles. 4:29509. doi: 10.3402/jev.v4.29509.

Lötvall, J., A.F. Hill, F. Hochberg, E.I. Buzas, D. Di Vizio, C. Gardiner, Y.S. Gho, I.V. Kurochkin, S. Mathivanan, P. Quesenberry, S. Sahoo, H. Tahara, M.H. Wauben, K.W. Witwer, and C. Thery. 2014. Minimal experimental requirements for definition of extracellular vesicles and their functions: a position statement from the International Society for Extracellular Vesicles. J.Extracell Vesicles. 3:26913. doi: 10.3402/jev.v3.26913.

Marcias, G., E. Erdmann, G. Lapouge, C. Siebert, P. Barthelemy, B. Duclos, J.P. Bergerat, J. Ceraline, and J.E. Kurtz. 2010. Identification of novel truncated androgen receptor (AR) mutants including unreported pre-mRNA splicing variants in the 22Rv1 hormone-refractory prostate cancer (PCa) cell line. Hum.Mutat. 31:74-80. doi: 10.1002/humu.21138.

Mihaly, J., R. Deak, I.C. Szigyarto, A. Bota, T. Beke-Somfai, and Z. Varga. 2017. Characterization of extracellular vesicles by IR spectroscopy: Fast and simple classification based on amide and CH stretching vibrations. Biochim.Biophys.Acta Biomembr. 1859:459-466. doi: 10.1016/j.bbamem.2016.12.005.

Milosevic, M., P. Warde, C. Menard, P. Chung, A. Toi, A. Ishkanian, M. McLean, M. Pintilie, J. Sykes, M. Gospodarowicz, C. Catton, R.P. Hill, and R. Bristow. 2012. Tumor hypoxia predicts biochemical failure following radiotherapy for clinically localized prostate cancer. Clin.Cancer Res. 18:2108-2114. doi: 10.1158/1078-0432.CCR-11-2711.

Mitchell, J.P., J. Court, M.D. Mason, Z. Tabi, and A. Clayton. 2008. Increased exosome production from tumour cell cultures using the Integra CELLine Culture System. J.Immunol.Methods. 335:98-105. doi: 10.1016/j.jim.2008.03.001.

Movasaghi, Z., S. Rehman & Dr. I.U. Rehman. 2008. Fourier Transform Infrared (FTIR) Spectroscopy of Biological Tissues. Appl. Spectrosc. Rev. 43:2, 134-179. doi: 10.1080/05704920701829043.

Paget, S. 1989. The distribution of secondary growths in cancer of the breast. 1889. Cancer Metastasis Rev. 8:98-101.

Palviainen, M., H. Saari, O. Karkkainen, J. Pekkinen, S. Auriola, M. Yliperttula, M. Puhka, K. Hanhineva, and P.R. Siljander. 2019. Metabolic signature of extracellular vesicles depends on the cell culture conditions. J.Extracell Vesicles. 8:1596669. doi: 10.1080/20013078.2019.1596669.

Pang, B., Y. Zhu, J. Ni, J. Thompson, D. Malouf, J. Bucci, P. Graham, and Y. Li. 2020. Extracellular vesicles: the next generation of biomarkers for liquid biopsy-based prostate cancer diagnosis. Theranostics. 10:2309-2326. doi: 10.7150/thno.39486.

Panigrahi, G.K., P.P. Praharaj, T.C. Peak, J. Long, R. Singh, J.S. Rhim, Z.Y.A. Elmageed, and G. Deep. 2018. Hypoxia-induced exosome secretion promotes

survival of African-American and Caucasian prostate cancer cells. Sci. Rep. 8:3853-13. doi: 10.1038/s41598-018-22068-4.

Paolini, L., S. Federici, G. Consoli, D. Arceri, A. Radeghieri, I. Alessandri, and P. Bergese. 2020. Fourier-transform Infrared (FT-IR) spectroscopy fingerprints subpopulations of extracellular vesicles of different sizes and cellular origin. J.Extracell Vesicles. 9:1741174. doi: 10.1080/20013078.2020.1741174.

Park, J., M. Hwang, B. Choi, H. Jeong, J.H. Jung, H.K. Kim, S. Hong, J.H. Park, and Y. Choi. 2017. Exosome Classification by Pattern Analysis of Surface-Enhanced Raman Spectroscopy Data for Lung Cancer Diagnosis. Anal.Chem. 89:6695-6701. doi: 10.1021/acs.analchem.7b00911.

Park, Y.H., H.W. Shin, A.R. Jung, O.S. Kwon, Y.J. Choi, J. Park, and J.Y. Lee. 2016. Prostate-specific extracellular vesicles as a novel biomarker in human prostate cancer. Sci.Rep. 6:30386. doi: 10.1038/srep30386.

Patel, D.B., K.M. Gray, Y. Santharam, T.N. Lamichhane, K.M. Stroka, and S.M. Jay. 2017. Impact of cell culture parameters on production and vascularization bioactivity of mesenchymal stem cell-derived extracellular vesicles. Bioeng.Transl.Med. 2:170-179. doi: 10.1002/btm2.10065.

Patel, D.B., M. Santoro, L.J. Born, J.P. Fisher, and S.M. Jay. 2018. Towards rationally designed biomanufacturing of therapeutic extracellular vesicles: impact of the bioproduction microenvironment. Biotechnol.Adv. 36:2051-2059. doi: S0734-9750(18)30158-7.

Patton, M.C., H. Zubair, M.A. Khan, S. Singh, and A.P. Singh. 2020. Hypoxia alters the release and size distribution of extracellular vesicles in pancreatic cancer cells to support their adaptive survival. J. Cell. Biochem. 121:828-839. doi: 10.1002/jcb.29328.

Peinado, H., M. Aleckovic, S. Lavotshkin, I. Matei, B. Costa-Silva, G. Moreno-Bueno, M. Hergueta-Redondo, C. Williams, G. Garcia-Santos, C. Ghajar, A. Nitadori-Hoshino, C. Hoffman, K. Badal, B.A. Garcia, M.K. Callahan, J. Yuan, V.R. Martins, J. Skog, R.N. Kaplan, M.S. Brady, J.D. Wolchok, P.B. Chapman, Y. Kang, J. Bromberg, and D. Lyden. 2012. Melanoma exosomes educate bone marrow progenitor cells toward a pro-metastatic phenotype through MET. Nat.Med. 18:883-891. doi: 10.1038/nm.2753.

Pellegrini, K.L., D. Patil, K.J.S. Douglas, G. Lee, K. Wehrmeyer, M. Torlak, J. Clark, C.S. Cooper, C.S. Moreno, and M.G. Sanda. 2017. Detection of prostate cancer-specific transcripts in extracellular vesicles isolated from post-DRE urine. Prostate. 77:990-999. doi: 10.1002/pros.23355.

Petrova, V., M. Annicchiarico-Petruzzelli, G. Melino, and I. Amelio. 2018. The hypoxic tumour microenvironment. Oncogenesis. 7:10-13. doi: 10.1038/s41389-017-0011-9.

Pitkäniemi, J., N. Malila, A. Virtanen, H. Degerlund, S.Heikkinen, K. Seppä. 2018. Syöpä 2018. Tilastoraportti Suomen syöpätilanteesta. Suomen Syöpäyhdistyksen julkaisuja nro 93. Suomen Syöpäyhdistys, Helsinki.

Probert, C., T. Dottorini, A. Speakman, S. Hunt, T. Nafee, A. Fazeli, S. Wood, J.E. Brown, and V. James. 2019. Communication of prostate cancer cells with bone cells via extracellular vesicle RNA; a potential mechanism of metastasis. Oncogene. 38:1751-1763. doi: 10.1038/s41388-018-0540-5.

Puhka, M., M. Takatalo, M.E. Nordberg, S. Valkonen, J. Nandania, M. Aatonen, M. Yliperttula, S. Laitinen, V. Velagapudi, T. Mirtti, O. Kallioniemi, A. Rannikko, P.R. Siljander, and T.M. Af Hallstrom. 2017. Metabolomic Profiling of Extracellular Vesicles and Alternative Normalization Methods Reveal Enriched Metabolites and Strategies to Study Prostate Cancer-Related Changes. Theranostics. 7:3824-3841. doi: 10.7150/thno.19890.

Ramteke, A., H. Ting, C. Agarwal, S. Mateen, R. Somasagara, A. Hussain, M. Graner, B. Frederick, R. Agarwal, and G. Deep. 2015. Exosomes secreted under hypoxia enhance invasiveness and stemness of prostate cancer cells by targeting adherens junction molecules. Mol.Carcinog. 54:554-565. doi: 10.1002/mc.22124.

Rice, M.A., S.V. Malhotra, and T. Stoyanova. 2019. Second-Generation Antiandrogens: From Discovery to Standard of Care in Castration Resistant Prostate Cancer. Front.Oncol. 9:801. doi: 10.3389/fonc.2019.00801.

Ringnér, M. What is principal component analysis?. 2008. Nat Biotechnol 26, 303–304. doi: 10.1038/nbt0308-303

Romano, S., F. Di Giacinto, A. Primiano, A. Mazzini, C. Panzetta, M. Papi, A. Di Gaspare, M. Ortolani, J. Gervasoni, M. De Spirito, G. Nocca, and G. Ciasca. 2020. Fourier Transform Infrared Spectroscopy as a useful tool for the automated classification of cancer cell-derived exosomes obtained under different culture conditions. Anal.Chim.Acta. 1140:219-227. doi: 10.1016/j.aca.2020.09.037.

Saari, H., E. Lázaro-Ibáñez, T. Viitala, E. Vuorimaa-Laukkanen, P. Siljander, and M. Yliperttula. 2015. Microvesicle- and exosome-mediated drug delivery enhances the cytotoxicity of Paclitaxel in autologous prostate cancer cells. J. Control. Release. 220:727-737. doi: 10.1016/j.jconrel.2015.09.031.

Saari, H., E. Lisitsyna, K. Rautaniemi, T. Rojalin, L. Niemi, O. Nivaro, T. Laaksonen, M. Yliperttula, and E. Vuorimaa-Laukkanen. 2018. FLIM reveals alternative EV-mediated cellular up-take pathways of paclitaxel. J.Control.Release. 284:133-143. doi: S0168-3659(18)30361-4.

Saleh, A.F., E. Lazaro-Ibanez, M.A. Forsgard, O. Shatnyeva, X. Osteikoetxea, F. Karlsson, N. Heath, M. Ingelsten, J. Rose, J. Harris, M. Mairesse, S.M. Bates, M. Clausen, D. Etal, E. Leonard, M.D. Fellows, N. Dekker, and N. Edmunds. 2019. Extracellular vesicles induce minimal hepatotoxicity and immunogenicity. Nanoscale. 11:6990-7001. doi: 10.1039/c8nr08720b.

Sampson, N., H. Neuwirt, M. Puhr, H. Klocker, and I.E. Eder. 2013. In vitro model systems to study androgen receptor signaling in prostate cancer. Endocr.-Relat. Cancer. 20:R49-R64. doi: 10.1530/ERC-12-0401.

Saxena, K., and M.K. Jolly. 2019. Acute vs. Chronic vs. Cyclic Hypoxia: Their Differential Dynamics, Molecular Mechanisms, and Effects on Tumor

Progression. Biomolecules. 9:10.3390/biom9080339. doi: 10.3390/biom9080339.

Schöning, J.P., M. Monteiro, and W. Gu. 2017. Drug resistance and cancer stem cells: the shared but distinct roles of hypoxia-inducible factors HIF1α and HIF2α. Clin. Exp. Pharmacol. Physiol. 44:153-161. doi: 10.1111/1440-1681.12693.

Senapati, S., A.K. Mahanta, S. Kumar, and P. Maiti. 2018. Controlled drug delivery vehicles for cancer treatment and their performance. Signal.Transduct Target Ther. 3:7-3. eCollection 2018. doi: 10.1038/s41392-017-0004-3.

Sfanos, K.S., A.L. Aloia, A.M. De Marzo, A. Rein. XMRV and prostate cancer--a 'final' perspective. 2012. Nat Rev Urol. 9(2):111-8. doi: 10.1038/nrurol.2011.225.

Sharma, B., R.R. Frontiera, A. Henry, E. Ringe, and R.P. Van Duyne. 2012. SERS: Materials, applications, and the future. Mater. Today. 15:16-25. doi: 10.1016/S1369-7021(12)70017-2.

Shiao, S.L., G.C. Chu, L.W. Chung. 2016. Regulation of prostate cancer progression by the tumor microenvironment. Cancer Lett. 380(1):340-8. doi: 10.1016/j.canlet.2015.12.022.

Soekmadji, C., J.D. Riches, P.J. Russell, J.E. Ruelcke, S. McPherson, C. Wang, C.M. Hovens, N.M. Corcoran, Australian Prostate Cancer Collaboration BioResource, M.M. Hill, and C.C. Nelson. 2016. Modulation of paracrine signaling by CD9 positive small extracellular vesicles mediates cellular growth of androgen deprived prostate cancer. Oncotarget. 8:52237-52255. doi: 10.18632/oncotarget.11111.

Sramkoski R.M., T.G. Pretlow 2nd, J.M. Giaconia, T.P. Pretlow, S. Schwartz , M.S. Sy, S.R. Marengo, J.S. Rhim, D. Zhang, J.W. Jacobberger. 1999. A new human prostate carcinoma cell line, 22Rv1. In Vitro Cell Dev Biol Anim. 35(7):403-9. doi: 10.1007/s11626-999-0115-4.

Stone, K.R., D.D. Mickey, H. Wunderli, G.H. Mickey, and D.F. Paulson. 1978. Isolation of a human prostate carcinoma cell line (DU 145). Int.J.Cancer. 21:274-281. doi: 10.1002/ijc.2910210305.

Strese, S., M. Fryknas, R. Larsson, and J. Gullbo. 2013. Effects of hypoxia on human cancer cell line chemosensitivity. BMC Cancer. 13:331-331. doi: 10.1186/1471-2407-13-331.

Sung, B.H., T. Ketova, D. Hoshino, A. Zijlstra, and A.M. Weaver. 2015. Directional cell movement through tissues is controlled by exosome secretion. Nat.Commun. 6:7164. doi: 10.1038/ncomms8164.

Tammela, T.L. 2012. Endocrine prevention and treatment of prostate cancer. Mol.Cell.Endocrinol. 360:59-67. doi: 10.1016/j.mce.2012.03.002.

Thery, C., K.W. Witwer, E. Aikawa, M.J. Alcaraz, J.D. Anderson, R. Andriantsitohaina, A. Antoniou, T. Arab, F. Archer, G.K. Atkin-Smith, D.C. Ayre, J.M. Bach, D. Bachurski, H. Baharvand, L. Balaj, S. Baldacchino, N.N. Bauer, A.A. Baxter, M. Bebawy, C. Beckham, A. Bedina Zavec, A. Benmoussa, A.C. Berardi, P. Bergese, E. Bielska, C. Blenkiron, S. Bobis-Wozowicz, E. Boilard, W.

Boireau, A. Bongiovanni, F.E. Borras, S. Bosch, C.M. Boulanger, X. Breakefield, A.M. Breglio, M.A. Brennan, D.R. Brigstock, A. Brisson, M.L. Broekman, J.F. Bromberg, P. Bryl-Gorecka, S. Buch, A.H. Buck, D. Burger, S. Busatto, D. Buschmann, B. Bussolati, E.I. Buzas, J.B. Byrd, G. Camussi, D.R. Carter, S. Caruso, L.W. Chamley, Y.T. Chang, C. Chen, S. Chen, L. Cheng, A.R. Chin, A. Clayton, S.P. Clerici, A. Cocks, E. Cocucci, R.J. Coffey, A. Cordeiro-da-Silva, Y. Couch, F.A. Coumans, B. Coyle, R. Crescitelli, M.F. Criado, C. D'Souza-Schorey, S. Das, A. Datta Chaudhuri, P. de Candia, E.F. De Santana, O. De Wever, H.A. Del Portillo, T. Demaret, S. Deville, A. Devitt, B. Dhondt, D. Di Vizio, L.C. Dieterich, V. Dolo, A.P. Dominguez Rubio, M. Dominici, M.R. Dourado, T.A. Driedonks, F.V. Duarte, H.M. Duncan, R.M. Eichenberger, K. Ekstrom, S. El Andaloussi, C. Elie-Caille, U. Erdbrugger, J.M. Falcon-Perez, F. Fatima, J.E. Fish, M. Flores-Bellver, A. Forsonits, A. Frelet-Barrand, F. Fricke, G. Fuhrmann, S. Gabrielsson, A. Gamez-Valero, C. Gardiner, K. Gartner, R. Gaudin, Y.S. Gho, B. Giebel, C. Gilbert, M. Gimona, I. Giusti, D.C. Goberdhan, A. Gorgens, S.M. Gorski, D.W. Greening, J.C. Gross, A. Gualerzi, G.N. Gupta, D. Gustafson, A. Handberg, R.A. Haraszti, P. Harrison, H. Hegyesi, A. Hendrix, A.F. Hill, F.H. Hochberg, K.F. Hoffmann, B. Holder, H. Holthofer, B. Hosseinkhani, G. Hu, Y. Huang, V. Huber, S. Hunt, A.G. Ibrahim, T. Ikezu, J.M. Inal, M. Isin, A. Ivanova, H.K. Jackson, S. Jacobsen, S.M. Jay, M. Jayachandran, G. Jenster, L. Jiang, S.M. Johnson, J.C. Jones, A. Jong, T. Jovanovic-Talisman, S. Jung, R. Kalluri, S.I. Kano, S. Kaur, Y. Kawamura, E.T. Keller, D. Khamari, E. Khomyakova, A. Khvorova, P. Kierulf, K.P. Kim, T. Kislinger, M. Klingeborn, D.J. Klinke, M. Kornek, M.M. Kosanovic, A.F. Kovacs, E.M. Kramer-Albers, S. Krasemann, M. Krause, I.V. Kurochkin, G.D. Kusuma, S. Kuypers, S. Laitinen, S.M. Langevin, L.R. Languino, J. Lannigan, C. Lasser, L.C. Laurent, G. Lavieu, E. Lazaro-Ibanez, S. Le Lay, M.S. Lee, Y.X.F. Lee, D.S. Lemos, M. Lenassi, A. Leszczynska, I.T. Li, K. Liao, S.F. Libregts, E. Ligeti, R. Lim, S.K. Lim, A. Line, K. Linnemannstons, A. Llorente, C.A. Lombard, M.J. Lorenowicz, A.M. Lorincz, J. Lotvall, J. Lovett, M.C. Lowry, X. Loyer, Q. Lu, B. Lukomska, T.R. Lunavat, S.L. Maas, H. Malhi, A. Marcilla, J. Mariani, J. Mariscal, E.S. Martens-Uzunova, L. Martin-Jaular, M.C. Martinez, V.R. Martins, M. Mathieu, S. Mathivanan, M. Maugeri, L.K. McGinnis, M.J. McVey, D.G. Meckes, K.L. Meehan, I. Mertens, V.R. Minciacchi, A. Moller, M. Moller Jorgensen, A. Morales-Kastresana, J. Morhayim, F. Mullier, M. Muraca, L. Musante, V. Mussack, D.C. Muth, K.H. Myburgh, T. Najrana, M. Nawaz, I. Nazarenko, P. Nejsum, C. Neri, T. Neri, R. Nieuwland, L. Nimrichter, J.P. Nolan, E.N. Nolte-'t Hoen, N. Noren Hooten, L. O'Driscoll, T. O'Grady, A. O'Loghlen, T. Ochiya, M. Olivier, A. Ortiz, L.A. Ortiz, X. Osteikoetxea, O. Ostergaard, M. Ostrowski, J. Park, D.M. Pegtel, H. Peinado, F. Perut, M.W. Pfaffl, D.G. Phinney, B.C. Pieters, R.C. Pink, D.S. Pisetsky, E. Pogge von Strandmann, I. Polakovicova, I.K. Poon, B.H. Powell, I. Prada, L. Pulliam, P. Quesenberry, A. Radeghieri, R.L. Raffai, S. Raimondo, J. Rak, M.I. Ramirez, G. Raposo, M.S. Rayyan, N. Regev-Rudzki, F.L. Ricklefs, P.D. Robbins, D.D. Roberts, S.C. Rodrigues, E. Rohde, S. Rome, K.M. Rouschop, A. Rughetti, A.E. Russell, P. Saa, S. Sahoo, E. Salas-Huenuleo, C. Sanchez, J.A. Saugstad, M.J. Saul, R.M. Schiffelers, R. Schneider, T.H. Schoyen, A. Scott, E. Shahaj, S. Sharma, O. Shatnyeva, F. Shekari, G.V. Shelke, A.K. Shetty, K. Shiba, P.R. Siljander, A.M. Silva, A. Skowronek, O.L. Snyder, R.P. Soares, B.W. Sodar, C. Soekmadji, J. Sotillo, P.D. Stahl, W. Stoorvogel, S.L. Stott, E.F. Strasser, S. Swift, H. Tahara, M. Tewari, K. Timms, S. Tiwari, R. Tixeira, M. Tkach, W.S. Toh, R. Tomasini, A.C. Torrecilhas, J.P. Tosar, V. Toxavidis, L. Urbanelli, P. Vader, B.W. van Balkom, van der Grein, S G, J. Van Deun, M.J. van Herwijnen, K. Van Keuren-

Jensen, G. van Niel, M.E. van Royen, A.J. van Wijnen, M.H. Vasconcelos, I.J. Vechetti, T.D. Veit, L.J. Vella, E. Velot, F.J. Verweij, B. Vestad, J.L. Vinas, T. Visnovitz, K.V. Vukman, J. Wahlgren, D.C. Watson, M.H. Wauben, A. Weaver, J.P. Webber, V. Weber, A.M. Wehman, D.J. Weiss, J.A. Welsh, S. Wendt, A.M. Wheelock, Z. Wiener, L. Witte, J. Wolfram, A. Xagorari, P. Xander, J. Xu, X. Yan, M. Yanez-Mo, H. Yin, Y. Yuana, V. Zappulli, J. Zarubova, V. Zekas, J.Y. Zhang, Z. Zhao, L. Zheng, A.R. Zheutlin, A.M. Zickler, P. Zimmermann, A.M. Zivkovic, D. Zocco, and E.K. Zuba-Surma. 2018. Minimal information for studies of extracellular vesicles 2018 (MISEV2018): a position statement of the International Society for Extracellular Vesicles and update of the MISEV2014 guidelines. J.Extracell Vesicles. 7:1535750. doi: 10.1080/20013078.2018.1535750.

Tian, T., Y.L. Zhu, Y.Y. Zhou, G.F. Liang, Y.Y. Wang, F.H. Hu, and Z.D. Xiao. 2014. Exosome uptake through clathrin-mediated endocytosis and macropinocytosis and mediating miR-21 delivery. J.Biol.Chem. 289:22258-22267. doi: 10.1074/jbc.M114.588046.

Tian, Y., S. Li, J. Song, T. Ji, M. Zhu, G.J. Anderson, J. Wei, and G. Nie. 2014. A doxorubicin delivery platform using engineered natural membrane vesicle exosomes for targeted tumor therapy. Biomaterials. 35:2383-2390. doi: 10.1016/j.biomaterials.2013.11.083.

Tran, M.G.B., B.A.S. Bibby, L. Yang, F. Lo, A.Y. Warren, D. Shukla, M. Osborne, J. Hadfield, T. Carroll, R. Stark, H. Scott, A. Ramos-Montoya, C. Massie, P. Maxwell, C.M.L. West, I.G. Mills, and D.E. Neal. 2020. Independence of HIF1a and androgen signaling pathways in prostate cancer. BMC Cancer. 20:469-6. doi: 10.1186/s12885-020-06890-6.

Usman, W.M., T.C. Pham, Y.Y. Kwok, L.T. Vu, V. Ma, B. Peng, Y.S. Chan, L. Wei, S.M. Chin, A. Azad, A.B. He, A.Y.H. Leung, M. Yang, N. Shyh-Chang, W.C. Cho, J. Shi, and M.T.N. Le. 2018. Efficient RNA drug delivery using red blood cell extracellular vesicles. Nat.Commun. 9:2359-8. doi: 10.1038/s41467-018-04791-8.

van Niel, G., G. D'Angelo, and G. Raposo. 2018. Shedding light on the cell biology of extracellular vesicles. Nat. Rev. Mol. Cell Biol. 19:213-228. doi: 10.1038/nrm.2017.125.

Varenhorst, E., R. Klaff, A. Berglund, P.O. Hedlund, G. Sandblom, and Scandinavian Prostate Cancer Group (SPCG) Trial No 5. 2016. Predictors of early androgen deprivation treatment failure in prostate cancer with bone metastases. Cancer.Med. 5:407-414. doi: 10.1002/cam4.594.

Watson, D.C., B.C. Yung, C. Bergamaschi, B. Chowdhury, J. Bear, D. Stellas, A. Morales-Kastresana, J.C. Jones, B.K. Felber, X. Chen, and G.N. Pavlakis. 2018. Scalable, cGMP-compatible purification of extracellular vesicles carrying bioactive human heterodimeric IL-15/lactadherin complexes. J. Extracell Vesicles. 7:1442088-16. doi: 10.1080/20013078.2018.1442088.

Watson, D.C., D. Bayik, A. Srivatsan, C. Bergamaschi, A. Valentin, G. Niu, J. Bear, M. Monninger, M. Sun, A. Morales-Kastresana, J.C. Jones, B.K. Felber, X. Chen, I. Gursel, and G.N. Pavlakis. 2016. Efficient production and enhanced

tumor delivery of engineered extracellular vesicles. Biomaterials. 105:195-205. doi: S0142-9612(16)30334-9.

Webber, J.P., L.K. Spary, A.J. Sanders, R. Chowdhury, W.G. Jiang, R. Steadman, J. Wymant, A.T. Jones, H. Kynaston, M.D. Mason, Z. Tabi, and A. Clayton. 2015. Differentiation of tumour-promoting stromal myofibroblasts by cancer exosomes. Oncogene. 34:290-302. doi: 10.1038/onc.2013.560.

Webber, M.M., D. Bello, H.K. Kleinman, D.D. Wartinger, D.E. Williams, and J.S. Rhim. 1996. Prostate specific antigen and androgen receptor induction and characterization of an immortalized adult human prostatic epithelial cell line. Carcinogenesis. 17:1641-1646. doi: 10.1093/carcin/17.8.1641.

Vergis, R., C.M. Corbishley, A.R. Norman, J. Bartlett, S. Jhavar, M. Borre, S. Heeboll, A. Horwich, R. Huddart, V. Khoo, R. Eeles, C. Cooper, M. Sydes, D. Dearnaley, and C. Parker. 2008. Intrinsic markers of tumour hypoxia and angiogenesis in localised prostate cancer and outcome of radical treatment: a retrospective analysis of two randomised radiotherapy trials and one surgical cohort study. Lancet Oncol. 9:342-351. doi: 10.1016/S1470-2045(08)70076-7.

Wilson, W.R., and M.P. Hay. 2011. Targeting hypoxia in cancer therapy. Nat.Rev.Cancer. 11:393-410. doi: 10.1038/nrc3064.

Vlaeminck-Guillem, V. 2018. Extracellular Vesicles in Prostate Cancer Carcinogenesis, Diagnosis, and Management. Front.Oncol. 8:222. doi: 10.3389/fonc.2018.00222.

Yang T., P. Martin, B. Fogarty, A. Brown, K. Schurman, R. Phipps, V.P. Yin, P. Lockman and S. Bai. 2015. Exosome delivered anticancer drugs across the blood-brain barrier for brain cancer therapy in Danio rerio. Pharm Res. 32(6):2003-14. doi: 10.1007/s11095-014-1593-y.

Yoshioka, Y., N. Kosaka, Y. Konishi, H. Ohta, H. Okamoto, H. Sonoda, R. Nonaka, H. Yamamoto, H. Ishii, M. Mori, K. Furuta, T. Nakajima, H. Hayashi, H. Sugisaki, H. Higashimoto, T. Kato, F. Takeshita, and T. Ochiya. 2014. Ultra-sensitive liquid biopsy of circulating extracellular vesicles using ExoScreen. Nat.Commun. 5:3591. doi: 10.1038/ncomms4591.

Yoshioka, Y., Y. Konishi, N. Kosaka, T. Katsuda, T. Kato, and T. Ochiya. 2013. Comparative marker analysis of extracellular vesicles in different human cancer types. J.Extracell Vesicles. 2:20424-9. doi: 10.3402/jev.v2i0.20424.

Zhang, W., X. Zhou, Q. Yao, Y. Liu, H. Zhang, and Z. Dong. 2017. HIF-1-mediated production of exosomes during hypoxia is protective in renal tubular cells. Am. J. Physiol. Renal Physiol. 313:F906-F913. doi: 10.1152/ajprenal.00178.2017.

Zhu, X., M. Badawi, S. Pomeroy, D.S. Sutaria, Z. Xie, A. Baek, J. Jiang, O.A. Elgamal, X. Mo, K. Perle, J. Chalmers, T.D. Schmittgen, and M.A. Phelps. 2017. Comprehensive toxicity and immunogenicity studies reveal minimal effects in mice following sustained dosing of extracellular vesicles derived from HEK293T cells. J.Extracell Vesicles. 6:1324730. doi: 10.1080/20013078.2017.1324730.

Zini, J., H. Saari, O-P. Nivaro, P. Ciana, J. Saarinen, M. Yliperttula. 2018. Raman and FTIR spectra of extracellular vesicles discriminating the purification. Data presented in ISEV annual meeting, Barcelona 2018 by Jacopo Zini.

Zlotogorski-Hurvitz, A., B.Z. Dekel, D. Malonek, R. Yahalom, M. Vered. 2019. FTIR-based spectrum of salivary exosomes coupled with computational-aided discriminating analysis in the diagnosis of oral cancer. J Cancer Res Clin Oncol. 145(3):685-694. doi: 10.1007/s00432-018-02827-6.

Zonneveld, M.I., T.G.H. Keulers, and K.M.A. Rouschop. 2019. Extracellular Vesicles as Transmitters of Hypoxia Tolerance in Solid Cancers. Cancers (Basel). 11:154. doi: 10.3390/cancers11020154. doi: 10.3390/cancers11020154.

8. Appendices

Appendix A Supplementary FTIR spectra

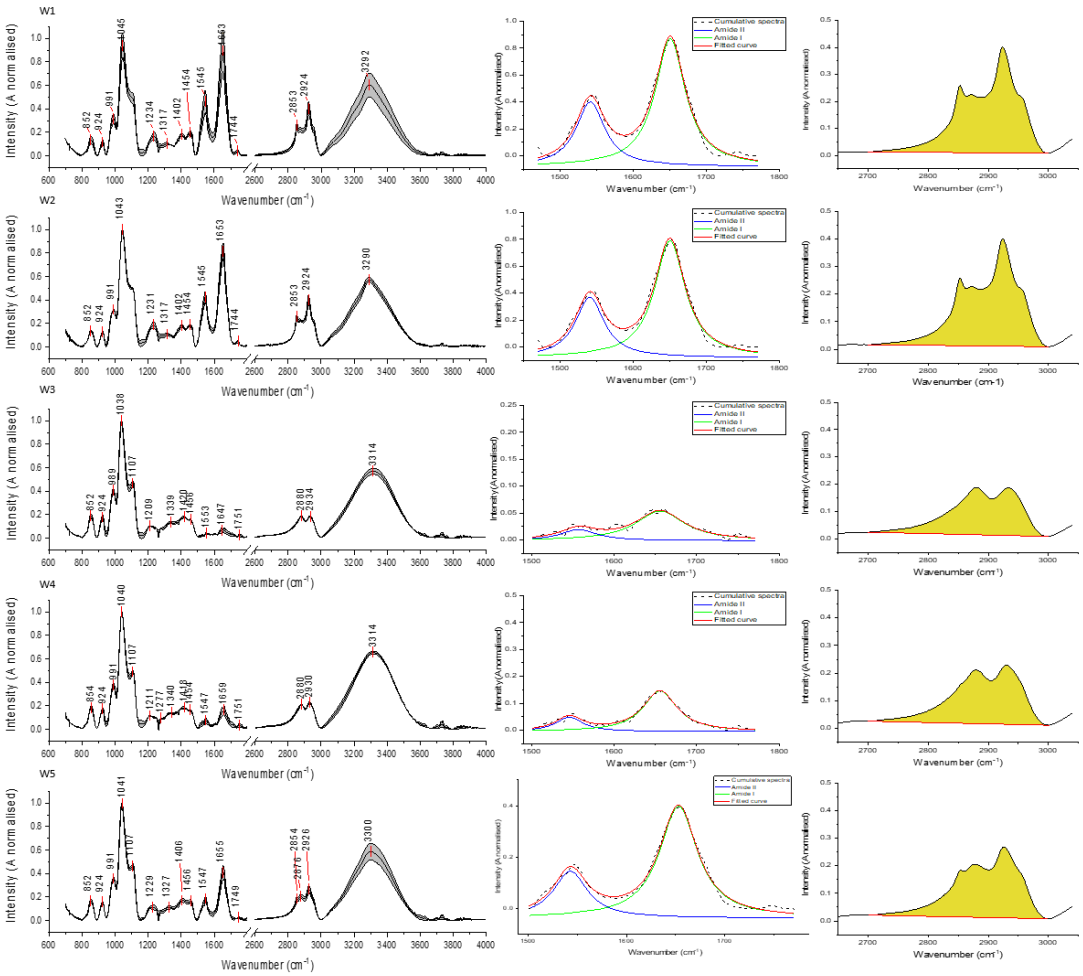

Figure 1 Apx A. FTIR spectra of EVs isolated from 22Rv1 cells cultured in bioreactor cell culture, purified using differential ultracentrifugation and size-exclusion chromatography, 1-5 weeks after bioreactor inoculation, presented as average (solid line)+-1 standard deviation(gray area) of 3 independent measurements (left). The area of the amide I peak centered at 1656 cm^{-1} (green line) was determined by peak deconvolution using curve fitting with Lorentz-function (red line) (middle). The area of the CH_2/CH_3 stretching vibration (2700 to 3000 cm^{-1}) representative of the lipid component was integrated (right).

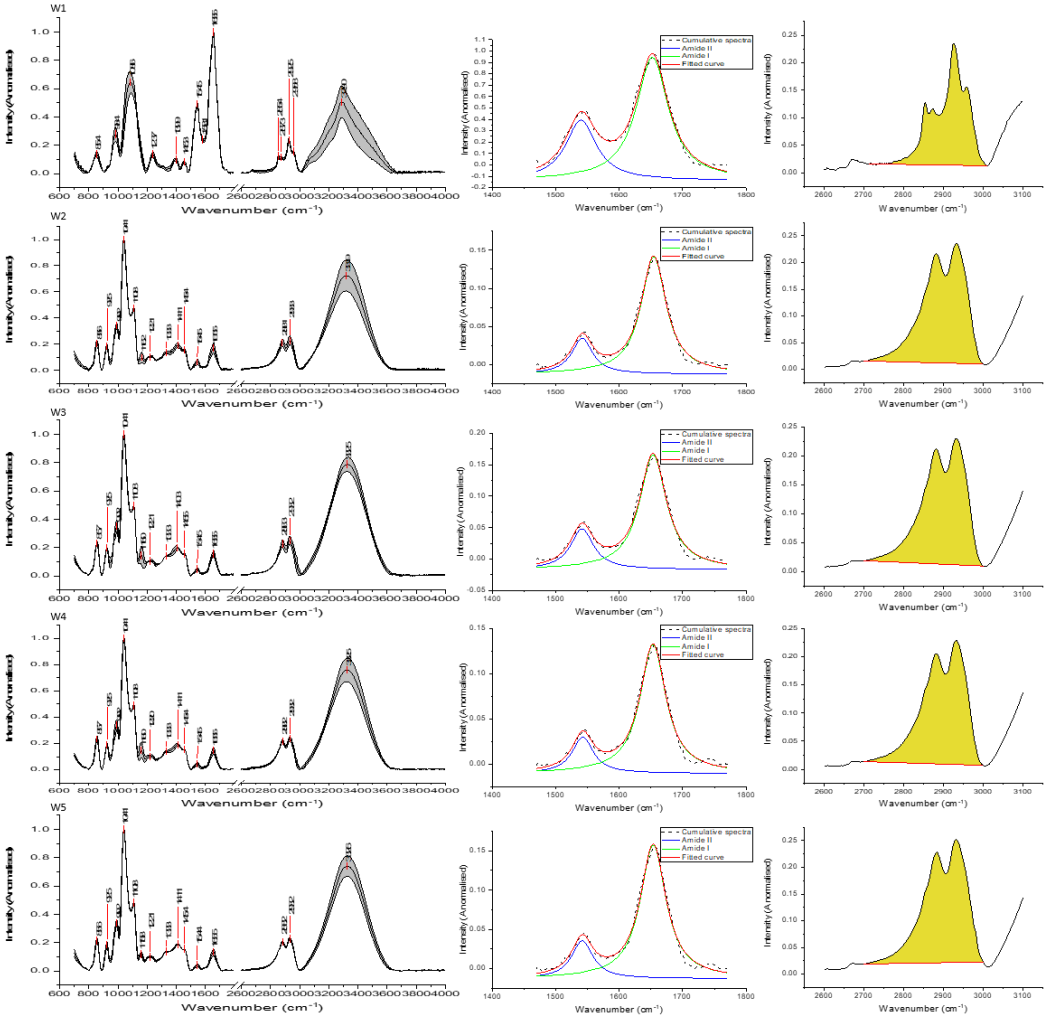

Figure 2 Apx A. FTIR spectra of EVs isolated from RWPE-1 cells cultured in bioreactor cell culture, purified using differential ultracentrifugation and size-exclusion chromatography, 1-5 weeks after bioreactor inoculation, presented as average (solid line)+-1 standard deviation(gray area) of 3 independent measurements (left). The area of the amide I peak centered at 1656 cm^{-1} (green line) was determined by peak deconvolution using curve fitting with Lorentz-function (red line) (middle). The area of the CH_2/CH_3 stretching vibration (2700 to 3000 cm^{-1}) representative of the lipid component was integrated (right).

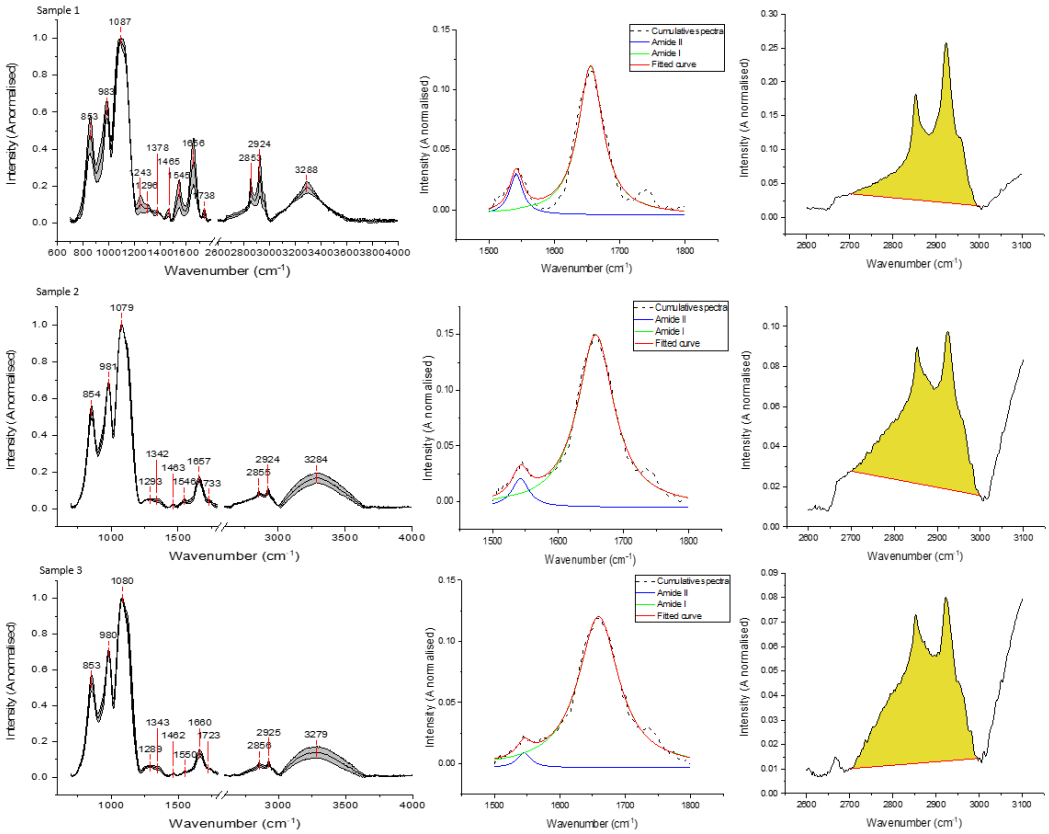

Figure 3 Apx A. FTIR spectra of three independent samples of EVs isolated from PC3 cells cultured in stable (3+ months since inoculation) bioreactor cell culture, purified using differential ultracentrifugation and size-exclusion chromatography presented as average (solid line)+-1 standard deviation(gray area) of 3 independent measurements (left). The area of the amide I peak centered at 1656 cm^{-1} (green line) was determined by peak deconvolution using curve fitting with Lorentz-function (red line) (middle). The area of the CH_2/CH_3 stretching vibration (2700 to 3000 cm^{-1}) representative of the lipid component was integrated (right).

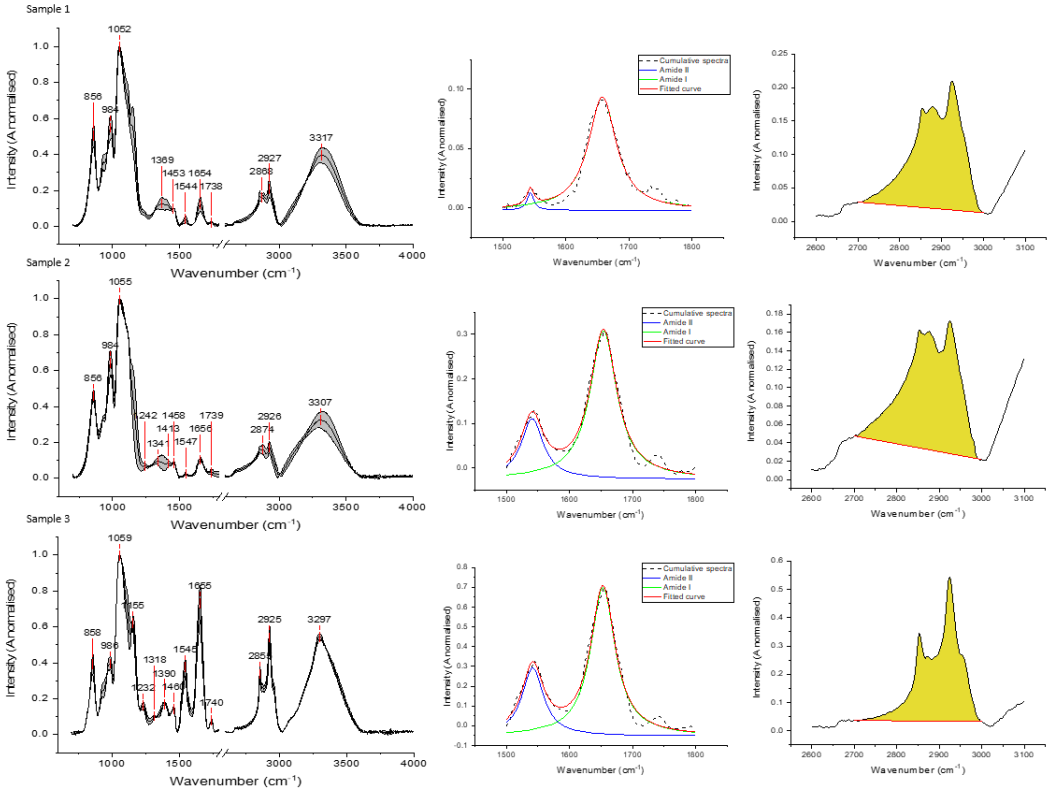

Figure 4 Apx A. FTIR spectra of three independent samples of EVs isolated from PNT2 cells cultured in stable (3+ months since inoculation) bioreactor cell culture, purified using differential ultracentrifugation and size-exclusion chromatography presented as average (solid line)+-1 standard deviation(gray area) of 3 independent measurements (left). The area of the amide I peak centered at 1656 cm^{-1} (green line) was determined by peak deconvolution using curve fitting with Lorentz-function (red line) (middle). The area of the CH_2/CH_3 stretching vibration (2700 to 3000 cm^{-1}) representative of the lipid component was integrated (right).

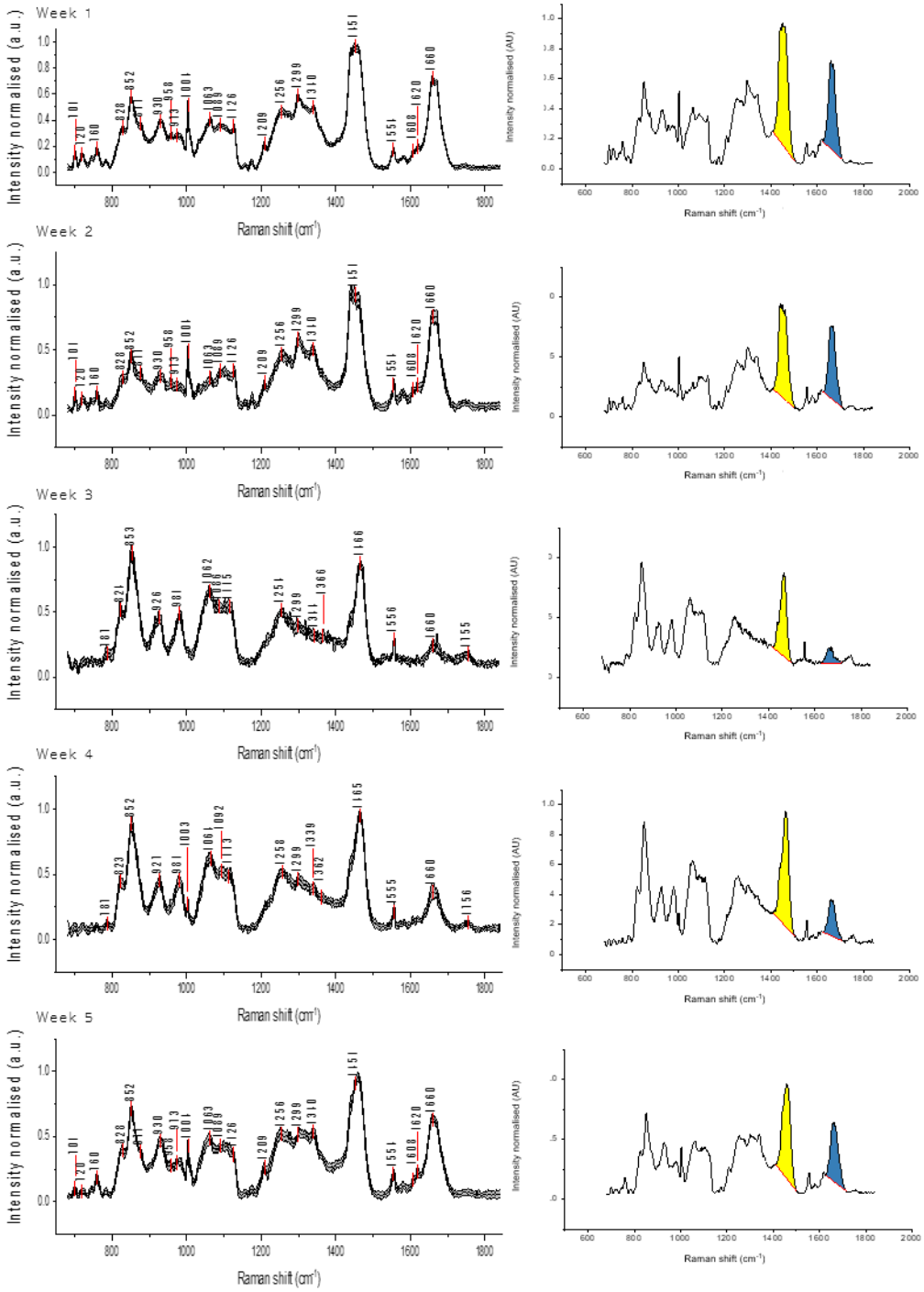

Figure 1 Apx B Raman spectra of EVs from 22Rv1 cells in bioreactor cell culture and purified using differential ultracentrifugation and size-exclusion chromatography, weeks 1-5 after bioreactor inoculation, presented as average (solid line) +/- 1 standard deviation (gray area) of 3 independent measurements (left). Integrated area of CH_2/CH_3 scissoring region (yellow 1416-1490 cm^{-1}) represents lipid component and C=O peak (cyan, 1630-1710 cm^{-1}) represents protein component (right).

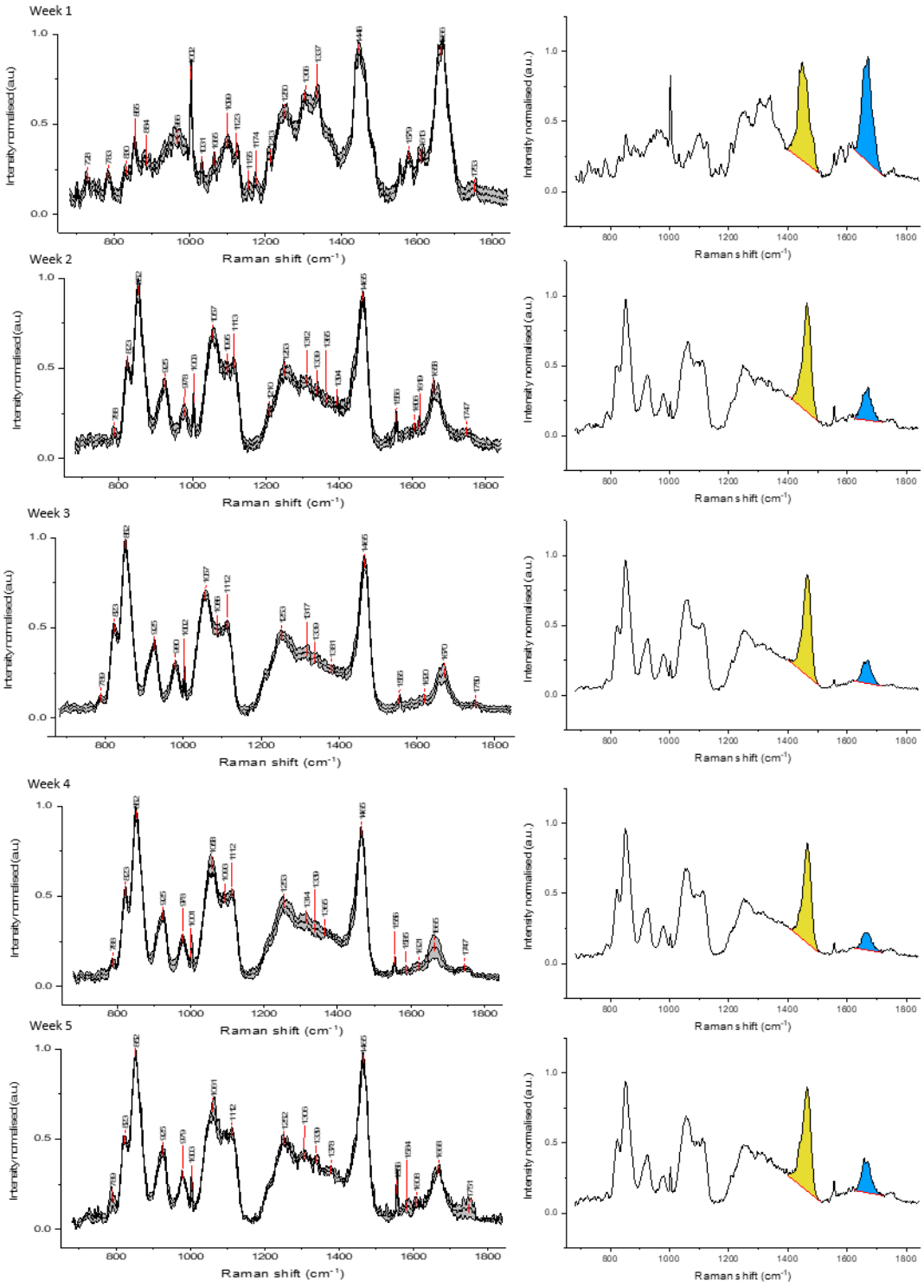

Figure 2 Apx B Raman spectra of EVs from RWPE-1 cells in bioreactor cell culture and purified using differential ultracentrifugation and size-exclusion chromatography, weeks 1-5 after bioreactor inoculation, presented as average (solid line) +/- 1 standard deviation (gray area) of 3 independent measurements (left). Integrated area of CH_2/CH_3 scissoring region (yellow 1416-1490 cm^{-1}) represents lipid component and C=O peak (cyan, 1630-1710 cm^{-1}) represents protein component (right).

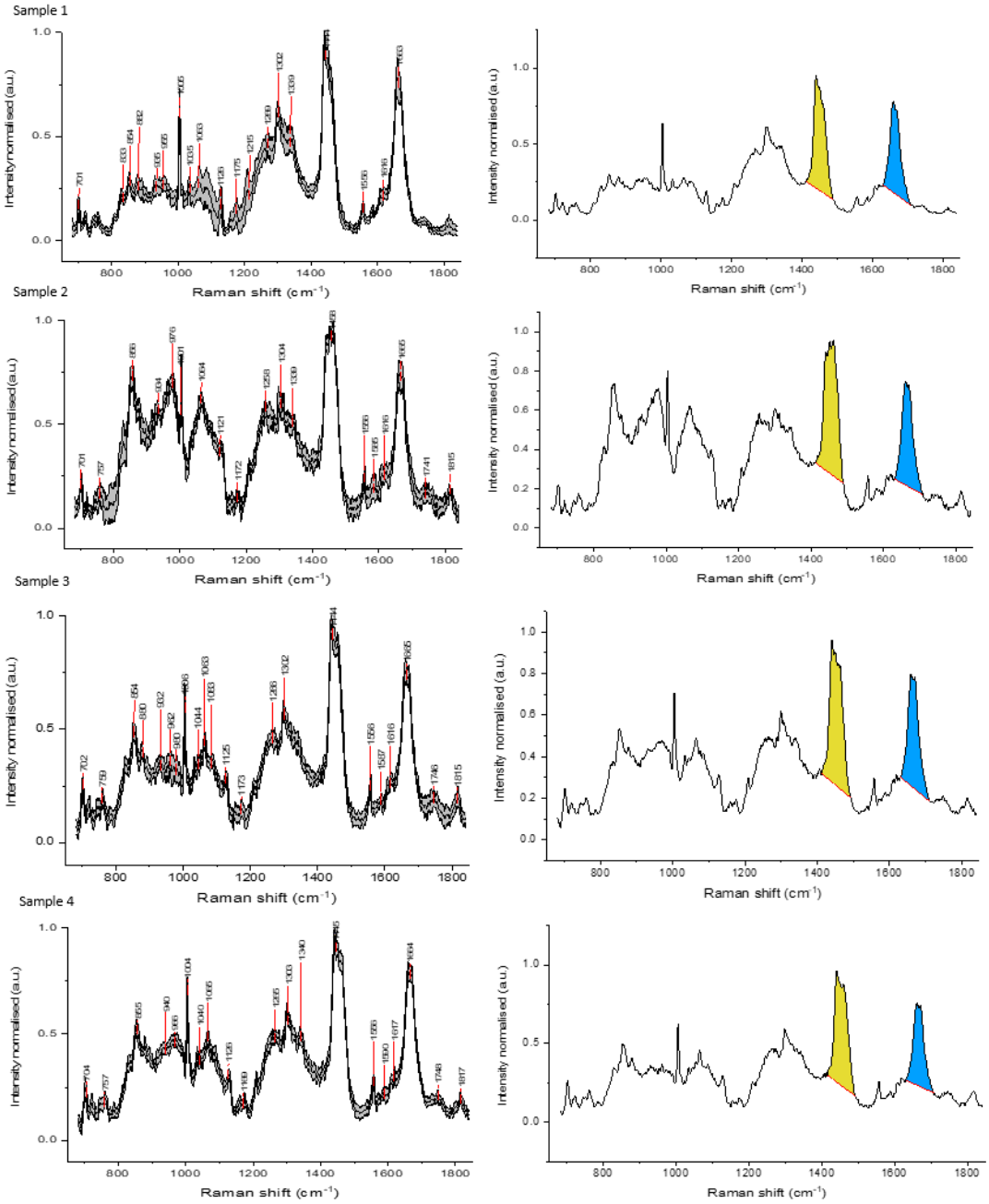

Figure 3 Apx B Raman spectra of four independent samples EVs from PC3 cells in stable (3+ months since inoculation) bioreactor culture and purified using differential ultracentrifugation and size-exclusion chromatography, as average (solid line) +/- 1 standard deviation (gray area) of 3 independent measurements (left). Integrated area of CH_2/CH_3 scissoring region (yellow 1416-1490 cm^{-1}) represents lipid component and C=O peak (cyan, 1630-1710 cm^{-1}) represents protein component (right).

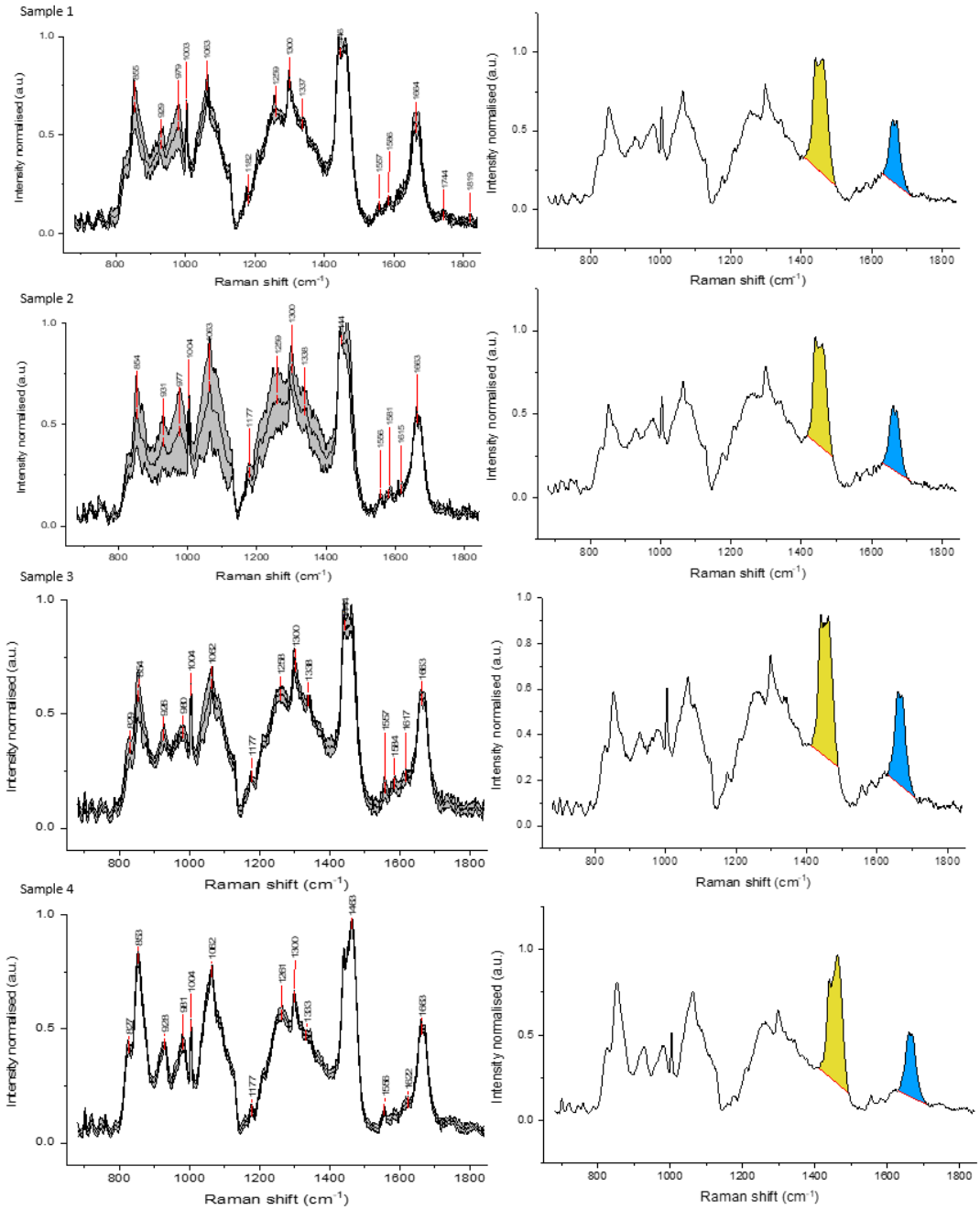

Figure 4 Apx B Raman spectra of four independent samples EVs from PNT2 cells in stable (3+ months since inoculation) bioreactor culture and purified using differential ultracentrifugation and size-exclusion chromatography, as average (solid line) +/- 1 standard deviation (gray area) of 3 independent measurements (left). Integrated area of CH_2/CH_3 scissoring region (yellow 1416-1490 cm^{-1}) represents lipid component and C=O peak (cyan, 1630-1710 cm^{-1}) represents protein component (right).